Blood clot microstructures: The role of engineered and combustion derived carbon particulates in thrombus formation.

Puckering, Oliver James

BLOOD CLOT MICROSTRUCTURES: THE ROLE OF ENGINEERED AND COMBUSTION DERIVED CARBON PARTICULATES IN THROMBUS FORMATION

Swansea University
Prifysgol Abertawe

BY
OLIVER JAMES PUCKERING
M.Eng (Hons.)(Swansea University)

Thesis submitted to Swansea University
in partial fulfilment of the requirements for the
Degree of Philosophiae Doctor

Department of Multidisciplinary Nanotechnology
School of Engineering
Swansea University

September 2009

Declaration

This work has not previously been accepted in substance for any degree and is not being currently submitted in candidature for a degree in any University.

Signed.. ..(candidate)

Date.....3/5/10.....

Statement 1

This thesis is the result of my own investigation except where otherwise stated. Other sources are acknowledged, giving explicit references. A bibliography is appended.

Signed.. ..(candidate)

Date.....3/5/10.....

Statement 2

I hereby consent for my thesis, if accepted, to be available for photocopying and for inter-library loan, and for the title and summary to be available to outside organisations.

Signed.. (candidate)

Date.....3/5/10.....

Certificate of Originality

This thesis is submitted to the University of Wales, Swansea, under the supervision of Prof. P.R. Williams in the department of Multidisciplinary Nanotechnology Centre, in Swansea University, in candidature for the degree of Doctor of Philosophy. The material in this thesis is the original work of the author except where acknowledgement ot other authors is expressed.

Signed.

Date.....3/5/10.....

Oliver James Puckering

(Candidate)

Signed.....

Date.....

Prof. P.R. Williams

(Supervisor)

Acknowledgements

I would like to thank my supervisor Prof. Rhodi Williams and the School of Engineering for enabling me to undertake the research in this thesis, Matthew Lawrence for all the help and advice, and together with all the other volunteers, for the kind donations of blood and time.

Thanks also to Dr. Adrian Evans and the staff in the Accident and Emergency department of Morriston Hospital without whom the blood work could not have taken place.

Finally to my partner and my family, for your patience, support and belief.

Abstract

This thesis deals with assessment of effects on thrombus structure brought about by the addition of carbon nanoparticles to blood in vitro.

Chapter 1 outlines the development of the rheological discipline and discusses viscoelastic systems. Whole blood is a transient viscoelastic system. Methods of locating the point of this change, the gel point, are discussed and briefly evaluated.

In Chapter 2 the development of fractal analysis is investigated and the method by which a phase angle measured at the gel point can be converted into a fractal dimension is outlined.

Carbon nanoparticles are discussed in Chapter 3 along with their methods of generation and an outline of the research into any associated health effects which has been carried out.

The means by which the nanoparticles, both individually and in suspension, can be assessed are outlined in Chapter 4. Tests which were carried out to determine the best solvent for this work are outlined and the results discussed.

Chapter 5 concerns blood and the cardiovascular system. The means by which thrombus generation and removal occur are discussed together with the TEG and Sonoclot clinical systems used to analyse haemostasis.

Chapter 6 states the hypotheses to be investigated in this work.

In Chapter 7 the materials and methods for the production of suspensions, their inclusion into extracted whole blood and the measurements taken on the resulting blood sample are outlined.

Chapters 8 - 12 present the results from each of the nanoparticles investigated.

Chapter 13 presents the conclusions drawn from the comparison of the results and discussions in Chapters 8-12. The most important of these conclusions is the order of effect of the nanoparticles on the blood: MCOOH $\geq$ SCOOH $\geq$ LPMN $\geq$ LPSN $\geq$ DIESEL.

Contents

List of Figures

Chapter 1

Rheology and Gels

παντα ρέι

Everything Flows

From the writings of the philosopher Simplicius, commonly mis-attributed to Heraclitus

1.1 Rheology

As can be seen from the quote with which this chapter begins, elements of the science of Rheology can be traced back as far as Ancient Greece. The following section briefly outlines the historical development of the subject through the ages to the coining of it as a specific discipline by Bingham and Reiner in 1929 [1]. In fact, the term *Rheology* was coined in reference to the quote above.

The development of rheological studies will be broken down into five distinct sections according to the particular type of material investigated and time periods over which the developments took place, as shown in figure 1.1. Therefore it is sensible to begin with a look at *ideal* materials.

1.1.1 Ideal Materials

This section can immediately be split into two sections, solids and liquids. The solids shall be dealt with first. The two types of ideal solid materials are at opposite ends of the spectrum. On one hand we have the rigid solids and on the other, elastic solids.

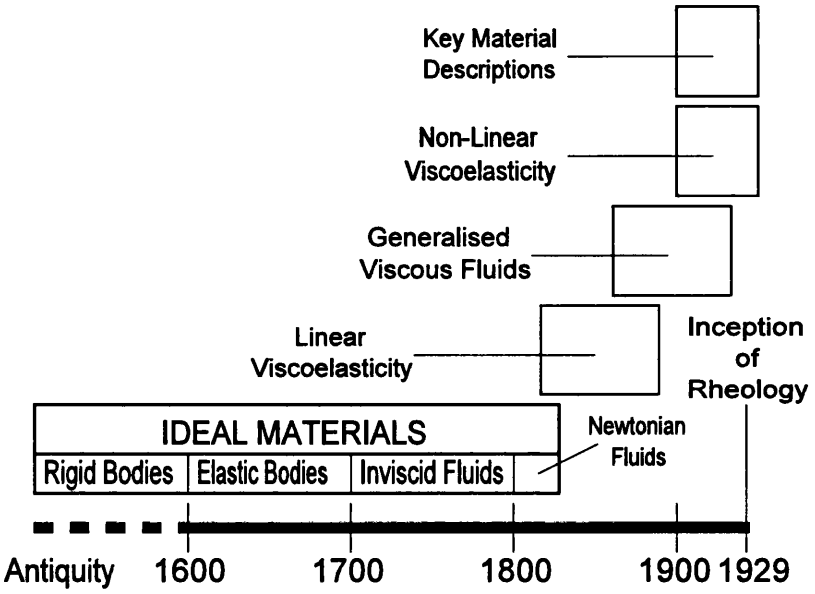

Figure 1.1: *An illustration of the key times of the developments of the science of rheology up to its official inception in 1929*

General mechanics is based upon the principles of Euclidean geometry such that it considers objects which do not deform. This is the oldest branch of mechanics and can trace its roots back to Archimedes (circa 250BC). The vast majority of the work in Newton's *Principia* [2]was concerned with the mechanics of rigid bodies.

Where the solids exhibit pure elastic behaviour, the governing rule was coined by Robert Hooke in 1678 [3].

'The power of any spring is in the same proportion with the tension thereof'

This can be written mathematically as:

$$\sigma \propto \gamma \tag{1.1}$$

where: σ is the applied stress and γ is the resultant strain. This is more commonly written as equation 1.2 and is known as Hooke's Law:

$$F \propto x \tag{1.2}$$

where F is the applied force and x is the corresponding extension observed in the spring. The constant of proportionality between the two variables is termed the spring constant, k, and is a property of the material under examination. This was identified as an intrinsic property of the material by Thomas Young in 1807 in his work on the elastic (known after as the Young's) modulus. The fundamental equations concerning small elastic deformations were laid down by Cauchy in 1827 [4], possible largely due to the work undertaken by Poisson, Navier and Coulomb [5].

The second set of ideal materials, the fluids, will now be discussed. Again, these fluids can be subdivided into two groups; Pascalian and Newtonian fluids.

The Pascalian fluids exhibit no resistance to flow. The statement by Pascal in 1663 equivalent to the pressure in a liquid being the same in all directions is the cornerstone of the field of hydrodynamics, a field dealing with the motion of fluids in which viscosity plays no part. This field was well developed in the early 19^{th} Century largely due to the work of Euler and Bernoulli in the mid 18^{th} Century.

The Newtonian fluids are so named following a definition by Newton in the previously mentioned masterpiece, *Principia*, in which he stated:

> 'The resistance which arises from the lack of slipperiness originating in a fluid - all things being equal - is proportional to the velocity by which the parts of the fluid are being separated from each other'

This can also be stated mathematically.

$$\sigma \propto \dot{\gamma} \tag{1.3}$$

In this case, the notation $\dot{\gamma}$, signifies the strain rate - the rate at which the parts of the fluid are separated such that the fluid exhibits continuous deformation: flow. This flow will continue to occur for as long as the force is applied, in comparison to the Hookean elastic solid which will deform a set amount, regardless of the timescale over which the force is applied as shown in figure 1.2.

In fact, the earliest recorded example of rheological application deals with the effects of viscosity. The ancient Egyptian Amenemhet (circa. 1600BC) is recorded as making a 7° correction in the angle of drainage in a water clock

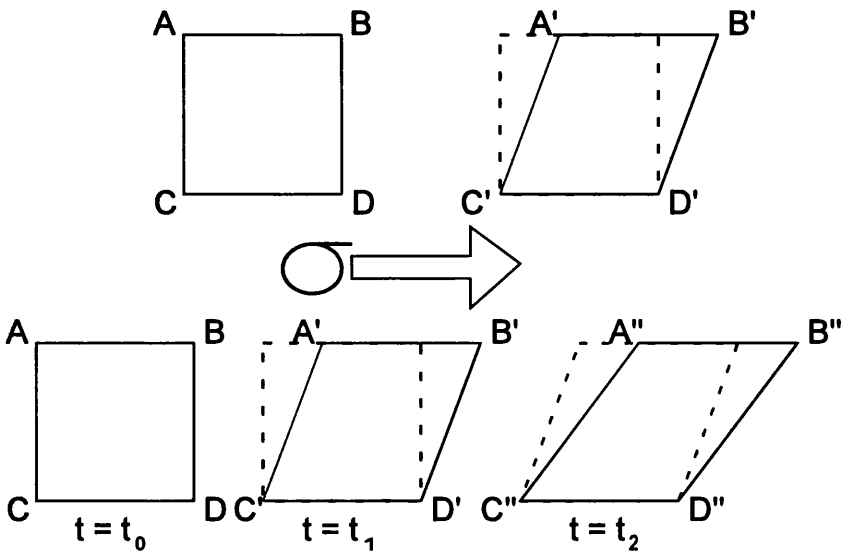

Figure 1.2: *Illustration of the Hookean (top) and the Newtonian (below) response to an applied stress.*

to account for the variation in viscosity with temperature. The temperature in Egypt can vary from 43°C during the day to 0°C at night.

There has been a massive body of work undertaken on Newtonian fluids, the most important aspects of which shall now be briefly covered.

The primary experiments on viscosity revolved around the pressure drop across a capillary tube. The seminal works by Hagen in 1839 [6] and Poiseuille in 1841 [7] were both empirical studies which resulted in the establishment of the proportionality of the flow rate to the pressure gradient and the radius raised to the fourth power.

Both Navier [8] and Stokes [9] undertook pioneering work on laws of motion for fluids with finite viscosities. While the Navier-Stokes combination provided a means by which, for example, a prediction of velocity distribution across cylindrical pipes, Stokes was unable to verify his work empirically. It was not until 1856 that another researcher, Weidemann [10], was able to show agreement between the prediction of Navier-Stokes and the data generated by Hagen-Poiseiulle.

1.1.2 Linear Viscoelasticity

Viscoelastic materials are those which exhibit both Hookean and Newtonian properties dependent on the timescale over which a force is applied. Viscoelasticity will be discussed in greater depth later in this chapter.

Prior to the rapid growth of the polymer industry, studies into viscoelasticity were focused on metallic behaviours of creep and relaxation. The first systematic study of viscoelastic behaviour in non metallic materials was undertaken on silk threads by Weber in 1835 [11]. (While this may seem a strange avenue to pursue, silk threads were widely used in the instrumentation of electromagnetism). In this way Weber was able to identify the stress relaxation phenomenon of viscoelasticity prior to the work undertaken by Stoke and Poiseuille.

In 1867, Maxwell [12] postulated the first-order differential equation which relates the shear stress to deformation and stress relaxation in a *fluid-like* viscoelastic material. This can be readily understood through the use of a model containing a spring and viscous damper in series as illustrated in figure 1.3. Interestingly it was Maxwell who came up with the definitions of the classical extremes of the Hookean solid and Newtonian fluid which enabled the study of materials in the region between the two.

> 'What is required to alter the form of a (soft) solid is sufficient force, and this, when applied, produces its effect at once. In the case of a viscous fluid, it is time which is required, and if enough time is given, the very smallest force will produce a sensible effect.'

This *process timescale* is now seen as critically important in the behaviour of viscoelastic materials.

If we now define the stress and strain components in the model in figure 1.3 thus:

$$\sigma_{Total} = \sigma_D + \sigma_S \tag{1.4}$$

$$\gamma_{Total} = \gamma_D + \gamma_S \tag{1.5}$$

Where the subscript S signifies the spring and the subscript D refers to the viscous damper. From equations 1.4 and 1.5 we get:

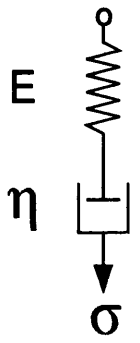

Figure 1.3: *The Maxwell model of a viscoelastic material.* ***E*** *is the elastic modulus of the spring and* η *is the coefficient of viscosity for the given material.* ***NB****: The spring and damper analogy for the Maxwell model was introduced by Thomson in 1902*

$$\frac{d\gamma_{Total}}{dt} = \frac{d\gamma_D}{dt} + \frac{d\gamma_S}{dt} = \frac{\sigma}{\eta} + \frac{1}{E}\frac{d\sigma}{dt} \tag{1.6}$$

As such it can be shown that the rates of change of stress and strain with respect to time are:

$$\frac{\dot{\sigma}}{E} + \frac{\sigma}{\eta} = \dot{\gamma} \tag{1.7}$$

However, the Maxwell models' ability to predict creep is limited. The introduction in 1874 of the Kelvin-Voigt model of viscoelasticity in a *solid-like* material went someway to address this. It is interesting to note as an aside, that the equations for this system were in fact introduced by Meyer, a rheologist from Poland and as such has an equal claim to that of Lord Kelvin and greater than that of Voigt. However, Meyer was embroiled in a dispute with Boltzmann which led to Meyer's discreditation.

The Kelvin-Voigt model is again much easier to comprehend through the use of the spring and viscous damper. In this instance they are connected in

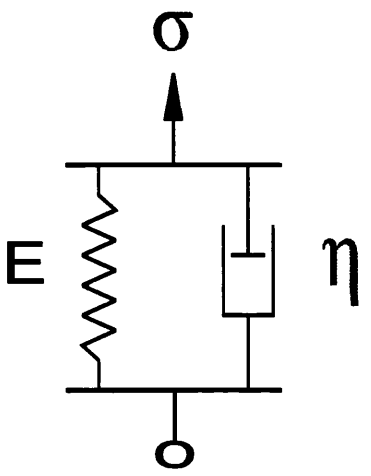

Figure 1.4: *The Kelvin-Voigt model illustrated using the spring and viscous damper.*

parallel as shown in figure 1.4. This results in both the spring and damper having identical strain components in response to the applied stress, while the total stress will now be the sum of the stresses in each component. Therefore equations 1.5 and 1.4 for the Maxwell model become:

$$\gamma_{Total} = \gamma_D = \gamma_S \tag{1.8}$$

$$\sigma_{Total} = \sigma_D + \sigma_S \tag{1.9}$$

These equations can then be used to obtain an equation for the rate of change of stress and strain with respect to time for the Kelvin-Voigt model.

$$\sigma(t) = E\gamma(t) + \eta\frac{d\gamma(t)}{dt} \tag{1.10}$$

Each of these models will be discussed in more depth later in this chapter.

One of the means by which a process can be defined as being linearly viscoelastic is by determining whether the function is separable in both creep and load, using a Volterra equation:

$$\sigma(t) = E_{inst-relax}\gamma(t) + \int_0^t F(t-t')\dot{\gamma}(t')dt' \tag{1.11}$$

or, in terms of strain

$$\gamma(t) = \frac{\sigma(t)}{E_{inst-creep}} + \int_0^t K(t-t')\dot{\sigma}(t')dt' \tag{1.12}$$

Where: *K(t)* is the creep function, *F(t)* is the relaxation function and $E_{inst-creep}$ and $E_{inst-relax}$ are the respective instantaneous elastic moduli.

The final important development to mention in this section concerns one of the scientist mentioned above, Boltzmann. The work of Weber in 1835 enabled Boltzmann to develop the *superposition principle* in 1878. This enabled him to arrive at a linear integration of viscoelasticity in three dimensions [13].

> 'The value of a characteristic function of a system is equal to the sum of all changes induced in the system by the driving functions which have been applied to it throughout its history.'

Superposition will also be dealt with further later in the chapter.

1.1.3 Viscous Fluids in General

One of the first pieces of experimental work on non-Newtonian fluid properties was underaken by Schwedoff in his studies of solutions of colloidal gelatin in 1890 [14]. His data indicated a non-linearity in the velocity profile and also required the consideration of a yield value in order that the results be accurately described. Viscosity was postulated to be a function of rate of shear by both Hess in 1910 [15] and Hatchek in 1913 [16], both of whose work was based on results analogous to those of Schwedoff. Following work on pitch by Trouton in 1904, in which they identified the need to take into account a small initial stress in order that the strain response be proportional, Bingham in 1922 [17] proposed his now famous *yield stress* in his descriptions of paint flow. These materials have since become known as Bingham plastics.

1.1.4 Non-linear Viscolelasticity

Many viscoelastic materials only exhibit linear behaviour within a certain range specific to the material under consideration. This is termed the *Linear Viscoelastic Range.*

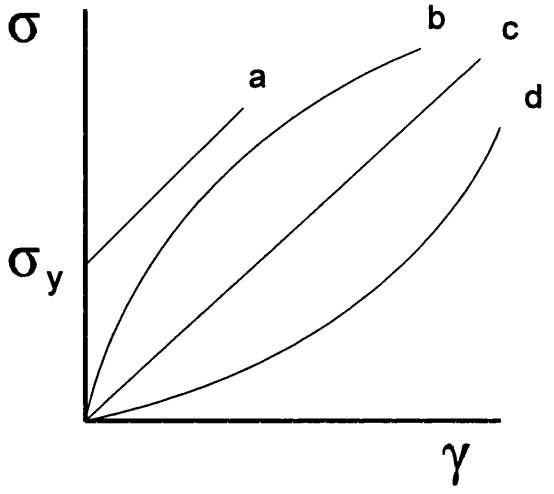

Figure 1.5: *The strain responses of various fluids to applied stress: a) Bingham plastic material with a yield stress, σ_y; b) A Thixotropic fluid; c) A Newtonian fluid; d) A Rheopexic fluid. (Fluids (b) and (d) are covered in later sections)*

Outside of this range the function in equation 1.12 is not separable into creep and load. The function will normally become inseparable due to large deformation of the material or if the material undergoes structural changes during the time over which the deformations occur. The early work was largely focussed on non-linear deformation in wires and so is not particularly relevant to this body of work.

1.1.5 The description of Key Materials

The important descriptions made prior to 1929 in terms of this thesis were those concerning polymers and suspensions. In the case of the former, the ability to define polymers and their formation is particularly critical.

The vast majority of the early work on polymers revolved around rubber and gutta percha due to the rapid expansion of the rubber industry.

The nature of suspensions is also of supreme importance as this is of direct relevance to blood. Blood can be viewed as a multicomponent colloidal suspension. The definition of colloidal dispersions as those comprising particles with diameters less than 1μm was made by Thomas Graham in the mid 18^{th} Century. This work was expanded by Einstein in 1906 [18] who developed an equation describing the effective viscosity in suspensions of less than 5%.

1.2 Viscoelasticity

The subject of viscoelasticity is of critical importance to the work in this thesis and shall now be discussed in more detail.

1.2.1 Response to Applied Stress or Strain

The strain responses representing the Maxwell and Kelvin-Voigt models outlined above will now be discussed. As described earlier, the process timescale is of critical importance in determining the nature of the measured response.

As can be seen from the dimensionless plots shown in figure 1.6, the responses to the application of a sudden force is markedly different between the Maxwell and Kelvin-Voigt models.

The Maxwell model experiences an immediate deformation limited by the elastic constant of the Hookean spring (figure 1.3). The stress in the system

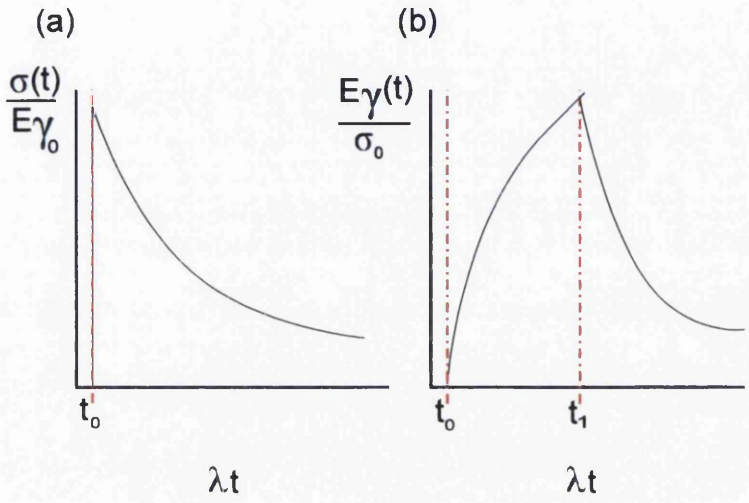

Figure 1.6: *Classic model responses to applied stress/strain: (a) Maxwell model, dimensionless stress against dimensionless time; (b) Kelvin-Voigt model, dimensionless strain against dimensionless time under constant stress.*

is then reduced as the process timescale increases by flow within the viscous damper. An important point to note here is that the viscous element of the system is unable to return to its original length and so a component of the deformation is irreversible. As the process timescale is increased, this irrecoverable deformation becomes increasingly dominant. This marks the Maxwell model as a viscoelastic fluid.

In comparison, the response of the Kelvin-Voigt model is deformation governed by the flow in the viscous damper, up to the limit imposed by the spring. If the stress is then suddenly released at time t_1, then the Kelvin-Voigt model will undergo a complete relaxation, it's speed governed by the viscous component. As all the deformation is reversible the Kelvin-Voigt model is a viscoelastic solid.

These two models are the extremes of viscoelastic material response. As such all viscoelastic materials will exhibit responses somewhere between these two. However, due to the dependence of the response upon the process timescale it can be difficult to accurately quantify a viscoelastic material through the application of a simple uni-directional stress or strain.

1.2.2 Oscillatory Stress Response and its Uses

In order to effectively study viscoelastic materials, dynamic measurement techniques are very useful. In these instances, either a small oscillatory stress or strain is applied. If the material is purely elastic the response will be completely in phase with the applied force, while if the material is a Newtonian fluid its' response will be 90° out of phase. All viscoelastic materials will have oscillatory shear responses somewhere between these two extremes, governed by whether they are elastically or viscously dominated.

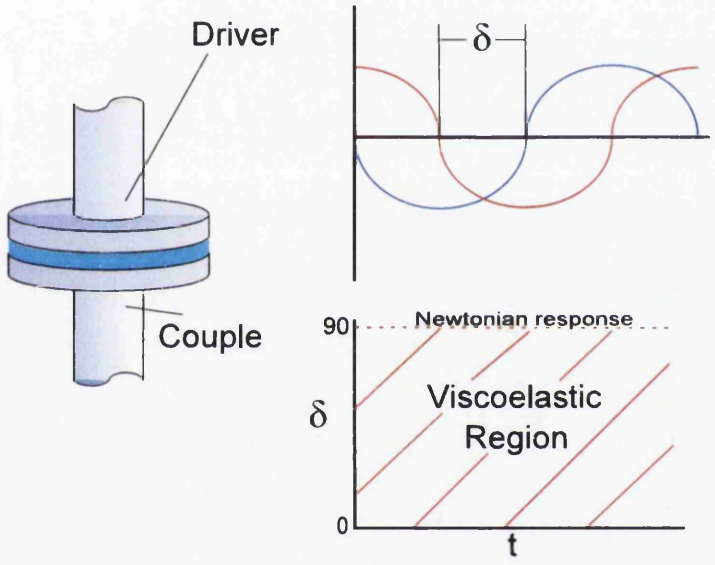

Figure 1.7: *Illustration of a simple plate-plate rheometrical device. The graphs on the right show: Top - The phase angle, δ, between the force applied by the driver and that measured by the couple as the response from the material: Bottom - The viscoelastic region of response as bounded by the Newtonian response at 90° and the Hookean at 0°.*

The relationship between the applied oscillatory stress and the resultant strain can be described using the *complex dynamic modulus*, G^*, through the following equation:

$$G^* = G' + G''i \tag{1.13}$$

Where G' and G'' are the storage and loss moduli respectively, defined as:

$$G' = \frac{\sigma_0}{\gamma_0} \cos \delta \tag{1.14}$$

$$G" = \frac{\sigma_0}{\gamma_0} \sin \delta \tag{1.15}$$

and

$$i^2 = -1 \tag{1.16}$$

thus

$$\frac{G''}{G'} = \tan \delta \tag{1.17}$$

Where: σ_0 is the amplitude of the stress, γ_0 is the amplitude of the strain and δ is the phase angle between them.

1.2.3 Linear Viscoelastic Range

In order that the theory of linear viscoelasticity proposed by Ferry in 1970 [19] may be invoked, the rheometrical measurements must be made within the specific linear viscoleastic range (LVR) of the material under investigation. Each measurement made outside of this range will be under a non-linear regime and thus will reveal a different behavioural aspect of the material.

When under dynamic testing systems such as oscillatory shear, the transition point between the linear and non-linear regimes is dependent upon the applied strain amplitude. This transition point is a characteristic of the material undergoing investigation, and is termed the critical strain, γ_c. Above this value the material will behave in a non-linear fashion. The linear viscoelastic response is therefore observed during low amplitude oscillation.

The above is of use when controlled-strain rheometrical techniques are to be used. In the event that a controlled stress rheometer is to be used, then the linear- non-linear transition will be governed by the critical stress, σ_c.

In order to determine the value of the critical stress or strain, the classical method is through the use of a stress or strain sweep respectively. The LVR is determined through analysis of the dynamic moduli defined earlier; G' and $G"$. Within the LVR, the dynamic moduli are independent of the magnitude of the applied stress or strain.

This method is not appropriate for use with systems which exhibit transient behaviour due to the fact that the dynamic moduli are then time-dependent. Location of the LVR therefore requires analysis of the response waveform measured at different levels of imposed stress or strain. This analysis is performed through the application of a single frequency of imposed stress or strain to the material under investigation. An appropriate fourier transform is then used to analyse the response waveform generated to determine linearity. If the test is the linear range, then the fourier analysis will result in a frequency spectrum with a clearly defined peak corresponding to the frequency of the test waveform applied. If the test occurs outside the linear range, the frequency spectrum will yield a distinct peak at the test frequency together with a number of additional peaks at harmonic frequencies.

1.2.4 Transient Materials

Transient viscoelastic materials are those which experience a change in structure, and as such a change in response, while under stress or strain. The material studied in this work, blood, exhibits transient behaviour and thus can be loosely described as a gelling system.

1.3 Gelling Systems

A gelling system is one which undergoes a structural, and thus behavioural, change from viscoelastic liquid to viscoelastic solid due to an external instigator, be it the addition of a chemical reagent, a change in temperature or the application of a particular stress or strain.

1.3.1 Types of Gel

Gels can be broadly categorised into a number of distinct groups: chemical gels, physical gels and colloidal gels. These groups are defined by the manner in which the gel is formed.

The formation of a chemical gel is characterised by gelation brought about through the formation of covalent chemical bonds between monomer functional groups. These bonds are highly stable and indeed can only be broken down by the addition of a suitable chemical agent, if at all. As such, these gels are termed *thermosetting.*

Physical gels are characterised by the formation of thermoreversible bonds such as Hydrogen bonding and Van der Walls interactions. Due to the fact

that these bonds can be broken by the application of heat, physical gels are termed *thermosoftening.*

1.3.2 Percolation Theory

The process of percolation was initially developed by Flory in 1941 [20] and Stockmayer in 1943 [21]. This process was used to describe the formation of large macromolecules within a system due to the reactions between small branching molecules.

The key concept behind percolation theory is the formation of a sample spanning network of chemically bonded molecules. The work of both Flory and Stockmayer was limited by the fact that all the theoretical development for their model of gelation was undertaken on a Bethe lattice, illustrated in figure 1.9.

Percolation Theory was further developed in 1957 to deal with fluid flow in random media. Rather than the direction and type of flow being defined by the fluid itself (a diffusion process), the randomness is defined by the media through which the flow occurs. If the medium is considered as a set of regular lattice points, then there can be two types of percolation. A *site* percolation considers the lattice vertices as the relevant entities for investigation, while a *bond* percolation process considers the lattice edges as important.

If the occupation of each site within the lattice is random and occurs with a probability, p, at low values of p (low concentration of fluid solution) the occupied sites are either isolated or form small clusters of 'nearest neighbour' sites.

As such, two occupied sites will belong to the same cluster if they are connected by a path of occupied nearest neighbour sites.

If the theory is applied to a viscoelastic gelling system, then at low values of p, the system will be a pre-gel fluid as no sample-spanning paths exist. At high values of p, the lattice is then traversed by paths connecting the sample edges and so the system will be a gel.

Therefore, a threshold concentration p_c must exist between low and high p values and is defined as the point at which, for the first time, a connection is made for one lattice edge to the other.

This is termed p_{cs} in the case of a site model and p_{cb} in the case of a bond

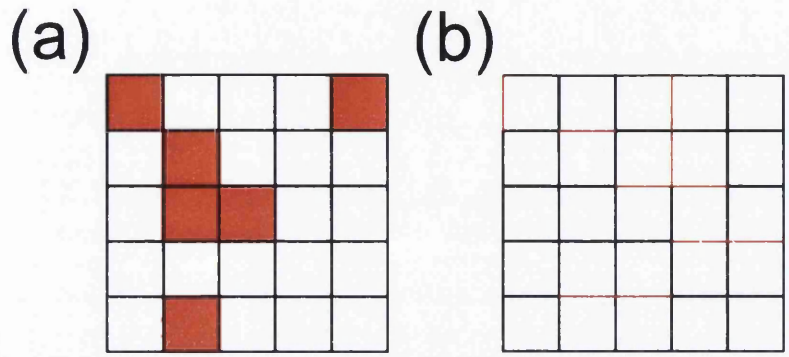

Figure 1.8: *Illustration of percolation types; (a) site percolation, (b) bond percolation.*

model. In general, $p_{cb} \leq p_c s$

The state in which the solution will be is dependent upon the timescale over which the reaction takes place. If this process time is shorter than the characteristic gel time, t_g, for the material then a number of finite branched polymer clusters within the solution, usually termed a 'sol'. This will be increasingly viscous as the process time approaches t_g. Once the process time exceeds t_g, then a solid, sample spanning network is formed. At this point the material is termed a 'gel'. The time at which the first sample spanning network appears during the transition from 'sol' to 'gel' is known as the Gel Point.

1.3.3 Lattice formation

The type of lattice formed will depend upon the coordination number, which defines the number of bonds made at a given vertice. All of the examples given above are shown as two-dimensional. It can be noted also that the Bethe lattice can be split into three symmetrical branches, each of which can be defined by the Caylee Tree. This states that from the end of each individual section, two more shall sprout.

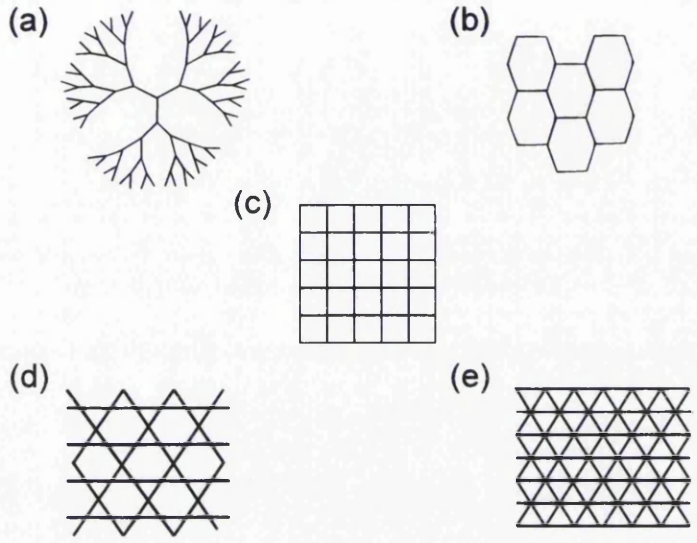

Figure 1.9: *Illustration of regular lattices with increasing coordination numbers; (a) Bethe Lattice (Z = 3), (b) Honeycomb Lattice (Z = 3), (c) Square Lattice (Z = 4), (d) Kagomé Lattice (Z = 6), (e) Triangular Lattice (Z = 6).*

The addition of more layers of lattice to the standard square lattice will enable the formation of either a diamond lattice or a standard cubic depending on the orientation of the extra lattice 'sheets'. Another diamond lattice can be formed from the addition of further sheets to the triangular lattice.

1.3.4 De Gennes' Ant and the Random Walk

The idea for comparing the manner in which bonds form in a percolation network to a person taking a random walk was first suggested by Brandt in 1975. In this instance the walker is placed on an occupied site within the network. The walker then takes a step to one of the unoccupied nearest neighbour sites to its current position. If it is assumed that all bonds have the same diffusion conductance, then the selection of the site to which the walker will go is dependent upon the coordination number of the lattice. Brandt used this idea to study diffusion of noble gases through glasses when modeled by a percolation network.

In 1976 the idea was expanded upon and popularised by de Gennes [22]

who compared the movement of the random walker to that of an ant in labyrinth.

The phenomenon of the random walk as explained by de Gennes ant has been modeled by a simple program developed by Langton, which utilises a square grid and an 'ant'. The grid begins with every square white. Simple rules control the motion of the ant: it always moves one square at a time, if it encounters a white square the square becomes black and the ant turns to the right, if it encounters a black square the square becomes white and the ant turns to the left.

Using this program, three distinct phases of order can be seen as the system develops:

1. Simplicity

   During the first two to three hundred moves, the ant creates tiny independent patterns which are very simple and often symmetric.

2. Chaos

   In this phase of the evolution of the system, the patterns degenerate into a large irregular patch of black and white squares without any discernable structure.

3. Emergent Order

   Finally, the ant locks into a particular kind of repetitive behaviour and builds a 'highway' over a cycle of 104 steps, at the end of which the ant has moved out two squares diagonally. The shape and colours along the edge of this highway are now the same as when the cycle began so the highway will now be rebuilt forever.

1.3.5 Backbone Formation

The backbone of any sample spanning network is that part which directly binds one edge to the other, such that transport can occur along it. For example, current in the case of an electrical network or material flow in the case of a diffusion process. Indeed, transport can only occur along the backbone as the rest of the structure consists of dead ends and loops which do not carry any flow. The structure of this backbone will define the transport properties of the network due to its tortuosity.

The formation of the backbone during the point at which the percolation threshold p_c is reached is very important. Work by Stanley [23] showed that the bonds in the backbone can be split into two distinct groups; those within the multiply connected backbone sections, and those termed *red* bonds. The cutting of any of these red bonds would result in the severing of the backbone into two distinct parts. They are termed red due to the fact that Stanley was working with electrical systems and these bonds carried all of the current causing them to become very hot.

1.4 Sol-Gel Transition and Attempts to Measure the Gel Point

Once the percolation threshold has been reached and a sample spanning network formed, the material exhibits increasingly Hookean behaviour with respect to its response to any applied force. As discussed earlier, the point at which the material changes from sol to gel is defined as the Gel Point. Identification and characterisation of the Gel Point, both in terms of time and with reference to the resultant gel structure has required a large degree of investigation. There have been a number of rheological methods put forward, involving both steady and dynamic techniques.

The steady state measurements have been used to investigate the changes in the zero-shear viscosity, η_0, as the material progresses towards the Gel Point. This is due to the fact that at the Gel Point the value for η_0 will tend towards infinity, coupled with a tend towards zero observed in the residual shear rigidity modulus, G_e such that at the Gel Point:

$$\eta \rightarrow \infty \tag{1.18}$$

$$G_e \rightarrow 0 \tag{1.19}$$

This is due to the conversion of the isolated molecular-scale clusters into a sample spanning network at the Gel Point.

In terms of dynamic investigation, it was postulated that at the Gel Point the dynamic moduli, G' and G'', would be equal. Thus the Gel Point could be determined by this 'cross-over'. From the definition given in equation 1.17 the Gel Point occurs where $\tan\delta = 1$, or at a phase angle, δ, of 45°.

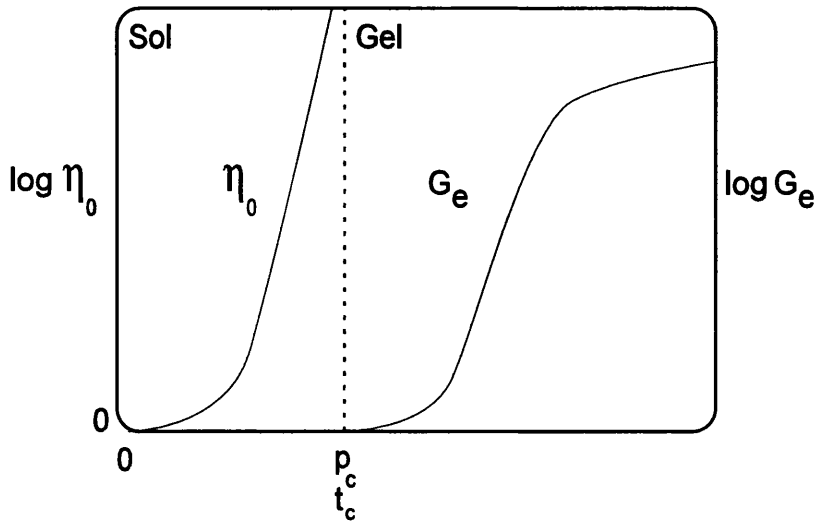

Figure 1.10: *Development of mechanical properties within a material as it undergoes gelation. The Gel Point is here determined by the critical values of reaction time, t_c, and the conversion, p_c*

Two other methods involved the linking of the Gel Point directly to changes in the values of G' and G". It was suggested that the rheological definition of the Gel Point occurs with the first development in the storage modulus, G'. However, this point is often indistinguishable from process noise when in practical use. This method therefore leads to a very rough approximation of the Gel Point as occurring at the point at which G'≥Experimental Noise. The second of these methods defined the Gel Point as the point at which G" is at a maximum. This is based on an analogue of the Kronig-Kramers equation which connects the real and imaginary components of any complex function. While a maximum G" value has been measured in gelatin immediately following an inferred Gel Point, the maximum is often drowned in experimental noise.

The most widely accepted method for the rheological determination of the Gel Point is based upon the rigorous work undertaken on polymer gels by Winter and Chambon in 1986 [24]. They characterised the transition of the material from sol to gel as exhibiting a power-law behaviour of G_t the linear, time-dependent shear stress relaxation modulus, such that at the Gel Point:

$$G(t) = St^{\alpha} \tag{1.20}$$

Where: S is the gel strength of the three dimension network formed at the Gel Point and α is the stress relaxation exponent.

This equation was developed from the equation describing the extra stress at constant density in any viscoelastic material:

$$\stackrel{\tau}{=}(t) = \int_{-\infty}^{t} G(t-t') \stackrel{\dot{\gamma}}{=}(t')dt' \tag{1.21}$$

Introducing the kinematics of oscillatory shear into the above equation allows analysis of the dynamic moduli:

$$G'(\omega) = \omega \int_{0}^{\infty} G(t)sin(\omega t)dt \tag{1.22}$$

$$G"(\omega) = \omega \int_{0}^{\infty} G(t)cos(\omega t)dt \tag{1.23}$$

In order for equations 1.22 and 1.23 to achieve congruency they must be equal and proportional to $\omega^{1/2}$. Fourier transforms were then used to obtain equation 1.20.

G(t) is calculated using a preset shear strain, γ_0, and the stress relaxation function, τ(t).

$$G(t) = \frac{\tau(t)}{\gamma_0} \tag{1.24}$$

Winter and Chambon demonstrated that their gel definition fulfilled the criteria for the Gel Point outlined by Flory in 1953 [25]. They followed this with work on gels of both balanced and unbalanced stoichiometry, and showed that their definition was applicable to both cases.

Their definition shows that the response of the dynamic moduli to an imposed oscillatory shear stress or strain is dependent upon the frequency of oscillation when the material is within the linear viscoelastic range. This allowed them to characterise the critical gel at the Gel Point as:

$$G'(\omega), G''(\omega) \propto \omega^{\alpha} \tag{1.25}$$

From equation 1.17:

$$tan\delta(\omega) = \frac{"(\omega)}{G'(\omega)} \tag{1.26}$$

From equations 1.25 and 1.26, it can be seen that at the Gel Point, the phase angle, δ, is frequency independent. This thereby enables the Gel Point to be characterised in terms of the gel equation given in equation 1.20.

Following this work, Winter [26] assessed the validity of the definition suggested by Tung et al[27] as outlined earlier. It was found that the location of the Gel Point only coincided with the G'-G" crossover when the stress relaxation modulus, α is equal to 0.5. The Gel Point occurs prior to the crossover if $\alpha<0.5$, and after the cross over if $\alpha>0.5$.

1.5 Rheological Techniques

1.5.1 Harmonic Frequency Phase Angle Response

The basis for this method is the speed at which different frequencies travel through solids and liquids: lower frequencies travel faster through solid materials, while higher frequencies travel faster through liquids.

As such the method involves the application of a base frequency and a number of harmonics (within the LVR) to the system under investigation. The materials' response to the applied frequencies will generate a different pattern of phase angles pre-gelling to the response pattern perceived when the same set of frequencies is applied to the system post gel.

The difference in the magnitude of the phase angle responses is due to the materials' response being dominated by the viscous and elastic components of the forces during the liquid and solid states respectively. The frequency response inversion enables the identification of the transitional point between the two states: the Gel Point, as discussed above.

1.5.2 Fourier Transform Mechanical Spectroscopy

However the above set of data can be time consuming to collect if the frequencies are applied and analysed independently. Completely individual frequency application is only possible when the gelation in the sample can be completely reversed and then initiated once again.

In order to facilitate faster application of the frequencies, and thereby a reduction in the time required for the measurements to be completed, Boltzmann's superposition principle which states that within the linear viscoelastic range the stress responses to successive strains are additive as are

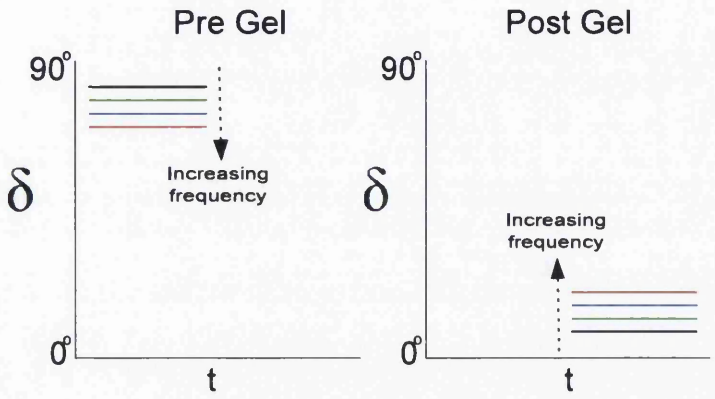

Figure 1.11: *The phase angle, δ response patterns observed pre- and post-gelation to a base frequency and a set of harmonics*

the strain responses to successive stresses. This allows for the combination of the base frequency waveform and the harmonics into a single composite waveform through fourier transform methods as shown in figure 1.12. The response waveform can then be separated into its component frequency responses through fourier transformation.

However, it was found to be very difficult to get good data from experiments on blood using this method. As such frequency sweep experiments were required. These procedures are outlined in the Materials and Methods chapter later in this thesis.

1.5.3 Increasing Sensitivity

Initial trials for this work were carried out on an ARES rheometer using a bob and cup geometry with a 1mm gap so as to replicate the geometry of the TEG machine. However, it was found that this set up was not sufficiently sensitive in Gel Point detection. The same geometry was trialled on an AR G2 rheometer with corresponding sensitivity issues. As such it was decided to use a double-gap geometry as outlined in figure 1.13.

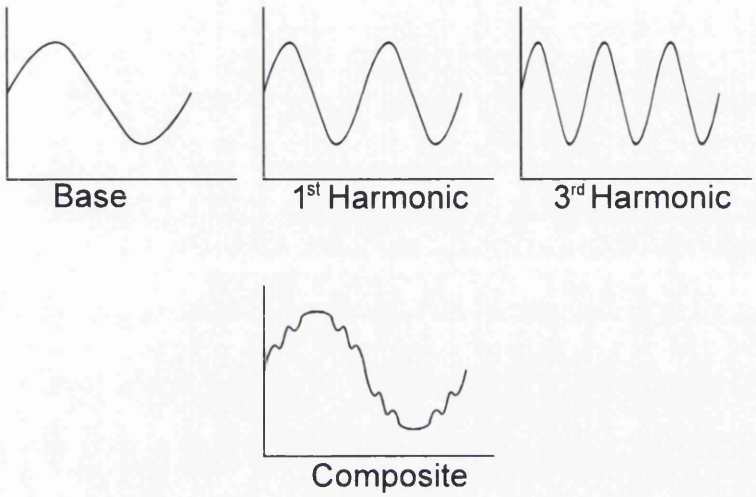

Figure 1.12: *Composite waveform created from the superposition of base and harmonic frequency components*

1.6 Nomenclature

σ	stress
σ_c	critical stress
σ_y	yield stress
γ	strain
$\dot{\gamma}$	strain rate
F	applied force
x	extension
k	spring constant
E	elastic modulus
η	coefficient of viscosity
η_0	zero shear viscosity
K(t)	creep function
f(t)	relaxation function
δ	phase angle between applied force and response
G'	storage modulus
G"	loss modulus
G*	complex modulus
G_e	shear rigidity modulus
p	probability
p_c	threshold concentration
p_{cb}	bond threshold concentration
p_{cs}	site threshold concentration
Z	co-ordination number
t	time
t_g	gel time
t_c	critical (reaction) time
S	gel strength

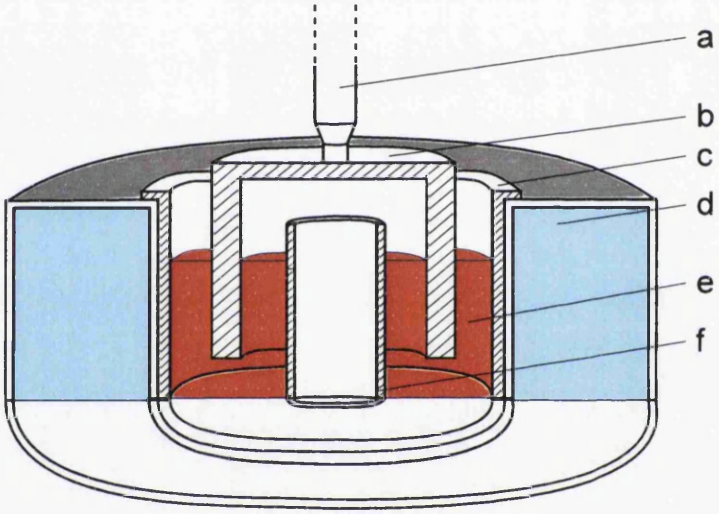

Figure 1.13: *Cutaway diagram of double gap concentric cylinder geometry. Labeled parts as follows: a - suspending rod mounted on an air bearing, b - detachable geometry, c - removable cup, d - temperature controlled water bath, e - blood sample, f - internal cylinder*

Chapter 2

Fractal geometry as a tool for structural analysis

The existence of these patterns challenges us . . . to investigate the morphology of the amorphous.

Benoit Mandelbrot, The Fractal Geometry of Nature, 1982.

2.1 Background

The worth of fractal geometry comes from the fact that it enables the characterisation and therefore comparison of structures which are scale-invariant and as such lie beyond the realm of standard Euclidean geometrical concepts. The term fractal was coined by Mandelbrot in 1975 while working on iterative processes for IBM [28]. It comes from the Greek *fractus* meaning broken or fractured.

It is to the principles of Euclidean geometry we refer when looking at the manner in which the volume, for regular objects such as a cube, changes with respect to length of the sides. In this instance, a doubling of the length of the sides of the cube would result in a fourfold increase in the area of each face, while the volume increases eightfold. The standard integer dimensions, d, (1,2 and 3) can be used to relate the way in which the mass, M, of the object alters as the linear size L, is changed, as long as certain conditions are met by the system such as constant density. In this instance, the dimension is characteristic. For example, if the value of d is 1 then the object is a line (thickness is taken to be infinitesimally small such that the only dimension is length), if d is equal to 2 then the object is a square, while if d is 3 then the object is a cube.

If a smaller part of the system is then studied, with a length, aL, such that $a \leq 1$ then an alteration in a will result in a change in M proportional to a^d.

$$M(aL) = a^d M(L) \tag{2.1}$$

However, scale invariant systems cannot be characterised by integer dimensions. The term scale-invariant means that the system has no characteristic length scale. A classic example of this is an overhead view of a coastline. A number of images of the coastline at different scales presented together without a scale reference will be relatively indistinguishable. A wide number of systems can be identified which possess fractal nature, for example biological structures as diverse as the Romanesco cabbage and the mammalian cardiovascular system. The examples of fractal expansion presented in figure 2.2 are constructed using set theory.

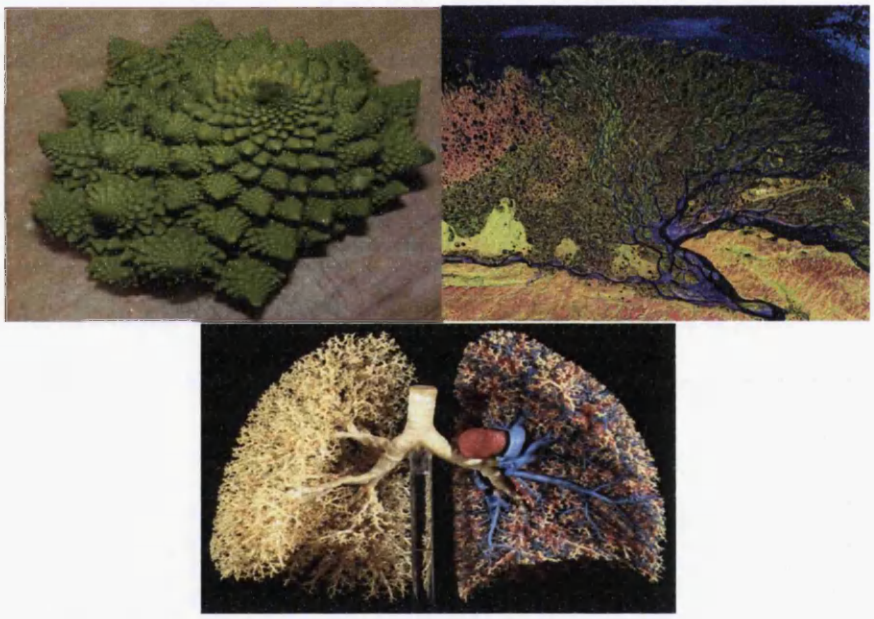

Figure 2.1: *Examples of natural fractal structures. Top row: The fractal cabbage chou Romanesco, and the Lena river delta. Bottom row; the fractal structure of the vascular and bronchial networks in the lung*

2.2 Set Theory in Brief

Before fractal systems can be looked at in depth, a brief introduction to set notation must be made.

The following definition of a set was made by Georg Cantor:

> By a set we understand any collection M of definite, distinct objects m of our perception or our thought (which will be called elements of m) into a whole.

As such, some examples of sets are: the Z set of all whole numbers (integers)and the sets Q, R and C of all rational, all real and all complex numbers respectively. Other sets can then be defined at will. Consider the words: set, collection and aggregate as synonymous in this instance. The elements of a set may be termed its members. If A is a set and if an object a is an element of A this can be written as;

$$a \in A \tag{2.2}$$

This symbolism means *a belongs to A*, while if a is not a member of A then this is written as;

$$a \notin A \tag{2.3}$$

Sets can be described by listing their members between pairs of curly parenthesis '{}' although sets containing an infinite number of members are clearly impossible to describe in this way. On such occasions it is possible to write $x : P(x)$ where P is a property which characterises only those elements of the set in question.

If A and B are both sets and if each element of A belongs to the set B then it can be said that *A is a subset of B* or *B contains A*. This can be written as:

$$A \subseteq B \tag{2.4}$$

Given the above, if we know that B contains elements not in A then this must be written as:

$$A \subset B \tag{2.5}$$

This last term is the most important for the fractal structures presented in figure 2.2 as it allows them to be described mathematically.

For example, the mathematical description of the Sierpinski Triangle presented below is as follows. Starting with a triangle with vertices (0,0) (1,0) (0,10) call it T_0, another three edges are included in the form of a middle triangle to get T_1. The process is then repeated in the three outer triangles thus created to get T_2. The limiting case of this expansion is the Sierpinski Triangle.

$$T_0 \subset T_1 \subset T_2 \subset T_3 \ldots \subset T_n \ldots \tag{2.6}$$

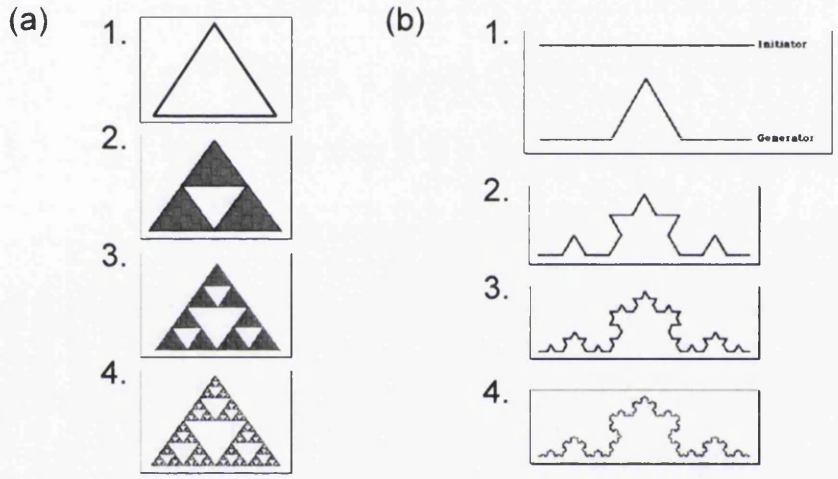

Figure 2.2: *Examples of Fractal Expansion; (a) Sierpinski Triangle, (b) Koch Curve*

The Koch curve presented above is perhaps one of the most famous mathematical fractals [29]. Both the Koch curve and the Sierpinski triangle are examples of deterministic fractals, systems which can modeled using computer algorithms. A comparison between the curve and the cube discussed above can now be undertaken using equation 2.1. Each step of the Koch curve iteration results in an increase in the length of the structure by 4/3. If a smaller segment of the structure is now considered in the same manner as above, a 1/4 decrease in the mass of the structure will be caused by a decrease in the segments' linear size of $a = 1/3$, such that:

$$M\left(\frac{1}{6}L\right) = \frac{1}{8}M(L) \tag{2.7}$$

In order that both equations 2.1 and 2.7 can be satisfied is through the use of non-integer fractal dimensions. The initial equation must now be altered to enable the inclusion of the fractal dimension thus:

$$M(aL) = a^{d_f} M(L) \tag{2.8}$$

Such that

$$M(L) \propto L^{d_f} \tag{2.9}$$

A return to the Euclidean geometrical concepts can be used in order to enable an instinctive evaluation of fractal structures. Again considering a standard 3-dimensional cube, if a cube of side b is expanded by a factor L then the original cube may be fitted into the resulting larger cube L^d times, where, d, is the dimension such that:

$$d = \frac{log(L^d)}{log(L)} \tag{2.10}$$

This then enables the assessment of the fractal dimension of the Koch curve. If the generator structure as shown in figure 2.2 is considered it can be seen that it is composed of a single cluster of 4 lines. The next iteration is composed of 4 clusters, each of which contains 4 lines, giving a total cluster size of 16 lines. The third iteration contains 16 clusters of 4 lines, giving a total cluster size of 64 lines, 4 times the number in the last iteration. As such it can be seen that for each iteration the number of lines in the total cluster increases by a factor of 4, while the maximum length increases by a factor of 3. If the iterations are continued to the N^{th} degree, then the number of lines will be equal to 4^N while the length will be equal to 3^N. It can therefore be stated that the Koch curve possesses a hierarchical structure. From the discussion above and with reference to 2.2, following the expansion of the curve by a factor of 3, 4 replicas of the original curve will be required to cover the new structure. Hence, the fractal dimension can be calculated as below:

$$d_f = \frac{log4}{log3} \approx 1.26 \tag{2.11}$$

In comparison,the fractal dimension of the Sierpinski triangle is;

$$d_f = \frac{log3}{log2} \approx 1.58 \tag{2.12}$$

Structures of a fractal nature are typically low density. The growth in the molecular weight of the fractal as the length is increased is smaller for

structures with a low fractal dimension than structures with high fractal dimension values.

2.3 Random Fractals

The method above, however, is only applicable to randomly generated fractals over a limited range of iterations. The fractals such as those used to mimic natural biological systems such as the cardiovascular system due to the fact that the structures cannot be directly mapped onto themselves following expansion or contraction outside of these upper and lower limits.

A method of statistical evaluation of self-similarity is therefore required. Two methods which enable the calculation of a statistical self-similarity average on fractal images are box-counting and the sandbox method.

2.3.1 Box-counting

The box-counting method utilises a rectangular grid consisting of N_1 squares which can be overlayed upon the fractal structure. The number of grid squares which are required to completely cover the structure, $S(N_1)$, can then be calculated. The size of the squares which make up the grid is then progressively reduced and the number of grid squares required to cover the structure at each iteration of the grid is then noted, $S(N_1)$,$S(N_2$, *etc.* $S(N_1)$ can be scaled with d_f such that:

$$S(N)\ N^{-d_f} \tag{2.13}$$

This enables the use of a plot of log[S(N)] against log[1/N], which will generate an asymptotic slope at d_f for large N. The minimum size of the squares which can be used in this method are limited to those which are greater than the size of the pixels which make up the image of the structure under investigation. This method is illustrated in figure 2.3.

2.3.2 Sandbox method

This method, shown in figure 2.4, utilises n circles of set radii, $r_1<r_2<\ldots,r_n$, placed over a single site on the fractal image. In order to enable collection an adequate level of data for statistical evaluation, a number of origin points must be used. The number of pixels, $M_j(R_i)$ where $j=2,3,\ldots$ within each of the circles is then assessed. The number of pixels around each point of origin can be averaged using the following formula:

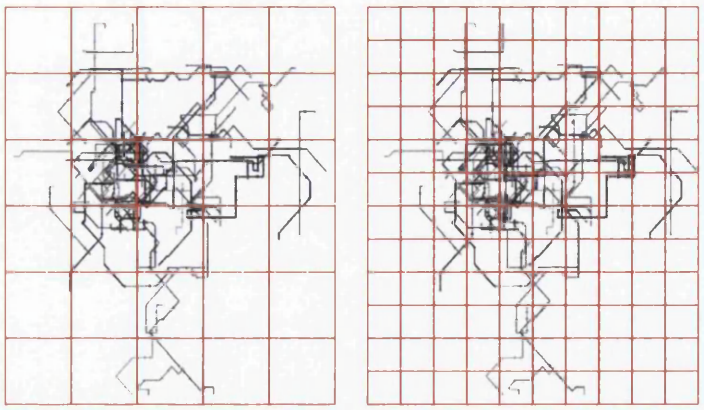

Figure 2.3: *Iterations of the box counting method for fractal dimension assessment, left to right: Using an N_1 grid; next iterative step, an N_2 grid.*

$$M(R_j) = \frac{1}{M} \sum_{j=1}^{m} M_j(R_i) \tag{2.14}$$

When using the above method, a plot of log[M(R_i)] against log[R_i] for large values of will give a slope of d_f.

2.4 Fractal models of gel network structures

The relationship between the relaxation exponent, α, as defined in Chapter 1.6, and the fractal dimension, d_f, has been investigated in terms of various theories concerning both cluster growth and gelation. The importance of this work in understanding the structural nature of the gel network is shown in this quote taken from the work of Martin [30].

> . . . the incipient gel, that fluid formed just at the sol-gel transition, is a viscoelastic intermediate between the liquid and solid state and a paradigm of fractal structure and fractal time.

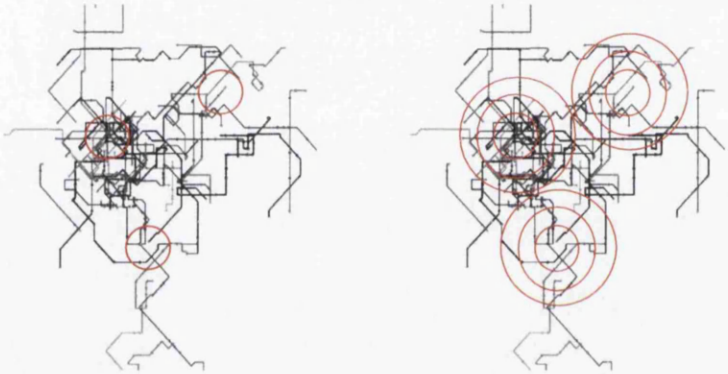

Figure 2.4: *Iterations of the sandbox method for fractal dimension assessment, left to right: Using circles of radius R_1 ; following two iterative steps, including circles of radius R_2 and R_3.*

2.5 Aggregation Models

The first of the aggregation models to be discussed here is the Smoluchowski Method [31], shown in equation 2.15. This theoretical approach to the modeling of gelation as an aggregation process is based upon the kinetic rate equation of Doi and Edwards [32]. The method utilises a reaction rate, K_{ij} which is used to determine the probability of a successful collision between the monomers (labeled i and j) extant in the system. The combination of these monomers results in the formation of m-mers. The equation expresses the rate of formation of $N(m)$. The right hand side of the equation can be readily split into two distinct sections: the first section is concerned with the creation of the m-mers, while the second section deals with their annihilation.

$$\frac{dN(m)}{dt} = \frac{1}{2}\sum_{i+j=m} N(i)K_{ij}N(j) - N(m)\sum_{j=1}^{\infty} K_{ij}Nj \qquad (2.15)$$

While this method is able to provide some level of qualitative analysis through the use of a mean-field description it is hindered by the difficulty in the determination of the form of the reaction kernel and its inability to predict the structure of the resulting cluster in part due to a number of underlying assumptions such as the use of a spatial average to represent the concentration of clusters with a given mass, and that the reaction rate between any two clusters is always the same.

2.5.1 Diffusion Limited Aggregation

This model for gelation involves the growth of a sample spanning cluster from a single seed within the middle of a lattice. Subsequent particles are released in turn from a random point located at a large radius from the seed point such that $r=r_{max}$. This particle proceeds upon a random trajectory (with a path possibly defined using the Langton - de Gennes ant defined in Chapter 1.6). If the introduced particles' trajectory is such that it approaches a point directly adjacent to the seed then the two are joined, in contrast, if the trajectory takes the particle on a course that is divergent from the seed to such an extent that a boundary $r \gg r_{max}$ then the particle is considered to be destroyed. In this way a particle is prevented from continuing on its path *ad infinatum*. Only once a particle has either joined with the seed at the origin or been destroyed is the next particle introduced into the lattice. This is illustrated in figure 2.5.

This method is not confined solely to standard square lattices, work has also been carried out a number of off-lattices such as the triangular and hexag-

onal which have been shown to generate more realistic structures. Bunde and Havlin [33] have published fractal dimensions for structures generated on off-lattices: where d=2, $d_f \cong 1.71$, while for d=3, $d_f \cong 2.4$.

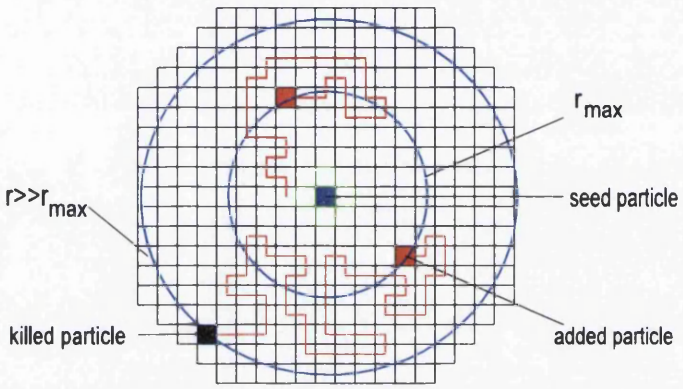

Figure 2.5: *An illustration of diffusion limited aggregation on a square lattice.*

2.5.2 Diffusion Limited Cluster Aggregation

In this case, the growth site for the fractal structure is not unique. When two particles come into contact, a cluster is formed. This cluster is not spatially fixed and so is able to diffuse throughout the lattice. This enables a wide variety of cluster sizes to be formed early on in the process. However, as the timescale increases, the number of clusters reduces as the clusters increase in size. At this point random branches begin to appear within the larger clusters. This continues until a single macroscopic structure is formed. DLCA results in much looser structures than simple DLA, with a $d_f \cong 1.4$ when d=2 and a $d_f \cong 1.8$ when d=3.

2.5.3 Reaction Limited Cluster Aggregation

While the two aggregation models described above assume that all contacts between particle and cluster or cluster and cluster result in a successful bond, a Reaction Limited aggregation allows for the possibility that a collision

will not result in a bond. This is assessed through the use of a stickiness coefficient, ξ, set between 0 and 1. This is used to decide whether or not a particle sticks to a cluster through the use of a random number generator. When the particle reaches one of the nearest neighbour sites on the lattice to the existing cluster, a random number between 0 and 1 is generated. If the number is greater than the stickiness coefficient then the particle sticks, if it is less then it continues to move. As the value of ξ approaches zero the likelihood that a given particle will stick when it reaches an adjacent site to the cluster becomes greater, leading to the formation of increasingly dense structures.

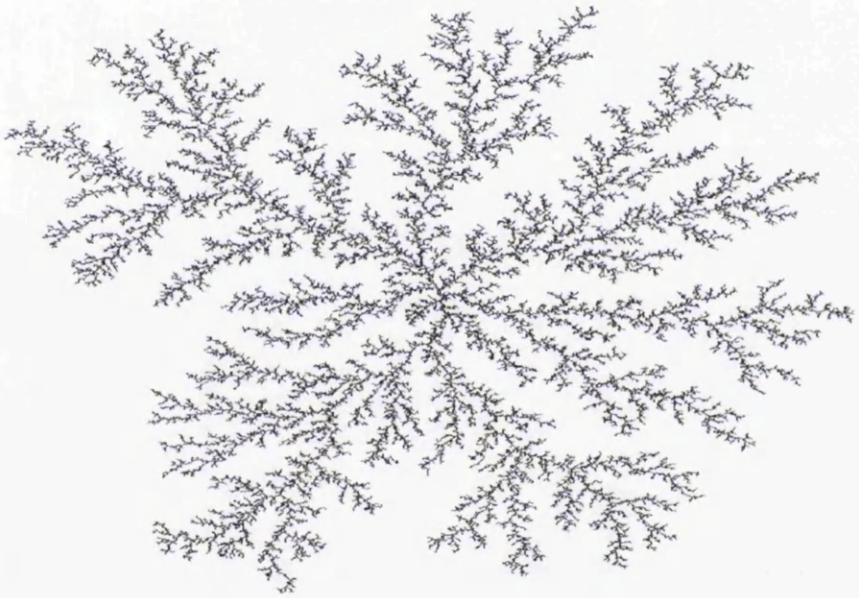

Figure 2.6: *An on-lattice fractal structure grown using RLA with a ξ value of 1.*

This sticking coefficient will also affect the rate at which the fractal structure is formed, and this has an impact on the nature of the structure. The faster the process of aggregation, the lower the fractal dimension of the resulting structure. It has been shown that the cluster radius in a reaction limited aggregation model follows an exponential growth curve and as such the fractal dimension values are higher than those found with diffusion limited aggregation, giving a $d_f \cong 1.56$ when d=2 and $d_f \cong 2$ when d=3

2.5.4 Mean Field and Percolation Theory

Percolation Theory was discussed in detail in the previous chapter and so only merits further mention in terms of its use in the development of fractal dimension assessment. The theory predicts power-law behaviour for the development of the molecular weight, M_w, and the radius, R_z of the clusters thus:

$$M_w \propto \epsilon^{-k} \tag{2.16}$$

$$R_z \propto \epsilon^{-\upsilon} \tag{2.17}$$

where:

$$\epsilon = |p - p_c| \tag{2.18}$$

The variables p and p_c were defined in the previous chapter. The theory predicts that the exponents are υ=0.5 and k=1. The theory has also been used to develop predictions for the changes in the dynamic viscoelastic properties η_0 and G_e which show that the viscosity grows logarithmically at the Gel Point:

$$\eta_0 \propto \epsilon^{-s} \qquad p < p_c \tag{2.19}$$

$$G_e \propto \epsilon^{z} \qquad p > p_c \tag{2.20}$$

Given that z=3 and s=0. Both z and s can be related to the stress relaxation component, α, as defined in the previous chapter through the following equation:

$$\alpha = \frac{z}{z+s} \tag{2.21}$$

As such, this gives a value for α of 1 from the s and z values stated above which are derived from the classic mean-field Flory-Stockmayer theory. However, this was found to predict non-physical results for branched polymers and so was developed into percolation by De Gennes and others as discussed in the last chapter.

Percolation theory predicts different theoretical values for the various exponents, dependent upon the structural model being considered. The Rouse dynamic model [34] considers the structure as a series of spheres (representing mechanical drag due to the friction factor) linked by springlike chains (representing Gaussian entropy).

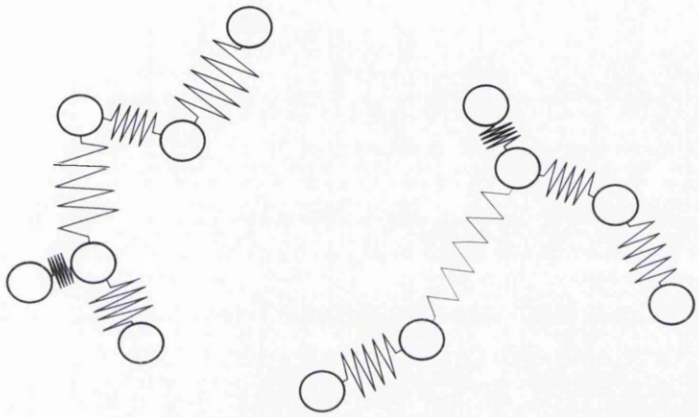

Figure 2.7: *Illustration of polymer chains as viewed with the Rouse dynamic model*

Using this model, together with hydrodynamic screening effects and rigid chains, enabled Muthukumar [35] to relate d_f and α by:

$$\alpha = \frac{d}{d_f + 2} \tag{2.22}$$

This was then developed to consider a mono-disperse system with flexible chains:

$$\alpha = \frac{d_f}{d_f + 2} \tag{2.23}$$

And finally to consider a poly-disperse system with complete hydrodynamic screening:

$$\alpha = \frac{d(d + 2 - 2d_f)}{2(d + 2 - d_f)} \tag{2.24}$$

Where d is the dimension of the system, in this case 3. Therefore, equation 2.24 becomes:

$$\alpha = \frac{15 - 6d_f}{10 - 2d_f} \tag{2.25}$$

Solving for d_f gives:

$$d_f = \frac{10\alpha - 15}{2\alpha - 6} \tag{2.26}$$

From Chambon and Winter, as discussed in the previous chapter, at the Gel Point α is equal to the phase angle, δ, divided by 90.

$$d_f = \frac{10\frac{\delta}{90} - 15}{2\frac{\delta}{90} - 6} \tag{2.27}$$

All fractal dimensions given in the results chapter are calculated using equation 2.27.

From this it can be seen that the transition from sol to gel is not a process purely reliant on percolation, but is also dependent on partial or complete hydrodynamic screening, dependent on the polymer under investigation.

A method by which a fractal dimension can be derived for a mature clot has been developed by Avrami[36] and Liu[37]. However, this method is unsuitable for use with blood due to the fact that it relies upon a value for G'_∞. This is not possible to measure, or even reliably infer in the case of thrombosis due to lysis, the means by which the clot is broken down, which occurs far before a value of G'_∞ is approached.

2.6 Nomenclature

d	dimension
L	length
M	mass
d_f	fractal dimension
α	stress relaxation exponent
δ	phase angle between applied force and response
N	square side length (box counting)
R	circle radius (sandbox)
K_{ij}	reaction rate
ζ	RLCA stickiness coefficient
M_w	molecular weight
R_z	cluster radius

Chapter 3

Carbon Nanoparticles

'Take carbon then, what shapely towers it constructs'
A.M Sullivan, Atomic Architecture

Carbon compounds and structures have been put to use in every stage of civilisation, from the charcoal drawings of the Neanderthal and Homo Erectus to the charcoal driven development of metallurgy, the rapid coal fueled mechanisation of the industrial revolution to the dependence of modern humanity on the internal combustion engine and hydrocarbon derived plastics. In this manner, humanity can be described as carbon based on far more than just an internal cellular level.

Carbon as an element is unique in that it can form widely varying structures which comprise of nothing but the element itself. The two most startlingly disparate examples of this are graphite and diamond.

The former consists of multiple sheets of Graphene, made of six sided carbon rings. Each sheet is weakly bonded to its neighbours through Van der Waal's interactions. This results in graphite being very soft, as the Van der Waal's forces can be easily overcome allowing the sheets to slide over one another. Diamond, on the other hand, is formed from tetrahedrally bonded carbon such that the single unit formed by 5 carbon atoms is a triangular pyramid with a central carbon atom and the other four located at the vertices. This results in an incredibly strong matrix structure, and has allowed diamond to be put to use in the drill bits used in mining operations. While tougher, diamond is less thermically stable and will decompose to graphite if heated to 1800°C.

With the advent of technologies which allow for the study of materials at ever smaller scales, the investigation into the differences in the structures of

carbon compounds together with the possibility of their manipulation became an ever more important goal. The rapid descent of science and technology into smaller and smaller scales of reference was first identified, and predicted, by Richard Feynmann in a talk given in 1959, in which he discussed the manufacture of substances within biological cells and urged his audience *to consider the possibility that we, too, can make a thing very small, which does what we want - that we can manufacture an object that maneuvers at that level.* The term Nanotechnology was not coined until the publication of the book 'Engines of Creation' by Eric Drexler in 1986 [38]. The term nano is derived from the Greek *nanos* meaning dwarf and is used to define a scale, in this instance of 10^{-9} meters, approximately 1/80,000 the width of a human hair.

Two distinct types of nanoparticles have been investigated for this thesis and so merit further discussion within this chapter. The first of these are the combustion generated carbon particulates which are one of the by-products of the internal combustion engine, whilst the second are the accidentally discovered and now deliberately engineered carbon nanotubes.

3.1 Urban Particulates

3.1.1 Composition and Generation

Atmospheric and urban particulate matter include a wide range of chemicals, covering particle sizes from diameters of one hundred micrometers down to a few nanometers. Elemental and organic carbon, sulphates and nitrates, both man-made and natural, along with various other minerals dependent on geographical location, maybe emitted directly into the air. Further particulate matter is also created through secondary reactions between both particulate and non-particulate material extant in the atmosphere. Some of the geographic deviation between chemical concentrations in urban particulate is due to the use of different fuels and indeed additives to fuels, such as the use of lead as a lubricant in petrol which is still the practice in few countries, while it has been phased out and now banned in others. This banning of lead was due to the health effects caused by the increasing levels of lead in the bloodstream of those exposed to exhaust.

3.1.2 Toxicology

Historical Cases

Airbourne particulate carbon can come from a variety of sources. While the coal industry still flourished in Britain, the effects of prolonged exposure to coal dust were well documented, with the respiratory problems being known commonly as black lung. These effects varied depending on the location of the mine, as the makeup of the coal and thus its dust were markedly different. The coal dust from South Wales was found to be the most toxic. It was suggested by Seaton et al [39] that this increase in toxicity was due to the shape of the particles within the Welsh coal dust. These were found to be flat and plate like, as opposed to the more spherical particles from mines in Yorkshire. This difference in shape may be what enabled the Welsh coal dust particles in certain orientations to penetrate deeper into the lungs, causing localised inflammation and a greater systemic response, and perhaps even some penetration into the bloodstream.

Effects of coal dust were largely limited to respiratory problems. This was due to the large size (PM_{10} (10μm diameter) or greater) of the particles produced. The effects of particle size are twofold; firstly, as mentioned above, particles of 10μm diameter and above will be more readily expelled by the lungs prior to their reaching the alveoli. Secondly, for a given mass of particles, a decrease in particle size will result in an increase in particle numbers and surface area, this is illustrated in figure 3.1.

This increase is most easily understood through the consideration of cubes. Taking a cube with sides of length ten as the initial particle (equivalent to PM_{10}). Each of the faces of the cube will have an area of 100 resulting in a total surface area of 600. If the cube is now divided into equal pieces such that each resulting cube has a side length of 1, then the surface area of each particle will be reduced to 6. However, there are now 1000 particles, resulting in a total surface area of 6000, with no change in volume. If this procedure is undertaken a third time, resulting in cubes with a side of 0.1, then the surface area of each particle is reduced to 0.06. However, there are now 1,000,000 particles, resulting in a total surface area of 60000.

Prior to the toxicological investigation into the effects of increased surface area, the hypothesis of the increased numbers of smaller diameter particles for a given mass was postulated by Seaton et al. in 1995 as being the cause of increased cardiovascular and cardiopulmonary mortalities during certain pollution incidents. This paper is partly credited with the creation of the

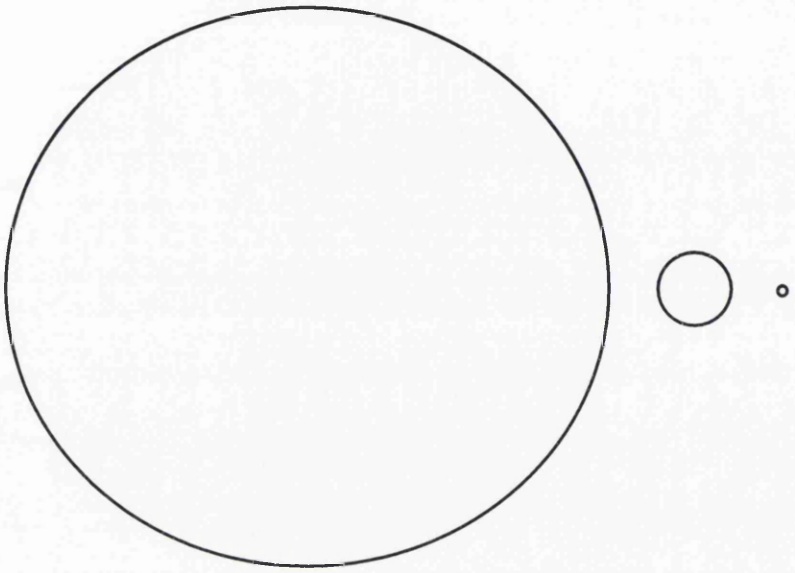

Figure 3.1: *Illustration of relative particle diameters. Left to right;* PM_{10}, $PM_{1.0}$ *and* $PM_{0.1}$.

nanotoxicology discipline. However, it had long been known within the chemistry discipline, especially by those studying reaction kinetics and catalysis, that a decrease in the particle sizes of the reactants (for example by grinding into powders) increased the rate of reaction as larger areas were available by which the materials could come into contact.

It had long been recognised that London had a particular problem with air pollution. The earliest attempt to deal with this was the banning of the burning of sea coal by Royal Proclamation in the Thirteenth Century. The problem persisted, and in 1661 John Evelyn presented a treatise to Charles II entitled, 'Fumifugium: or the Inconvenience of the Aer and Smoake of London Dissipated', in which he suggested that the lives of London's population would be shortened by smoke pollution.

The first time in which urban pollution was directly linked to respiratory and cardiovascular problems, and even mortalities, was in London in December 1952.

A large drop in winds together with the prevalent weather patterns on the night of the 4th of December resulted in the formation of a temperature

inversion over the Thames Valley [40]. This occurs when warmer air moves on top of cold air, trapping the colder air at lower altitudes. This prevented the dissipation of smoke and pollutants from all sources, coal fires used for heating and power stations for example.

This caused a rapid and dramatic increase in ambient pollution concentrations. On the 4th, the concentrations of smoke and sulphur dioxide measured at 12 sites across London were both between 0.12 and 0.44mg/m^3. As the fog began to appear and the smoke was prevented from dissipating, concentrations on the 5th reached 2.46mg/m^3 of smoke and 2.15mg/m^3 sulphur dioxide. The peak was not reached until the 7th and 8th however, when concentrations of smoke and sulphur dioxide rose to 4.46mg/m^3 and 3.83mg/m^3 respectively.

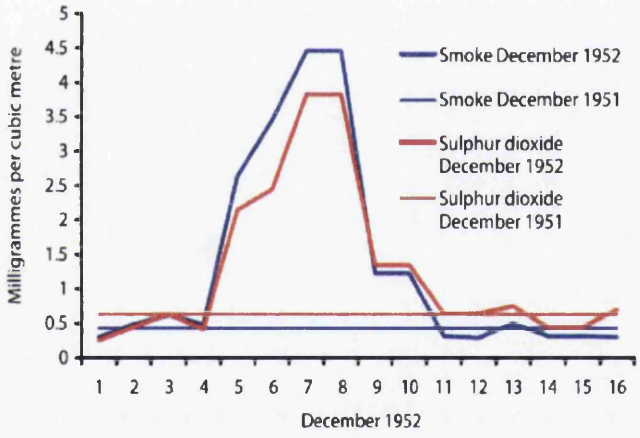

Figure 3.2: *Increase in levels of smoke and sulphur dioxide during 1952 smog compared to average data from the same period in 1951. (LCC 1953)*

This smog forced a number of schools to close due to fears that children would become lost between their houses and the school gates, together with recommendations that no journeys be undertaken unless completely necessary. In fact, the smog was so thick that fire engines were forced to employ men carrying flares to walk in front of them to enable the firemen to find the desired destination.

A Ministry of Health committee formed in 1953 estimated that the number of deaths during the incident were between 3,500 and 4000 more than would be expected under normal conditions. In fact, the number of deaths attributable to the smog were similar to those that occurred over the same time period caused by the cholera epidemic in London of 1854, and the pandemic of influenza in 1918.

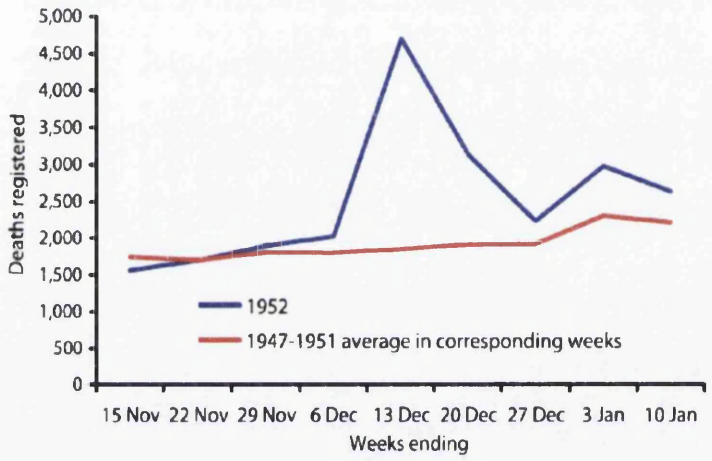

Figure 3.3: *Increase in mortality during London smog of 1952. (Ministry of Health 1953).*

Following this incident and the evident link between the high levels of black smoke fog or smog, a term coined by Dr. Des Veoeux in 1905 to describe the combination of smoke and natural fog which London frequently suffered, measures were made to reduce airbourne pollution levels within towns and cities. This was done primarily by relocating industry (both manufacturing and power generation) away from urban areas. However, while these steps reduced respiratory disorders as the levels of black smoke were brought down, the numbers of cardiovascular and cardiopulmonary related mortalities were not reduced. This was due to the fact that black smoke largely consists of particles in the PM_{10} range and larger, which are unable to penetrate as far into the lung. The largest generator of airbourne particulates following the relocation of the factories was exhaust gases from internal combustion engines, particularly diesels. These particulates however were much smaller, with an average of $PM_{0.1}$. As such these particles could penetrate deeply

into the lung, where they would be retained within the mucous membrane and alveolar tissue far more readily than the larger particles from the black smoke.

Another air pollution episode occurred over central and western Europe during 1985. Over a 13 day period in January, high concentrations of total suspended particles and sulphur dioxide were recorded with means of $98\mu g/m^3$ and $200\mu g/m^3$ and peaks of $238\mu g/m^3$ and $176\mu g/m^3$ respectively. High concentrations of carbon monoxide were also recorded. During this period, a pronounced increase in ambulance requests, hospital admissions and mortalities were recorded. People suffering from cardiovascular diseases were most affected with an increase in hospital admissions of 19%.

Data was taken from a MONICA survey carried out in Augsberg between 1984 and 1985 [41]. The authors investigated the hypothesis that the increases in cardiovascular mortalities associated with air pollution episodes were due to changes in the blood coagulability by comparison of blood plasma viscosity measurements taken during the episode and on less polluted days. The viscosity of the blood plasma is determined by large asymmetrical plasma proteins such as fibrinogen and immunoglobulin M. It was found that the pollution incident led to an increased risk for both men and women of extreme high values of plasma viscosity. The high concentrations of carbon monoxide were associated strongly with increased plasma viscosity in the women sampled.

The majority of the studies thus far have been made in developed countries. It cannot be assumed that the effects recorded in developed countries will match those in developing countries. This is true for a number of reasons. Firstly levels of air pollution will be markedly different due to industry types, location and local government emission limits. The chemical composition and size of the airbourne particulate particles will also differ depending on local industries. The prevalent meteorological conditions play a large part in ambient particulate concentrations: strong winds will tend to disperse particulate matter, while temperature inversions will contain any particulates close to the ground. The effects of particulate exposure will also differ depending upon local societal disease patterns, the age structure and socio-economic status of the populace.

A number of studies have recently attempted to address this lack of data, such as the work by Huang carried out in Shanghai between the 4th of March 2004 and December 31 2005 [42][43]. Prior to this work, most studies under-

taken in Asia had focused on total suspended particles or occasionally PM_{10} as particle measures.

At present, China only sets limits for levels of PM_{10}, at $50\mu g/m^3$ for a 24 hour average and $150\mu g/m^3$ for an average annual exposure. This is despite the fact that particles in the $PM_{2.5}$ range and smaller have been shown to be of far more dangerous. Work by Oberdorster et al in 1994 [44] and Venkataraman et al in 1999 [45] showed that most of the particles that deposit in the alveolar region of the lungs are $PM_{2.5}$ or smaller. These areas are cleared far more slowly than in the conducting airways. It has also been shown that $PM_{2.5}$ can cause oxidative stress due to lung inflammation.

The Shanghai study measured 24 averages of $PM_{2.5}$ at $56.4\mu g/m^3$ and $PM_{10-2.5}$ at $52.3\mu g/m^3$, with $PM_{2.5}$ constituting 53% of the total PM_{10} mass. The study found that $PM_{2.5}$ was associated with all causes of mortality, especially cardiovascular diseases. No significant effect was noticed from particles in the $PM_{10-2.5}$ range. The effects from PM_{10} were attenuated and thus less precise. The results revealed an increase in $PM_{2.5}$ levels of $10\mu g/m^3$ corresponded to a 0.36%, 0.41% and 0.95% increase in total, cardiovascular and respiratory mortality within the Shanghai area.

An additional issue that arises from the increase in finer airbourne particulates is environmental penetration. While larger particles can be prevented from entering internal living spaces by window and door seals for example, the same is not true for particles smaller than $1\mu m$. This means that people are under a relatively permanent exposure regime to very fine airbourne particulates.

There are two main factors which affect the amount of urban particulates a person is exposed to: location and seasonal variation.

Location

A study was carried out by Roemer and van Wijnen [46] in Amsterdam over the autumn and winter of 1998 and 1999 into the variations in levels of black smoke and fine particulate matter (PM_{10}, $PM_{2.5}$ and $PM_{1.0}$) between three measurement locations. The first of these was a background reading. A background site was defined as being at the center of a circle of radius 35m through which fewer than 2,750 motor vehicles passed over a 24 hour period. The second location was at an intersection with traffic lights of a pair of central urban streets with speed limits of 50km per hour. The final location was at the side of the 6 lane motorway which encircles Amsterdam.

The black smoke was measured for two reasons. Firstly because black smoke is historically linked with mortalities in Amsterdam more closely than particulate matter, and secondly because black smoke levels are a good indicator for the concentration of diesel traffic. As would be expected, a much higher average level of both black smoke and fine particulate matter was recorded on the 6 lane motorway compared to the background site.

Exposure is also dependent on global location. This variation in exposure levels is due to a number of factors, the most important of which is economic and industrial development.

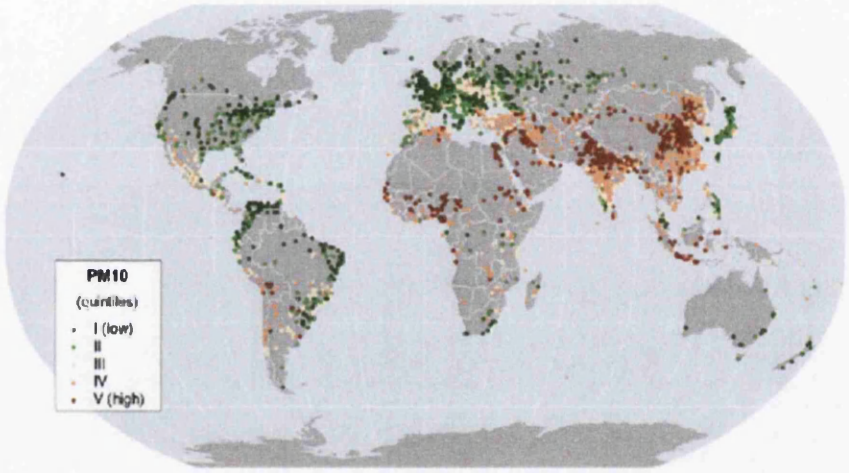

Figure 3.4: *airbourne particulate levels in major cities (WHO).*

3.1.3 Seasonal Variations

The variations exhibited between seasons are due to a number of factors: the ambient meteorological variations; seasonal variations in road traffic together with variations in the levels of particulates generated from other sources such as oil fired heating for buildings; and pollutants released from industrial processes. In 2005 Peng at al. [47] ran an investigation to determine the seasonal variance in urban particulate levels (PM_{10}) and mortality in one hundred different cities in the United States. The cities were divided into seven categories depending upon their location: the Industrial Midwest; the Northeast; the Northwest; Southern California; the Southeast; the Southwest; and the Upper Midwest.

3.1.4 Ingress Into Body

In order for the ambient particulates to enter the body they must be inhaled.

The mechanisms by which airbourne particulates enter the cardiovascular system have been studied using ultrafine carbine particles chemically labeled with radioactive isotopes of Iridium which were then aerosolised. Healthy volunteers were exposed to the aerosolised particulates and the distribution of radioactivity within them was then measured.

Work undertaken by Seaton involved the exposure of healthy volunteers to airbourne particulates with diameters less than $10\mu m$ (PM_{10}) over a three day period. A negative correlation was found with the haemoglobin levels, packed cell volume and red blood cell count as the exposure level increased. The subjects were also exposed to larger diameter particles. These did not result in inflammation of the alveoli or cardiovascular tissue, perhaps due to their ejection by cilia or mucous membrane as described earlier.

Calculation of Exposure Levels

The levels of daily exposure can be roughly calculated using an average tidal lung volume. While the human lung capacity can vary from 4 to 6 litres depending on age, health and sex, it is very rarely fully utilised. At rest, only a very small proportion is used during respiration. This is the air that is actually exchanged with each breath in a tidal flow, hence being known as tidal lung volume. An average tidal lung volume for an average size (5'8, 80kg) adult male is 500ml. At rest, an average respiration rate is between 10 and 20 breaths per minute. Given an average ambient fine particulate concentration of $30\mu g/m^3$, a daily exposure can now be calculated.

Taking an average of the resting breaths a minute as 15, the total air respired over a 24 hour period is 10800L, or $10.8m^3$. With an average ambient particulate concentration of $30\mu g/m$, this gives a daily intake of $324\mu g$. It has been postulated, that while short term exposure to high levels of pollution (during an incident) are of concern, the long term effects of low level exposure are more important for an assessment of the risks posed to population health. In this instance, a yearly exposure may be relevant. Following on from the previous calculations then, the yearly intake of particulate matter into the lung is approximately 118mg.

Very little research has been undertaken into how effectively these fine particles can be removed from the intratracheal system. However, should a

significant amount remain entrenched local build up may then ensue, possibly resulting in similar effects to that found from tobacco smoke. In fact, it has been shown that the mortality risk increases as the age bracket considered is increased. While age has an effect on general health and thus susceptibility to the detrimental effects of exposure, it will also increase the exposure timescale. For example, a 30 year old will have been exposed to approximately 3.5g of particulate matter, while a 60 year old will have been exposed to 7.1g. While these may seem like very small amounts it is once again important to stress the minuscule size of the particles involved, and thus the incredibly massive numbers of particles and the corresponding surface area.

In contrast to this, the daily particulate intake (assuming continuous exposure) during the worst period of the London smog mentioned above was approximately 48.2mg.

Particulate Reduction

Various proposals have been made for the setting of particulate level targets to be reached by 2010. These latest targets are focused on the reduction of levels of particles in the $PM_{2.5}$ range as these are a better marker for health effects, as put forward by the CAFE (Clean Air For Europe) programme in 2005. The suggested targets are the reduction to levels of 25, 20, 15 or $10\mu g/m^3$. These reductions have been proposed by a new European Directive, European Parliament, the US EPA, and the World Health Organisation respectively. While the differences in reduction levels may appear minuscule, the difference in the accompanying reduction in mortality rates is worth mentioning. These reductions occur in people aged 30 years and over are 0.4%, 1.0%, 1.6% and 3.0% respectively.

Epidemiological studies published between 1989 and 1996 showed that even at unexpectedly low concentrations of particulate pollution adverse health effects were still reported. Following these studies, the US Environmental Protection Agency adopted new standards for ambient air quality which imposed limits on the levels of $PM_{2.5}$. These new standards were contested by industry, whose case was upheld in a Federal Appeals court. The standards were ratified by the US Supreme Court, forcing industry to comply. It has since been shown that for each $10\mu g/m^3$ increase in fine particulate air pollution is associated with a 4%, 6% and 8% increase of all cause, cardiopulmonary and lung cancer mortalities respectively.

3.1.5 Ambient Concentration Measurement Procedures

The necessity for methods by which levels of urban particulates could be measured arose to enable the application of regulatory limits by governmental authorities. A comprehensive government maintained monitoring site network was already in existence. The problem with the network was that different measurement devices gave systematic differences in results. In order to combat this in Europe, a European Union directive (EN12341) has been put in place, specifying three reference methods for determination of PM_{10} levels. High- and low-volume samplers are used to obtain daily samples both for weighing and subsequent chemical analysis.

Many collection and analysis methods involve the collection and assessment of all particulate matter, termed Total Suspended Particles. This collected material can then filtered and fractionated to enable investigation of composition, thus giving data for levels of PM_{10} and $PM_{2.5}$.

3.1.6 Effects of Exposure

Pollutants in environmental tobacco smoke (ETS) include many found in ambient air due to combustion of bio-derived organic material and are toxicologically very similar. Indeed, a number of papers report effects on the peripheral and coronary circulation systems following inhalation of diesel particulates which are similar to those recorded in patients with a history of smoking. Indeed, a number of papers report effects on the peripheral and coronary circulation systems following inhalation of diesel particulates which are similar to those recorded in patients with a history of smoking.

The following hypothesis has been put forward for the effects of chronic exposure. Firstly, that inhaled particulate matter, with individual particle diameters small enough to reach the alveoli, may set up inflammation in the lung. This inflammation would then lead to changes in the control mechanisms that govern the formation of clots within the blood. Any changes caused in the chemical factors within the blood can affect the stability of atherosclerotic plaques in the arterial walls - especially those which supply blood to the muscular tissue of the heart itself.

A large body of research has recently been undertaken with respect to ascertaining the toxicological effects of both urban and purely diesel exhaust particulate upon the cardiovascular system. The hypotheses under examination are that transient exposure to traffic derived air pollution may be a trigger for acute myocardial infarction, especially where an individual has a

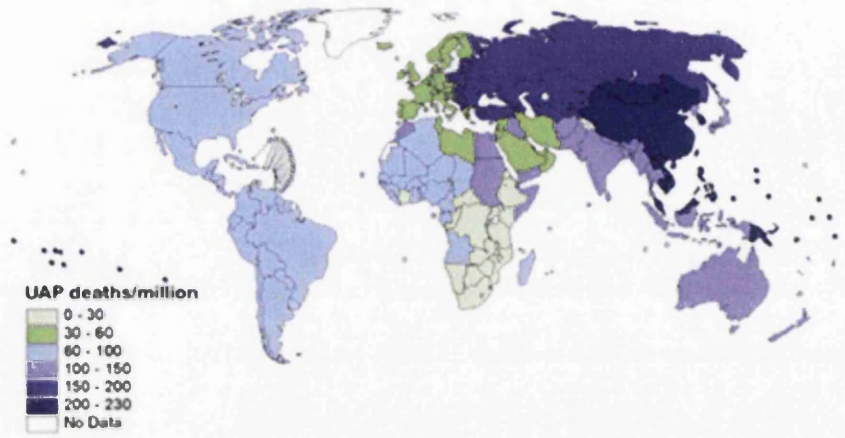

Figure 3.5: *Global deaths linked to aibourne particulate exposure.*

previous history of the problem.

A study by Mills et al published in Circulation in 2005 [48] investigated the effects of diesel exhaust inhalation on the vascular and endothelial function in 30 adult males. They exposed the volunteers to either clean air or dilute diesel exhaust at particulate concentration of $300\mu g/m^3$ for one hour during intermittent exercise. They found that inhalation of diesel exhaust particles at concentrations found within urban environments impair two important complementary factors in the human circulation system. These are endogenous fibrinolysis and the regulation of vascular tone. These findings suggested a potential mechanism by which air pollution may enhance or exacerbate atherothrombosis and acute myocardial infarction.

3.2 Carbon Nanotubes

The synthesis of micro- and nanoscale carbonaceous compounds did not begin with carbon nanotubes. They were discovered by accident among the deposited carbon formed in the creation of another, now widely known, carbon compound: fullerenes.

Fullerenes, named after the geodhesic structures of architect Buckminster-Fuller, take the form of highly stable spherical or ellipsoidal structures. They are based on the graphene sheet of which graphite is constructed but contain a number of pentagonal rings together with the standard hexagonal rings

which allow them to form the three dimensional structures. They were first discovered by Kroto and Smalley in 1986 [49], by subjecting graphite to arc evaporation within a helium atmosphere. This process will be discussed in more detail later in this chapter. The most famous fullerenes are C60 and C70, which resemble a football and a rugby ball respectively. Carbon nanotubes were discovered by Iijima in 1991 [50] while undertaking microscopic analysis of the carbon soot produced using the methods of Kroto and Smalley.

For experimental purposes, carbon nanotubes can be split into two distinct groups; as-produced (which will be referred to as AP), and functionalised. As the functionalisation of nanotubes is a process which takes place after the initial generation, it shall be discussed later in the chapter.

3.2.1 As-Produced Nanotubes

As-produced nanotubes can be readily split into two subsets determined by structure; multi-walled and single-walled. Each subset, while structurally similar, has differing methods of generation. As such, the underlying structure of as-produced nanotubes will first be discussed, followed by the production methods of the two subsets which will be discussed chronologically with reference to their discovery.

Structure

The basic structure from which nanotubes are derived is the graphene sheet mentioned previously. A nanotube consists of cylinders capped at both ends with hemispheres containing precisely six pentagonal rings as defined by Euler's Law which states that a flat hexagonal sheet can only be made into a sealed three dimensional object by the inclusion of twelve pentagonal rings. These hemispheres are formed by the splitting of a C_{60}. This method of formation leads to the generation of nanotubes with structures commonly described as 'armchair' and 'zig-zag', The type of nanotube formed is determined by the way in which the C_{60} molecule is split. If the split is along the 3-fold axis then the nanotube formed will have a zig-zag configuration, while a C_{60} split along the 5-fold axis will form an armchair nanotube.

However, nanotubes can exist with structures in between the two extremes presented above and so a method of characterisation known as the chiral angle is used. In order to understand the chiral angle, firstly a single graphene layer needs to be considered. The atoms at each of the vertices are given coordinate numbers using (n,m) vector notation.

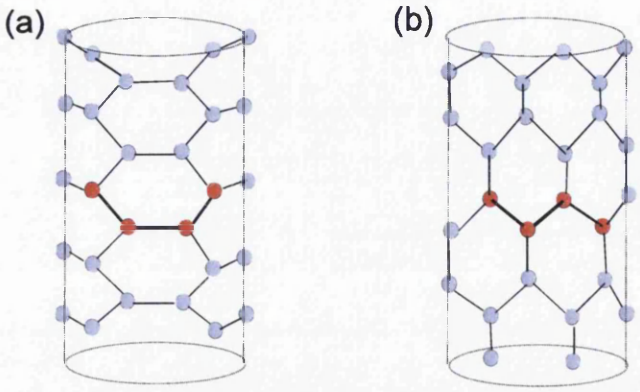

Figure 3.6: *Representation of the two extremes of nanotube structural variation; (a) armchair, (b) zig-zag. The structural arrangements from which the names are derived are highlighted in red.*

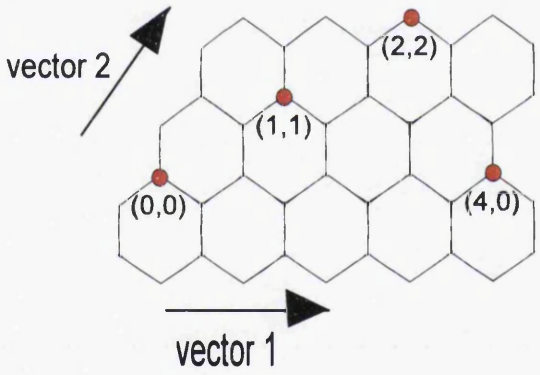

Figure 3.7: *Illustration of n,m vector notation as applied to a single layer of graphene.*

The armchair and zig-zag nanotubes presented in figure 3.6 can now be described in terms of the vectors of their unit cells [51], the structural area of the sheet from which they are constructed, and thus their chiral angle can be calculated using the formula given below.

$$\Theta = \arcsin \frac{\sqrt{3m}}{2\sqrt{n^2 + nm + m^2}} \tag{3.1}$$

It can be shown that m = n for all armchair tubes, while m = 0 for all

zigzag tubes. All the tubes in between are defined by their chiral angle. For example, taking a nanotube composed from a unit cell (7,3) the chiral angle Θ can now be calculated using equation 3.1 thus:

given: n = 7, m = 3

$$\Theta = \arcsin \frac{\sqrt{9}}{2\sqrt{7^2 + 21 + 3^2}} = \arcsin \frac{3}{2\sqrt{79}}$$

$$\Theta = \arcsin 0.169 = 9.73^\circ$$

The structures described above only deal with single-walled nanotubes, multi-walled consist of a number of tubes arranged concentrically. However, while successive cylinders will exhibit the same orientation with respect to the unit cell, they will differ in their structures slightly due to the increase in diameter between the inner tube and its surrounding neighbour. It has also been suggested that multi-walled nanotubes contain both concentric cylinders and some scroll like elements. These scroll like elements occur due to edge dislocations and in fact, multi-walled nanotubes can only have a zig-zag structure if dislocations are present.

Multi-walled Nanotubes

It was multi-walled nanotubes which were identified by Iijima during the microscopic analysis carried out on carbon soot produced using the process developed by Smalley as outlined earlier.

Synthesis

There are three main methods through which multi-walled nanotubes are synthesised: Arc ablation; Laser ablation; and chemical vapour deposition.

Arc Evaporation

This is the classic method of production identified by Iijima in Nature 1991. It involves the use of two graphite electrodes (not necessarily of very high

purity) held a small distance apart within a stainless steel vacuum chamber. This differs from the method used for fullerene production in which the electrodes are in contact. The chamber is connected to a supply of helium and a vacuum line. The electrodes are not similar. The anode is usually a thin rod with a diameter of 6mm, while the anode is shorter and thicker with a diameter of 9mm. It has been shown that water cooling the cathode is essential in high quality nanotube production. The arcing is usually undertaken at a voltage of 20V resulting in a current between the electrodes of 50 - 100A. Presented in figure 3.8 is a basic schematic diagram of the arc ablation apparatus.

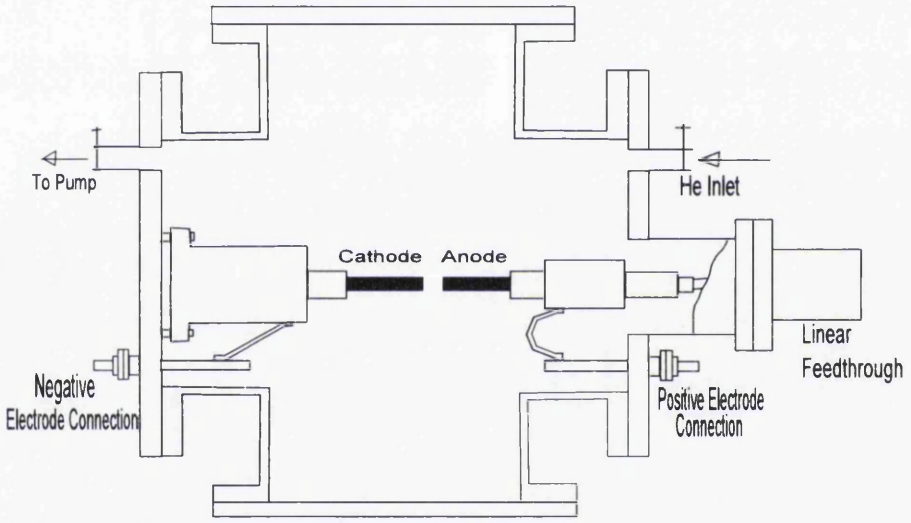

Figure 3.8: *Basic Schematic Diagram of Arc Evaporation Apparatus*

A number of other factors have also been shown to be important to the quality of arc discharge nanotubes: chamber helium pressure and current. The optimum pressure for a good yield of high quality nanotubes has been identified as 500 Torr. This is markedly different from the pressures of 100 Torr used by Kroto for the production of fullerenes.

The current on the other hand needs to be kept as low as possible, both in order to maintain a stable plasma and to prevent the generated material

being sintered and thus containing very few free nanotubes.

While the cathode is cooled as standard, it has been shown that effective cooling of both the anode and the chamber itself is important both to the quality of the nanotubes produced and to reduce sintering.

The arc ablation method tends to produce relatively long, straight nanotubes.

Laser Ablation

Described by Chernozatinskii et al in 1994 [52], this method evaporated graphite by subjecting it to an electron beam while under a high vacuum. The material was then condensed onto a quartz substrate and collected. This film of condensed material was shown to contain some imperfect multi-walled nanotubes following examination using high magnification electron microscopy. This method was further developed at Rice University by a group lead by Smalley, which resulted in the report of carbon nanotube synthesis using oven laser vaporisation in 1995.

Smalley's technique involves the mounting of a graphite target in a controlled-environment oven held at 1200° C in a carrier gas of argon. The laser is then used to vaporise the graphite target which then condensed onto a cooled copper substrate. Upon investigation the collected condensed carbon film was found to contain a significant amount of structurally perfect nanotubes. This technique was further developed for the production of single-walled nanotubes .

Chemical Vapour Depostion

This method consists of a quartz reactor that is heated in two zones;: a preheater and a furnace. A carbon source such as xylene is mixed with a catalyst such as iron or cobalt and fed continuously into the reactor. In the preheating section the liquid carbon compound is vapourised, followed by decomposition in the furnace section at temperatures beween 600° and 1200° C. The nanotubes grow around the catalyst particles and form mats on the walls of the quartz tube had on the substrate. They are then harvested once the process has been terminated. By including a plasma chamber, better control over length, diameter and structure of the resulting nanotubes can be achieved together with straighter and more uniformly aligned mats.

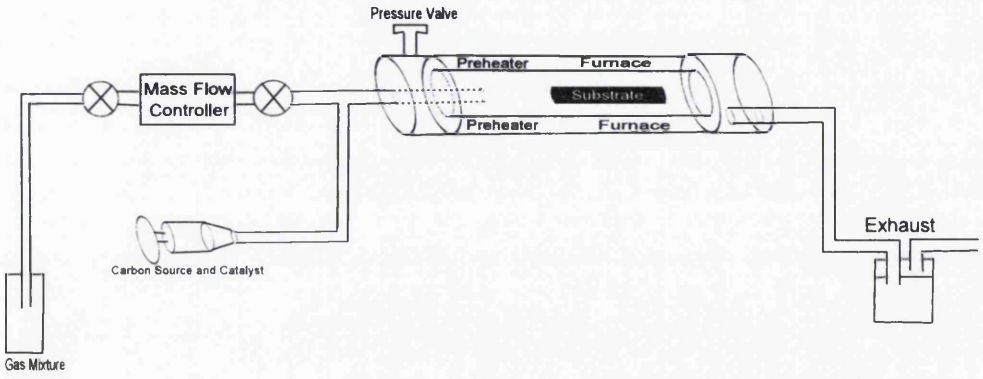

Figure 3.9: *Basic Schematic Diagram for the Chemical Vapour Deposition Process.*

Purification

There are three main methods in use for the purification of multi-walled nanotubes [53]: selective copper catalysed oxidation; flocculation and filtration; and size exclusion chromatography.

The oxidation process can be broken down into a number of distinct steps.

Firstly, the crude cathodic deposit is immersed in molten $CuCl_2$-KCl held at 400°C for one week. The resultant material is then washed in ion-exchanged water, following which it is heated to 500°C in a combination of He and H_2 for one hour. The product is then oxidised in flowing air through a ramped temperature of 10°C/min up to 550°C.

The flocculation and filtration method uses Sodium Dodecyl Sulphate (Lauryl Sulphate) to solubilise the nanotube/nanoparticle blend in water. The nanotubes are then allowed to flocculate, leaving the nanoparticles in suspension. The sediment is then removed and further flocullation allowed to occur. This enables removal of the nanoparticles from the sample, and some initial degree of length separation of the nanotubes. This separation

is then further heightened using microfiltration membranes with a pore size corresponding to the upper end of the desired length spectrum.

Size exclusion chromatography [54] again involves the dispersion of the nanotubes in water using sodium dodecyl sulphate. This technique is widely used in the biological sciences for separation of macromolecules. This method is based upon the fact that molecules of different sizes will diffuse through a medium at different rates. The apparatus consists of a column, typically packed with gel beads which serve to provide a variety of pore diameters. Evidently, larger particles will be unable to pass through many of the pores and so are separated out of the eluate. However, this technique is more useful for separating an already purified sample of nanotubes into fractions defined by length.

Single-walled Nanotubes

The discovery of single-walled nanotubes stemmed from work undertaken by several groups in early 1993 [55]. It was found that by using modified electrodes during arc evaporation, foreign materials could be encapsulated within carbon nanotubes.

This work was of great interest to a group at IBM led by Bethune, who were working on the application of magnetic materials for the storage of data, particularly that of ferromagnetic metal crystals embedded in carbon shells. By enclosing the metal crystals, the magnetic moments of the individual crystal would be maintained while isolating it both magnetically and chemically from its neighbours.

This had been attempted using a very small number of crystals encapsulated within fullerenes. It was felt that increasing the crystal cluster size inside the shells may be important. As such Bethune et al doped electrodes with nickel, cobalt and iron prior to arc evaporation [56]. The resulting soot showed completely unexpected properties. When this soot was examined at high magnification using electron microscopy it was found to contain single-walled nanotubes. Similar experiments were also being undertaken concurrently by Iijima et al who also investigated the effect of the local atmosphere on single-walled tube production, finding that a blend of methane and argon was more productive than the standard helium.

Synthesis

Arc Evaporation Developments

The methods discovered by Bethune and others have been further developed using a wide variety of catalysts for the doping of the electrodes. These catalysts affect the diameter of the resultant tubes and will be briefly outlined here. As described above, cobalt was initially used as a doping agent. This was found to produce single-walled nanotubes with diameters between 0.6 and 2nm. The inclusion of a small amount of sulphur, lead or bismuth into the anode along with the cobalt was shown to increase this range of diameters to between 1 and 6nm.

In late 1993 Subramoney et al [57], working for Du Pont, grew single-walled nanotubes using electrodes doped with gadolinium. The structures formed by these tubes were markedly different from those achieved using other catalysts. The formations were described as 'sea-urchins' and consisted of a large number of single-walled nanotubes growing outwards from a single particle of gadolinium carbide. These tubes were much shorter than those grown using ferric metals, but exhibited a similar spread of diameters.

Using a similar technique to that pioneered by Bethune, a high yield of single-walled nanotubes was achieved by a French group in 1997 using an yttrium/nickel catalyst in place of the cobalt and utilising a slightly different geometry for the reactor. This method achieved a 70 - 90% yield and subsequent investigation revealed multiple tube bundles, with individual tube diameters of 1.4nm.

Laser Vaporisation

This technique was developed and improved upon the technique of laser vaporisation described above in order to produce a high yield of single-walled nanotubes. This led to the formation of nanotubes with incredibly uniform diameters. Instead of the pure graphite target used in the formation of multi-walled nanotubes, a composite target of graphite and a blend of cobalt and nickel was used. An improvement in the evenness of vaporisation was achieved by utilising a double laser pulse. Due to the increased uniformity of diameter these nanotubes exhibit a tendency to form 'ropes', highly aligned bundles, which occasionally were found to have formed in the direction of the beam. This enabled them to be imaged end-on in an electron microscope. Further investigation of these ropes using both electron microscopy and X-ray diffraction showed the bundles to primarily consist of armchair structure

nanotubes with diameters of 1.38nm.

Catalytic Methods

Further work by Smalley et al has shown that single-walled nanotubes can be grown using a method that is purely catalytic [58]. This method is broadly similar to chemical vapour deposition as described above. In this case, the catalyst was nanometer sized particles of molybdenum which were supported on alumina. The furnace was run at 1200°C, through which carbon monoxide was passed. This is higher than the initial temperatures defined earlier, as at lower temperatures multi-walled nanotubes are preferentially formed.

The single-walled nanotubes produced in this manner were markedly different in a number of ways from those produced by the vaporisation methods described previously. The wide range of particle diameters, 1-5nm, was determined for each tube by the size of the catalyst particle around which it had grown. Each of the tubes still contained the catalytic particle, embedded in, or attached to, one end. These nanotubes were more often to be found individually rather than formed into bundles.

Through the use of a magnetic field, and the careful location and sizing of the catalyst particles, it is possible to grow a mat of highly regularly spaced and uniform single-walled nanotubes. These are currently being investigated for their electronic properties with proposed uses as lighting and television screens using field emission.

Purification

Due to the nature of the single-walled nanotubes, the harsh oxidation methods available for the purification of the multi-walled nanotubes are not viable. The challenge is further increased due to the metal contamination within the produced nanotube containing carbon soot. As such, purification methods have focused on filtration [59].

One such method has been described by a Japanese group [60]. This method involves the refluxing of the soot in distilled water for 12 hours after which it is filtered and dried to remove the amorphous carbon. Toluene was then used to remove the fullerenes followed by treatment with concentrated hydrochloric acid to remove the metal particles. While this method was shown to have removed most of the contaminants, some nanoparticles, both filled and empty, remained.

A method pioneered by Smalley involved the use of microfiltration. This used a cationic surfactant in which the nanotubes were suspended prior to filtration, followed by passing the resulting solution through membrane filter in order to trap the tubes. The required multiple filtration and sample resuspension rendered this procedure very inefficient and time consuming. By incorporating ultrasonics in order to keep the material suspended, these drawbacks were overcome, allowing the continuous filtration of large amounts of sample. This technique enables the purification of material to a final product containing over 90% singlewalled nanotubes.

Nanotube Properties

The initial assumptions made were that the nanotubes would exhibit similar properties to macro-scale carbon compounds, the most important of which is chemical inertness. A number of scientifically important properties of nanotubes have been identified in the two decades since their discovery. However, the vast majority of these properties are of little or no importance to the work undertaken for this thesis and so merit only a very brief discussion here.

Carbon nanotubes exhibit an electrical conductivity that is either metallic or semi-conductive. Which category a given nanotube falls into is determined by its helicity as described by the chiral angle defined earlier. Metallic nanotubes can have an electrical conductivity as high as copper.

Nanotubes have a strength one hundred times that of steel at less than one sixth the weight, rendering them one of the strongest materials known to man. This also means that nanotubes have an incredibly high strain to failure ratio. The thermal conductivity can be as high as diamond, again this is determined by helicity, and this property has enabled the targeting of tumours with infrared.

The most important properties for the possibility of application in the medical field are: chemical inertness and internal storage space. This inertness presents opportunities within drug delivery and imaging due to the possibility of attaching molecules to the surface by which the nanotube may be targeted to a specific organ or location within the body. The ability to both open and seal nanotubes, thus gaining access to the space inside them enables the nanotubes to be used to carry drug molecules internally (provided the tubes are sealed with a molecule that will allow to reopen at the desired destination). This also enables the inclusion of radioactive molecules incorporated within the nanotubes to enable medical imaging, while preventing

chemical interaction between the radioactive material and the surrounding tissue.

However, the interaction with blood and tissues within the body will also be affected by the surface roughness exhibited by the nanotube. This surface roughness characteristic will determine the both the contact and wetting angles between the blood and the nanotube.

The property which has thus far presented the largest problem to progress in many fields of nanotube research is that of their solubility. This difficulty in getting nanotubes into solution may be in part due to their electronic interaction properties. Both multiwalled nanotubes and bundles of single-walled nanotubes are stabilised by the competition between long range van der Waals binding, intermediate range dipole-dipole interactions and kinetic-energy induced repulsion. It is important to note that the term long range when used to describe van der Waals forces is 3 - 3.5$\dot{A}$.

Due to the low electron density exhibited by nanotubes, they exhibit a localised screening effect. This may be another factor which limits their interaction with surrounding solvent molecules causing hydrophobicity.

Nanotube Functionalisation

The ability to functionalise nanotubes by the adsorption of molecules, whether biological or simple organic, to their surface is of massive importance. The attachment of these surface molecules is at present mainly used to change the interaction of the nanotubes with solvents, both water and organics, allowing them to be effectively dispersed. The use of poly(propionelthylenimine-co-ethylenimine) and poly(vinyl acetate)-co-(vinyl alcohol) for the functionalistion of singlewalled nanotubes and a polysterene co polymer for the functionalisation of multi-walled nanotubes have resulted in the nanotubes becoming soluble in water. This change in interaction and thus solubility may be due to the effect on charge and electron density. By wrapping the nanotubes in polymers which present effective dipoles or other systems to the solvent while inhibiting the local screening effects of the nanotubes the hydrophobic tendencies of unaltered nanotubes are overcome.

Functionalisation is also being investigated as a method of targeting the nanotubes to specific regions within the body, both for drug delivery and medical imaging, and to attempt to disguise them from the bodies immune system.

In the case of the work carried out for this thesis, the ability to solubilise the nanotubes is the most critical. The functionalisation methods have been selected to enable the ready dispersion of the nanotubes into water or low concentration medical salts solution.

A number of functionalisations of both single-walled and multi-walled nanotubes have been developed to enhance the solubility of the nanotubes in various solvents. The following chemical groups are bonded to the nanotubes in order to enhance solubility in water: carboxyl groups, Poly Ethylene Glycol (PEG) and poly-(m aminobenzene sulfonic) acid (PABS). These groups are attached over the entire length of the nanotube. The spacing between attached carboxyl groups can be specified and is often only one or two atoms.

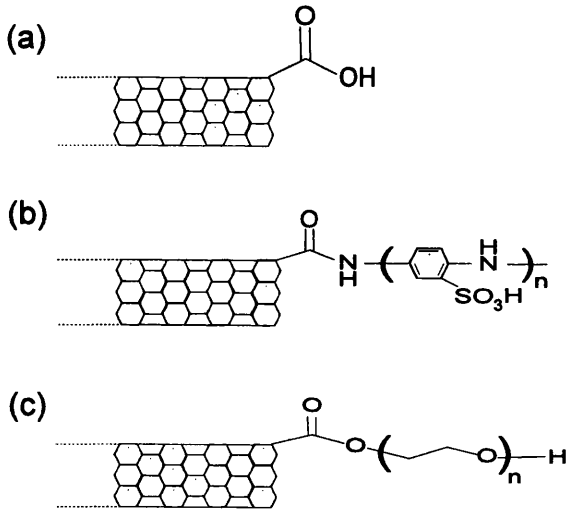

Figure 3.10: *Single-walled nanotubes showing funcionalisation with; (a) - COOH (b) PABS and (c) PEG.*

Another form of functionalisation which will be important for medical imaging and would also enable a study on confocal further to the work here, is fluorescent labelling. One method for this utilises enzymatic biotinylation to bond isomers of a biotinyl tyramide radical which can then be bonded to a singlewalled nanotube.

The main problem with the attachment of flourophores directly to the nanotube is that of quenching. This is yet to be overcome. In contrast,

attached quantum dots do not undergo quenching. This may be due to the differences in magnitude between the dots and the nanotubes - quantum dots are an order of magnitude larger than the nanotubes, while the fluorophores are of similar dimensions. The low electron density properties mentioned above may also have a quenching effect on the flourophores as the electrons may be removed from the higher energy states by the nanotubes, thus preventing them from releasing the photons which would normally be ejected during the transition of the electrons to the lower energy states.

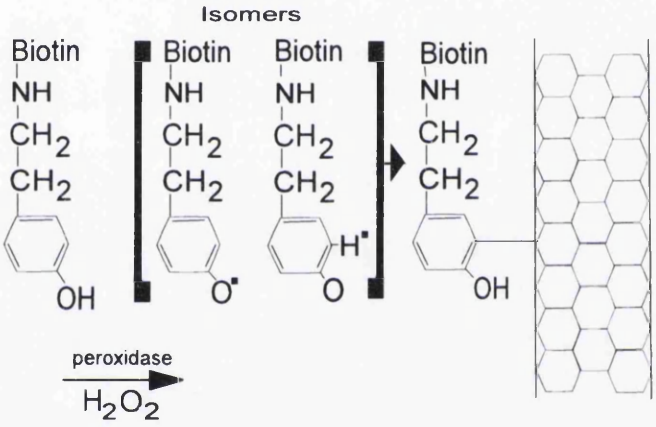

Figure 3.11: *Reaction mechanism using peroxidase to create isomers of a biotinyl-tyramide radical. These radicals are then able to bond with single-walled nanotubes.*

The reaction proposed above may enable the fluorophore, in this case Biotin, to remain active as it is not directly attached to the nanotube. This mechanism is based upon work undertaken by Gross et al in 1959 [61].

Nanotube Toxicity

The study of the toxicological effects of carbon nanotubes, in fact all nanoparticles, is still in its infancy. This is shown most starkly by the material safety data sheets supplied with carbon nanotubes by the producing companies.

On these sheets, exposure is broken down into the following categories: inhalation; skin contact; eye contact; and ingestion. For exposure in each of these categories medical advice is recommended. For skin and eye contact, washing the area with soap and water or rinsing with running water are recommended. As the nanotubes are insoluble in water the most this will result in is a smearing of the particles over a larger area.

The most important point to note with regards to nanoscale particulate toxicology is that the effects are not due to mass as would be the case with macroscale compounds, but are due to the high surface area exhibited.

There are two methods by which nanotubes may be caused to enter the bloodstream: injection and inhalation.

While injection is evidently a deliberate act and thus assumes the nanotubes are placed within the immediate area of the target organ or system, inhalation requires the presence of airbourne nanotubes. However, in order for any nanotubes which enter the respiratory system to pass into the bloodstream, the systems defensive measures must be passed. These defences consist of: the cilia - the tiny hairs lining the trachea; and the mucous membrane lining the alveolal wall. Particulate materials caught by these hairs are ejected from the body via the cough reflex. In order for a particle to pass the cilia and reach the membrane it has been shown that it must have a diameter less than 10μm (PM_{10}). This has been calculated using spherical particles. Evidently nanotubes themselves are not spherical, however, due to the tendency of nanotubes to agglomerate, some spherical particles may result. Even so, the transport of individual nanotubes through the respiratory system may well be length determined, assuming that the largest dimension is the most critical for rejection.

The presence of nanoparticles within the lung has also been hypothesised to cause localised inflamation within the alveoli, thus triggering a corresponding effect and the systems of control within the blood which regulate the clotting process.

It has also been suggested that changes in the chemical factors in blood due to the presence of nanoparticles can affect the stability of the atherosclerotic plaques (fatty deposits) found in the walls of arteries, especially those which supply the blood to the heart muscle itself.

The change in plaque stability causes the uptake of lipids into the endothelium resulting in lesion formation. It is the rupture of these lesions

which is suggested to then induce localised clotting of the blood, potentially leading to embolism or deep vein thrombosis if the clot cannot be readily removed.

It has been hypothesised that inhalation of nanoparticles may be of a greater danger than injection due to the fact that the nanoparticles embedded within the mucous membranes within the lung will remain there for a much greater time as they cannot be removed effectively, compared to those in the blood stream.

Following intratracheal nanotube installation in mice, inflammation and the formation of epitheloid granuloma have been recorded. These reactions are dose dependent.

Once the nanotubes have made ingress to the blood, clotting may potentially be induced in a number of other ways. If the surface roughness of the nanotubes causes the contact angle between them and blood to resemble collagen then platelet aggregation may be induced.

It has recently been shown that nanotubes produced using arc discharge can resemble asbestos fibres and ehibit similar proerties when placed into the bodies of mice [62]. This not only poses the risks associated with asbestos, but due to the structural nature of these nanotubes (long and straight), lymphocytes and phagocytes are unable to effectively engulf them and thus enable their removal from the bloodstream.

The response of the immune system to the introduction of nanotubes into the cardiovascular system is under only preliminary investigation. It is likely that further functionalisation utilising specific antigens and other protein molecules will be required to prevent the nanotubes coming under attack. Any large scale response could be potentially life threatening to the patient and thus it may be found to be necessary to suppress the immune system if treatment with nanotubes is decided upon. This course of action carries its own health risks.

Another issue with the use of nanotubes within the body is that the blood may well transport the nanotubes to undesired locations. While functionalised nanotubes can be tailored somewhat to concentrate to a particular point in the body, AP nanotubes have a relatively free reign.

It has been shown recently that nanoparticles may have the ability to cross the blood-brain boundary (BBB), which may be both a blessing and a curse.

Medical science has for many years been attempting to effectively enable certain drugs to more readily cross the BBB and this finding may allow the development of delivery systems that can achieve that. However, the ability of nanoparticles to cross the BBB has serious implications. The effect of nanoparticulate build up within the brain has obviously never been studied. It seems to have been assumed that once the drugs have been delivered the nanotubes will either somehow be ejected from the brain (although if targeted proteins have been used to concentrate them to a location this seems unlikely) or that they will simply exist in dormancy within the cortex.

While not an accurate allegory for primates in any way, work on earthworms has found that nanotubes can accumulate within the reproductive system. In the case of the earthworms this led to the nanotubes being passed on the next generation. The effect on primate reproductive systems should the nanotubes be found to accumulate there is unknown.

The three locations within the body which function to remove foreign or otherwise unwanted material are also likely sites for accumulation. These organs are the liver, the kidneys and the spleen. Effects on these three organs are disputed, with some studies finding very little effect whatsoever and no evidence of nanoparticle storage, while other studies have found clear evidence of nanoparticle storage together with localised inflammation. However, these studies have so far focused on rats and mice. No atherosclerotic lesions have been found, however, rodents are far less prone to the developments of plaques than primates.

The non biodegradability of the nanotubes due to their chemical inertness is another cause for concern linked to build up within a given bodily system if exposure occurs over a longer timescale. While functionalisation has thus far been studied in order to facilitate solubilisation or targeting, the issues of the interactions between the resulting nanotube-polymer compound and blood are not well understood. Wrapping the nanotubes in heparin has been suggested as a means of allowing them passage through blood. However, heparin is well known to affect the clotting cascade, causing differences in clot structure. Interestingly, it has been shown that the ability of blood to clot around multi-walled nanotubes is greatly reduced following wrapping with heparin.

3.3 The Effects of Nanoparticles on Blood

The seminal study on the effects of various carbon nanoparticles on blood was carried out by Radomski et al [63]. The similarities between carbon nanotubes and the carbon particulates generated from combustion led to questions arising as to the toxicology of the newly discovered material. Studies have been carried out to attempt to ascertain the effects of exposure to exhaust particulates with regards to haemostatic function.

3.3.1 Studies on Urban Particulates

A number of papers [64][65] demonstrate that diesel exhaust inhalation can impair vascular function in humans. They show an impairment of both vascular tone regulation and endogenous fibrinolysis. The impairment of vasomotor function in the forearm bed is associated with increased risk of acute cardiac events including cardiac death. The inhalation of exhaust had an immediate pro-ischemic effect;: an important mechanism for the observed increase in myocardial infarction in the hour after exposure to heavy traffic. A second peak for myocardial infarction 5-6 hours after exposure to traffic is reported by Peters et al [66], also at this point in time reductions in tPA were recorded as presented in the second paper. These reductions reduced the efficacy of endogenous fibrinolysis. For discussions of all terms relating to blood and thrombosis please refer to chapter 5.6.

3.3.2 Expansion of Investigation

The study by Radomski et al mentioned above expanded this research to cover a broader spectrum of carbon nanoparticles: single and multi walled nanotubes; fullerenes; standard urban particulate matter (average size 1.4μm); and a mixed carbon nanoparticle blend. This study used in vitro platelet function assays and in vivo vascular thrombosis in rats as means of assessing deviations in haemostatic function.

Platelet Assessment Methods

The following methods were used to assess platelet function: lumi aggregation; phase contrast,; immunofluorescence; transmission electron microscopy; flow cytometry; zymography; and pharmacological inhibitors of platelet aggregation.

Sample Preparation Techniques

The desired nanoparticle was added to Tyrode's solution. Samples are then sonicated for 2 minutes. While this aids in dispersing the nanoparticles, the ultrasonic vibrations result in rapid heating of the sample. This leads to solvent boil off, changing the sample concentration. This is overcome in the current work by immersing the sample tube in a cold water bath. The samples were then vortexed for 20 seconds. This was found in the current work to have the opposite effect to that stated as centrifugal forces caused the nanoparticles to migrate to the edge of the sample container resulting in very high localised concentrations and thus rapid agglomeration.

Some of Radomski et al's suspensions were filtered through 0.1um filters. Studies of the filtrate concentration using photospectrometry has shown that the final concentration of the samples following filtration fall on the almost vertical region of the calibration curve, meaning that accurate concentration assessment is very difficult. Nanoparticle concentrations in the range 0.2 - 300mug/ml were investigated.

Radomski et al obtained blood from healthy volunteers. This blood was then spun down to obtain platelets which were washed prior to re-suspension in Tyrode's solution. Nanoparticles were added following pre-incubation of the platelets at 36°C. No mention is made of any alteration of particle concentration pre-injection to account for the dilution due to the Tyrode's solution already present in the platelet solution.

The various platelet assays showed that, bar the C60 fullerenes, all the nanoparticles induced platelet aggregation with an order of efficacy as follows: mixed carbon nanoparticles = single walled nanotubes $\geq$ multi walled nanotubes $\geq$ urban particulate matter.

Rat carotid arteries were used as models for the effects of nanoparticle infusion in vivo. The nanoparticles caused an increase in the rate of thrombosis with a rank order of efficacy matching that found from the work undertaken on platelets in vitro.

3.4 Nomenclature

PM_x	particle diameter (μm)
Θ	chiral angle

Chapter 4

Nanoparticle Characterisation and Dispersion

Nanoparticle characterisation is undertaken to assess a number of variables: particle size (both individual and as agglomerates),; particle composition; and surface roughness. The instruments most commonly used for these measurements are scanning and transmission electron microscopy, EDX and atomic force microscopy. There are also methods available for the investigation of the particles once they are in a suspension: particle size analysis; zeta potential assessment; and photospectroscopy.

4.1 Procedures

4.1.1 Electron Microscopy

Electron microscopy involves the study of the products of the interaction between an applied electron beam and a solid sample. The type of electron microscopy used will depend on the size of the sample. A bulk sample will require the use of scanning electron microscopy (SEM) while if the sample is a thin foil or a single layer of particles then transmission electron microscopy (TEM) may be used.

A visualisation of the interactions and the material responses with references to SEM and TEM can be seen in figure 4.1. A number of issues must be overcome to enable successful imaging of carbon nanoparticles with electron microscopy. These issues can be separated into those arising from the sample preparation and those arising from the machine itself.

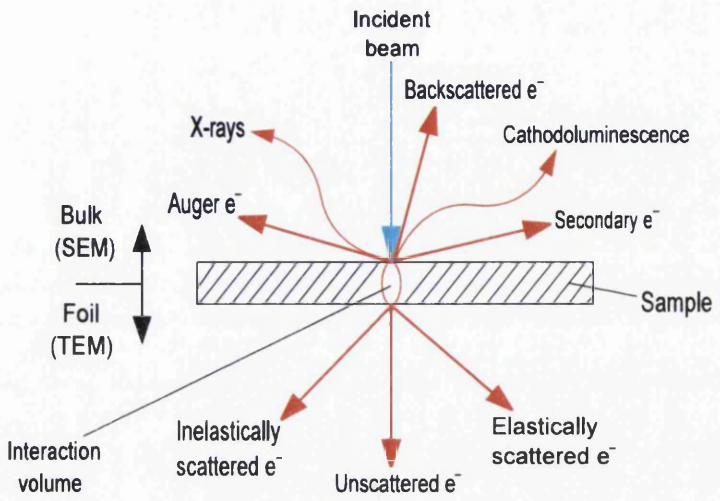

Figure 4.1: *Interactions between an applied electron beam and a solid sample*

The issues arising from sample preparation techniques are primarily due to the selected solvent. The selection of solvents which are compatible with biological materials (critical for the work in this thesis) results in a common problem when samples are viewed under the SEM; residual solvent surface structure. This structure may take the form of distinct crystals or dendritic structures depending on the solvent, but always results in prevention of nanotube location. Examples of residual solvent surface structure are presented below.

Due to these issues, harsher solvents were required. This resulted in the use of ethanol as a solvent for this part of the characterisation process. Another advantage of ethanol is the rapidity of evaporation, reducing the time at which the sample is at risk from external contamination. Sample preparation is discussed in more detail in a later chapter.

4.1.2 Energy Dispersive X-ray Spectrometry

This technique allows the assessment of the composition of nanoparticles through the interaction between matter and a beam of charged particles such as electrons. This interaction causes the release of X-rays. The number and energy level of the X-rays emitted are measured by an energy dispersive spectrometer. These X-rays are released to remove energy allowing electrons

Figure 4.2: *Residual surface structure from biologically viable solvents at varying magnification on the SEM.*

within the element to return to their ground states following excitation by the applied particle beam. The difference between the excitation energy level and the ground state of the electron is a characteristic of the element and will correspond directly to the energy present in the X-ray.

In the case of carbon nanoparticles, this technique provides composition data for diesel particulates and enables assessment of contamination of nanotubes by catalyst materials used in some production methods.

4.1.3 Atomic Force Microscopy

Atomic force microscopy can be used to study the surface topography of nanoparticles and their agglomerates and to provide dimensional analysis. However, it was found to be incredibly difficult to obtain good images using this equipment.

4.1.4 Particle Sizing

The main technique used for particle size analysis for suspensions is scattering spectrophotometry. This method measures light scattered through a set angle

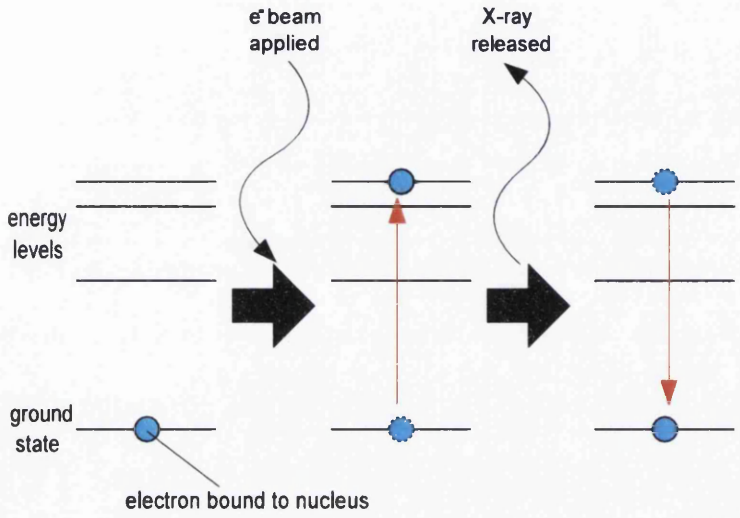

Figure 4.3: *Changes in electron energy states corresponding to particle beam application and x-ray release in EDX analysis.*

as a function of its wavelength. Through the use of a broad spectrum of light, from ultraviolet to infra red, with a wavelength variation of 1100nm to 190nm, it is possible to measure particles in the size range of 5nm to 15μg. The process of measurement relies upon the variance in the amount through which light is scattered due to the size of the particles (Mie scattering).

The uses of this method in respect to this thesis are twofold. Firstly as an assessment of the size of the particles within suspension to ascertain whether the particles are in suspension individually or as agglomerates. Secondly, by taking particle size measurements over a period of time, the rapidity with which the particles agglomerate can be assessed.

However, particle sizing has limited applications to nanoparticles in the case of nanotubes due to the fact that the aspect ratio between the diameter and the length is so massive, and in terms of all nanoparticles, due to the rapidity with which agglomeration occurs. While this may suggest that the technique would lend itself to the assessment of the rate at which agglomeration occurs in various solvents, the risk of blocking the inlet or outlet tubes due to agglomerates severely limits this possibility.

4.1.5 Zeta Potential

Study of the zeta potential enables an assessment of the stability of particles in a suspension. This reflects on the rapidity with which the particles will agglomerate, and therefore how rapidly sedimentation will occur. Interactions between particles and a solvent are dependent on the surface charge of the particles. This surface charge may be a function of the ionic charges at the surface of the particle itself due to dissociation of surface groups, or may be brought about by the presence of ions adsorbed onto the particle surface. The interactions between particles due to surface charge do not occur at the particle surface itself, rather they are felt at a distance. These interactions are a resolution of two forces: attractive molecular forces (Van der Waal's attractions) , V_A; and the repulsive electrostatic BORN forces, V_R. It is the resolution of these forces that is termed the zeta potential.

This potential cannot be measured directly. In order to obtain a value for it, the mobility of the particles is studied. The most common method for this is electrophoresis. This method uses laser doppler velocimetry (LDV) to study the particle migration rate upon application of an electromagnetic field. The elecrophoretic mobility, μ_ϵ, is a function of the particle velocity, v, and the applied electric field, E.

LDV machines utilise two beams, a reference and a 'scattering' beam. Obviously, Brownian motion may result in a smearing of the velocity profile obtained. This is addressed by reducing the angle in which the scattering beam and reference beam cross in the sample vessel to approximately 12°. The electrophoretic mobility is related to the zeta potential through the Henry equation.

$$\mu_\epsilon = \epsilon\zeta\frac{f(\kappa.a)}{6\pi\eta} \tag{4.1}$$

Where ϵ and η are the dielectric constant and the viscosity of the solvent medium respectively, f(κ.a) is a correction factor to take into account the particle diameter and the thickness of the double layer. For dispersions in polar media (water, saline solutions etc.) f(κ.a) is approximately 1.5. This is the Smolochowski approximation and reduces the Henry equation (4.1) to the following (4.2).

$$\mu_\epsilon = \epsilon\frac{\zeta}{4\pi\eta} \tag{4.2}$$

This can be further simplified in practice to the approximation at 25°C:

$$\mu_\epsilon = \frac{\zeta}{12.85} \tag{4.3}$$

In order to remove the effect of Brownian motion on the determined mobility, measurements are carried out both with and without the applied field. This reduces the width of the velocity profile measured in the presence of the field to purely account for the electrophoretic mobility. This peak is then analysed using Fourier transforms to obtain spectra corresponding to particle velocity and zeta potential.

The stability of the particles in the suspension can be broadly characterised by the zeta potential in the following way:

Zeta Potential mV	Suspension Stability
0 to ±5	Rapid Flocculation
±10 to ±30	Incipient Instability
±30 to ±40	Moderate Stability
±40 to ±60	Good Stability
≥±61	Excellent Stability

4.1.6 Transmission Spectrophotometry

Transmission photospectrometry involves the measurement of the percentage of light that is able to pass through a solution or suspension, termed the percentage transmission. It can be used to assess nanoparticle suspensions in a number of ways. Firstly, once a calibration curve has been obtained using set concentrations, concentrations of nanoparticles remaining in suspensions following treatments such as vortexing or filtration can be assessed by comparison between the transmission percentage measured for the sample and the calibration curve. Secondly, the effectiveness of a given medium for keeping the nanoparticles within suspension can be assessed through a timelapse method. This involves taking a number of readings on a sample containing a set concentration over a given time. As the particle agglomerate and sink over time, the transmission percentage will increase. Again, these readings can be compared to the calibration curve to assess the change in the concentration of nanoparticles remaining in suspension.

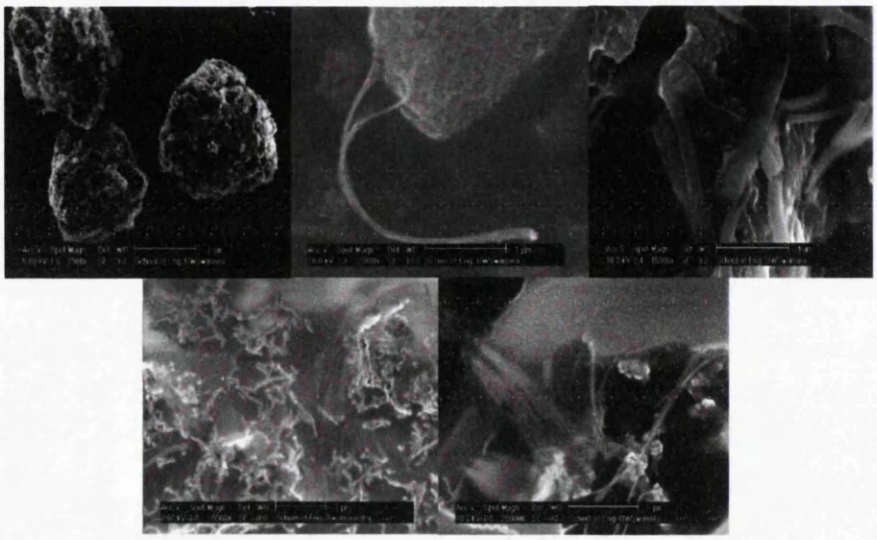

Figure 4.4: *SEM images of the nanoparticles used in this work. Top row L-R; Diesel, As-produced single walled nanotubes, As-produced multi-walled nanotubes. Bottom row L-R; COOH-functionalised single-walled nanotubes, COOH-functionalised multi-walled nanotubes.*

4.2 Characterisation Results

4.2.1 SEM and TEM

Figure 4.4 shows scanning electron micrograph images of the nanoparticles used in this thesis. While the diesel particulates proved relatively simple to image, the location and capture of images of the nanotubes was markedly more difficult.

Figures 4.5, 4.6 and 4.7 show transmission electron micrograph images of the three types of diesel particulates in the blend supplied by Cardiff University. The images were taken by the Cardiff Materials Engineering department.

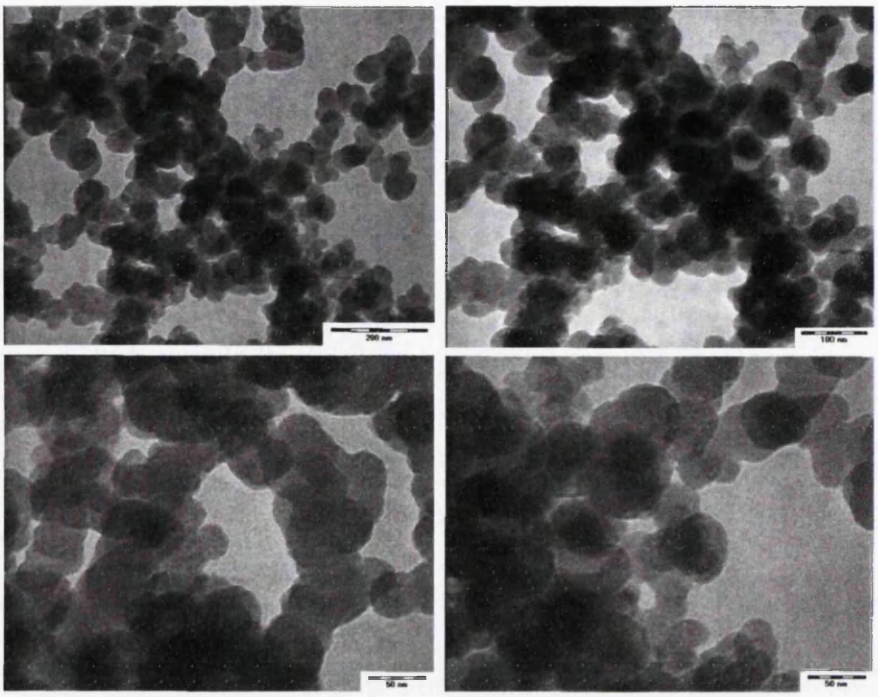

Figure 4.5: *TEM image of combustion derived particulates of standard diesel*

4.2.2 EDX

Nanoparticle	Composition (%)		
	Carbon	Sulphur	Metallic Impurities
Diesel	90	10	0
AP-SWNT	99.9	0	0.01
AP-MWNT	99.9	0	0.01
SWNT-COOH	99.9	0	0.01
MWNT-COOH	99.9	0	0.01

Presented above are the compositional values for the nanoparticles as measured on the EDX. It is important to note however that carbon is not considered to be heavy enough for the EDX to give absolutely accurate values for it. However, in the case of the nanotubes, the incredibly low value for the metallic impurities suggests that the carbon reading can be considered reliable.

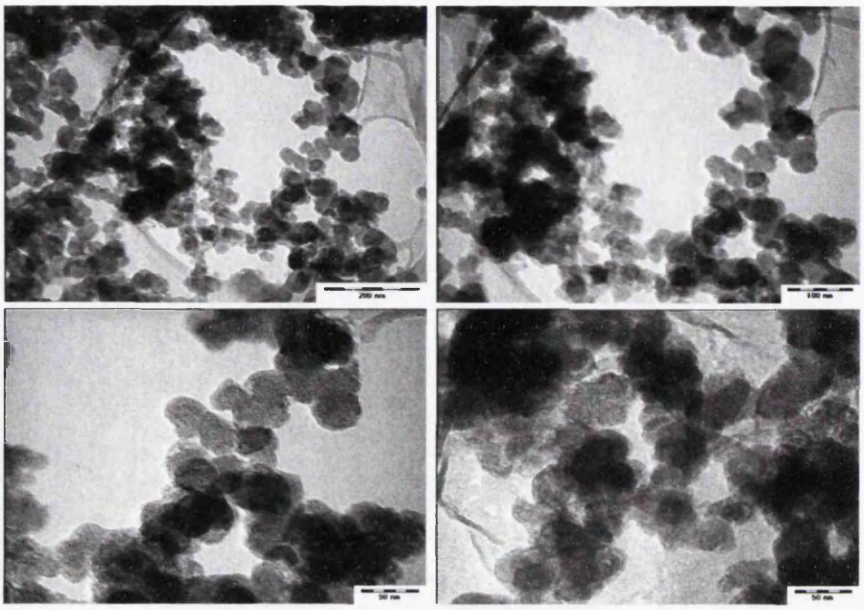

Figure 4.6: *TEM image of combustion derived particulates from bio-diesel*

4.3 Potential Solvents for Nanoparticle Solubilisation

Strictly, the issue of nanoparticle solubility is a misnomer, as the nanoparticles do not dissolve. A more accurate view would be to refer to the resulting blend as a colloidal suspension. This aside, the fluid into which the nanoparticles were suspended prior to their introduction into blood required careful investigation. As discussed in nanotubes section above, getting carbon nanotubes into suspension is incredibly difficult. Standard strong solvents such as ethanol or acetone do achieve results but cannot be considered for this research due to their effects on blood.

As such, the following fluids were evaluated for use: 1wt% sodium dodecyl sulphate; Tyrode's solution; medical saline solution; gelofusine plasma replacement solution; Hartmann's Solution; tris buffered saline; and rpmi 1460 cell culture medium. The fluids were evaluated using the following criteria:

1. Literature usage
2. Ease of solubility

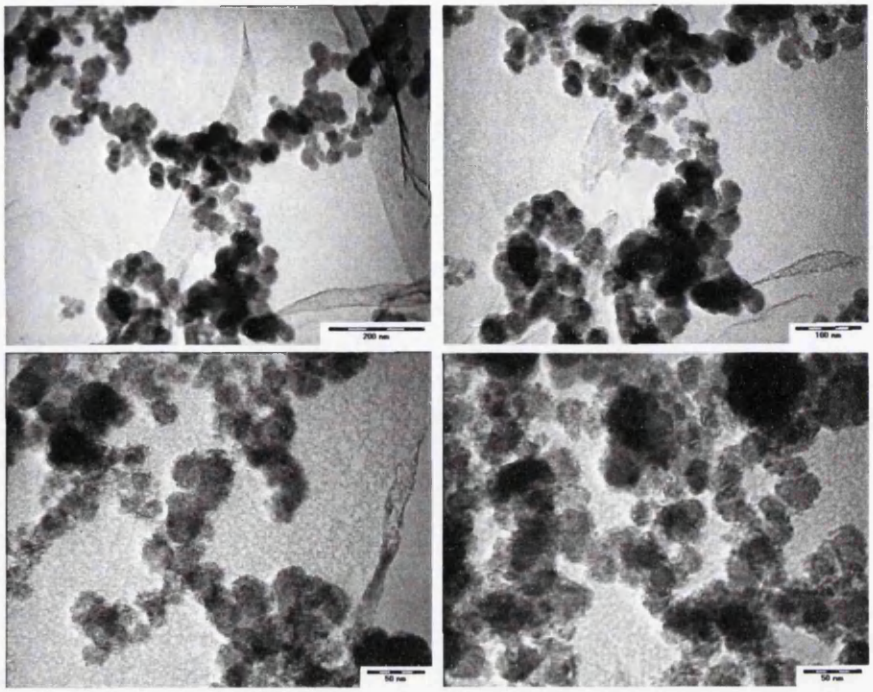

Figure 4.7: *TEM images of combustion derived particulates from red diesel*

3. Effect on blood

4.3.1 Literature Usage

Very few of the solvents used in literature to attempt to achieve a quasi-stable nanoparticle suspension are appropriate for the work in this thesis. The two which can be readily identified as possible solvent candidates are sodium dodecyl sulphate (SDS), which has been used both as a solvent and for nanotube functionalisation, and Tyrode's solution used in the work of Radomski et al. Other solvents were tested following discussion with medical professionals, identified from use in fibrinogen (an important component of blood clots) gelation work undertaken by colleagues or recommended by colleagues working with nanoparticles.

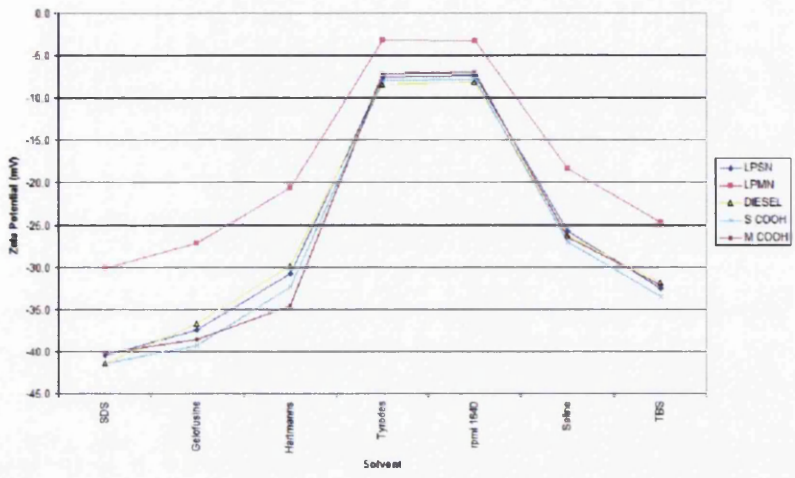

Figure 4.8: *Zeta Potential measurements for each of the nanoparticles when suspended in each of the solvents investigated.*

4.3.2 Ease of Solubility

Zeta Potential Measurements

Figure 4.8 presents the data from the assessment of the zeta potential of each of the nanoparticles in the solvents under examination. As can be seen, a suspension of nanoparticles in either Tyrode's solution or rpmi 1640 is highly unstable leading to rapid agglomeration and either sedimentation or flotation resulting in the rapid removal of the nanoparticles from suspension. Sodium dodecyl sulphate and gelofusine produced the most stable suspensions.

Particle Sizing

The particle sizer was of very limited use for the sizing of individual nanotubes. The results from timelapse experiments showed very good agreement with the results from the agglomeration rate experiments discussed below.

Agglomeration Rate

Figure 4.9 presents the results of a time lapse assessment of each of the potential solvents using photospectrometry. In each case, a suspension of

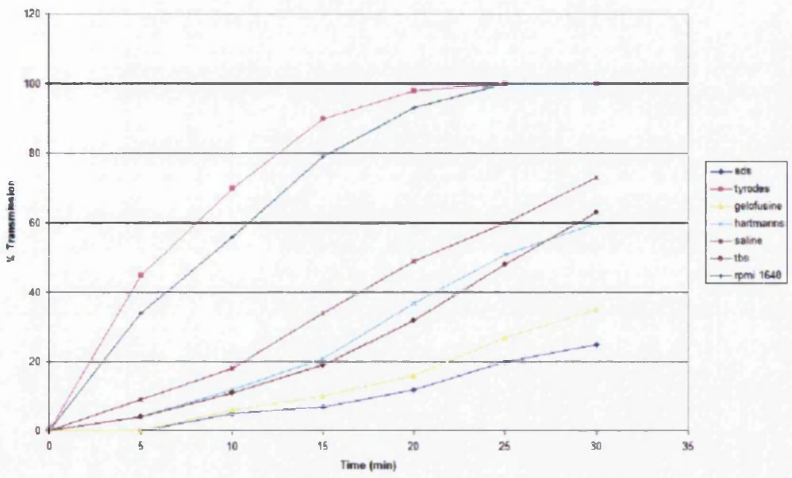

Figure 4.9: *The variance in % transmission in a photospectrometer over time for the solvents under investigation.*

100mg/l was made up with the solvent to be tested. As-produced single walled nanotubes were used for this as they had proved to be the least stable in suspension.

Each sample was made up directly prior to testing and was sonicated for 20s at an amplitude of 60 units. This was done while the sample was immersed in a water bath in order to minimise solvent boil off. Each sample was then placed into the photospectrometer for 30 minutes, with transmission readings taken every 5 minutes. The best results occurred with sodium dodecyl sulphate, used in the literature for solubilisation of nanoparticles, and gelofusine, a plasma substitute suggested by medical colleagues. However, SDS is unsuitable for inclusion into blood as it is a detergent. Gelofusine was found to denature somewhat following sonication and I was advised by medical consultants that it would punch holes in the clot. As such it too was discounted.

Radomski et al utilise Tyrode's solution, a culture medium, as is rpm 1640. It was found that both these solutions were incredibly bad at retaining any nanoparticles in suspension due to the tendency of the particles to flocculate and float very readily. It was very difficult to prepare samples for

the tests above for these two potential solvents.

Medical saline seemed to offer a viable possibility but while it was fairly good at getting nanoparticles into suspension it proved to be very difficult to get good gel point data upon inclusion of even pure saline into blood.

Hartmann's solution is another medical drip solution. Again this was found to be very difficult with which to get good gel points. It was also more difficult to obtain a ready supply of this solution.

TBS was chosen due to it's use in work on fibrin gelation. It performed reasonably well as a solvent, showed no complications with sonication and, importantly, did not inhibit the ease of gel point detection.

4.3.3 Effect on Blood

As sodium dodecyl sulphate is a surfactant and a detergent, it is not suitable for inclusion into blood. Preliminary gel point trials with both Tyrode's solution and the culture medium rpmi 1640 showed that each of the solvents had a marked effect. Both produced much looser gel points that were thus much harder to obtain an accurate phase angle value for.

4.3.4 Conclusions

Tris buffered saline was selected as the most suitable solvent for this thesis.

4.4 Nomenclature

V_A	attractive Van der Waal's forces
V_R	repulsive Born forces
ζ	zeta potential
μ_ϵ	electrophoretic mobility
v	particle velocity
E	applied electric field
ϵ	dielectric constant
f(κ.a)	correction factor for particle diameter and double layer thickness

Chapter 5

Blood

'Once more unto the breach'
Henry V, William Shakespeare

5.1 The Cardiovascular System: An Overview

The cardiovascular system is the means by which bodily tissues can be supplied with fuels and oxygen and the waste products of carbon dioxide and lactic acid can be removed. It also enables the transport of control compounds such as hormones throughout the body.

It can be split into two distinct sections, the pulmonary circulation in which carbon dioxide rich blood is circulated to the gas exchange surfaces of the lungs where the gas is exchanged for oxygen, and the systemic circulation which feeds the body. In the systemic circulatory system oxygen-rich blood is pumped from the heart throughout a network of arteries to the tissues of the body. Oxygen-depleted blood is then carried back to the heart through a network of veins.

5.1.1 Arterial and Veinous Construction

The structure of the arterial and venous components within the cardiovascular system is markedly different. This is due to the nature of the flow within them. Higher pressures are experienced within the arteries requiring a thicker wall containing a larger percentage of elastic and muscular tissue than is found in a comparable vein.

Components of the vessel construction can become triggers of thrombus formation following disruption or injury to the endothelial lining of the Tu-

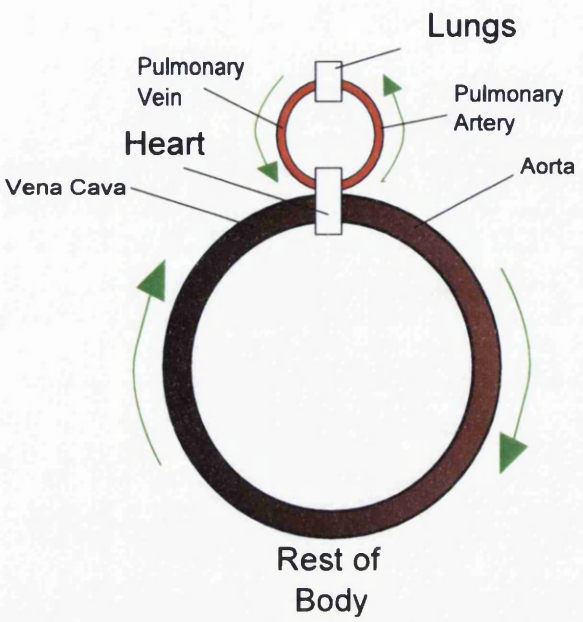

Figure 5.1: *Basic schematic representation of the cardiovascular system.*

nica Intima and the muscular Tunica Media. Injury to these two layers can result in exposure to the collagen fibres which make up the Tunica Adventita. The roughness of these collagen fibres trigger a response from the platelets resulting in the commencement of the clotting cascade described later in this chapter.

5.2 Main Blood Constituents

5.2.1 Red Blood Cells

The red blood cells or erythrocytes (from the Greek, *erythros* meaning red and *kytos* now taken to mean cell although originally meaning hollow) are the gas transport cells within the blood. They are bi-concave in order to maximise the surface area available for gas exchange.

5.2.2 White Blood Cells

Leukocytes are immune system cells which hunt down foreign materials such as bacteria, fungi and parasites in the blood system. There are five distinct types of leukocyte, each of which is focused on the removal of a particular

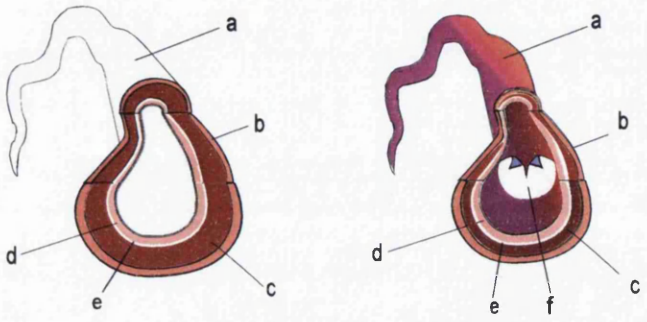

Figure 5.2: *Left, Arterial Structure: a) External arterial wall; b) Tunica Adventita composed of collagen fibers; c) Tunica Media, composed of smooth muscles cells and elastic fibers; d)Tunica Intima, the endothelium that lines the lumen of all vessels; e) elastin sheath. Right, Veinous Structure: a-e are the same as for the artery (note the much thinner Tunica Media); f) Non-return Valve.*

foreign body or bodies. These five are: Eosiniphils, Basophils, Lymphocytes, Monocytes and Neutrophils.

Eosiniphils' primary function is the removal of parasites from the system and are the primary cellular response in allergic reactions.

Basophils are also largely involved in the allergic and antigenic response through the release of the inflammatory chemical histamine.

While more common in the lymphatic system, there are three distinct types of lymphocyte which are found in the blood:

1. Natural Killer Cells

   These are able to directly kill cells of the body which display signal markers designating them as infected or cancerous.

2. B Cells

   The function of the B Cells is the manufacture of the antigens by which the body combats invading pathogenic bodies. A small number of these cells which survive a pathogenic attack will retained the ability to produce the required antigen in order that a level of immunity to a repeated attack is achieved.

3. T Cells

   T Cells have two main functions: the coordination of the immune response; and the ability to kill cells infected with viral parasites or which are cancerous.

4. Monocytes and Neutrophils

   These cells are discussed together as they can both be described as phagocytes. This is due to the way in which they attack and remove pathogens such as microbial infections. This is done by engulfing the invading foreign body (phagocytosis). The difference between the two types of cell lies largely in their lifespan. The monocytes are much longer lived than the neutrophils which are unable to regenerate and thus die after they have engulfed relatively few microbes. In contrast, the monocytes live longer to enable them to fulfill their secondary role; the presentation of pieces of the pathogens to the T Cells mentioned above, in order that a repeated invasion by the microorganisms can be readily repelled.

5.2.3 Platelets

Also known as thrombocytes, the platelets are irregularly shaped cells without nuclei, with a typical lifespan of between 8 and 12 days. They are between 2 and 4μm in diameter and are derived from the products of the fragmentation of megakaryocytes within the bone marrow, with each megakaryocyte fragmentation resulting in the generation of between 5 and 10,000 platelets. This process is regulated by thrombopoietin, a hormone produced by the liver.

5.2.4 Clotting Factors

Blood contains a large number of clotting factors which act at different stages during the coagulation process.

1. Factor I (Fibrinogen)

   Fibrinogen is a soluble non-globular plasma glycoprotein generated in the liver [67]. It is a hexameric molecule consisting of two sets of three different protein chains, α, β and γ. The chains terminate in N-terminals at one end and C-terminals at the other. The α and β chains have small protein molecules, fibrinopeptides (A and B respectively), bound to them. These molecules prevent the spontaneous bonding of the fibrinogen chains to themselves.

   Normal concentration of the protein within blood is between 1.5 and 2.77g/l. The protein is able to form bonding bridges between platelets when in it's natural state by binding to the GpIIb/IIIa membrane proteins exhibited on the platelet surface. Thrombin causes the fibrinogen to cleave and to begin to form an insoluble fibrin mesh, the basis for the thrombus structure. These reaction steps are discussed in more detail later.

   Disfunctionality of the liver can lead to abnormal levels of fibrinogen production or to the production of fibrinogen molecules with abnormal structure leading to reduced activity levels. In either case, this decrease in the levels of viable fibrinogen available causes a reduction in the ability of the blood to form thrombi, resulting in a raised potential for haemorrhage following injury.

2. Factor II (Thrombinogen)

   The gene for thrombinogen is located on the eleventh chromosome. Thrombin, the active form of factor II is the most important of the bioregulation enzymes involved in haemostasis. However it is only relatively recently that this has come to be accepted in both arterial and venous thrombosis. It was widely thought in the 1960s and -70s that an arterial thrombus was of the nature of a primary plug formed due to the action of platelet aggregation alone, exclusive of the rest of the clotting system [68]. In contrast, a thrombus formed within the venous network would more closely resemble a complete clot. Despite attempts

to maintain the importance of thrombin generation within thrombus formation it was not until 1980 that opinions were largely changed due to the publication of a study by Loeliger et al [69]. It has since been shown that thrombin is the most potent of all platelet activators, and activated platelets result in the explosive generation of thrombin which serves to promote secondary haemostasis.

The mechanism by which thrombin activates the platelets was resolved in the work by Vu et al [70]. They showed that thrombin acts upon a trans-membrane molecule within the lipid bilayer of the platelet membrane. The exposed N-terminal of this membrane is cleaved by thrombin, with the resulting new N-terminal acting as a ligand for protein receptor molecule on the platelet surface. This binding enables the transference of a procoagulant protein from the inside of the platelet membrane to the outside. This protein is phophatidyl serine (PS), a procoagulant phospholipid. In common with all other cells, this protein is located on the inside of the plasma membrane of the platelet. It is this fact which prevents intact cells from having procoagulant effects, as opposed to ruptured or lysed cells in which the protein is then able to contact the surrounding plasma. However, the actions of thrombin and collagen enable the translipid migration of the PS protein, causing the intact platelet surface to become an active coagulant. At normal concentrations of the platelets within the plasma, this migration can be brought about through the action of thrombin alone, with any increase in rate due to simultaneous collagen exposure being negligible.

Thrombin, as mentioned above, also acts to cleave fibrinopeptide A (FpA) from the ends of the α chains on fibrinogen molecules. The resulting molecule is termed fibrin I. The new α terminals on fibrin I can then bind to complementary sites on the fibrinogen chains which require no activation. The complexing of fibrin with fibrinogen enables the former to be kept in solution as long as the local concentration does not exceed a critical level. As such, these complexes are termed soluble fibrin. Once the critical concentration is passed the fibrin I molecules will aggregate to form fibrin I polymers. These polymers can then be cross-linked by factor XIIIa which causes isopeptide formation between adjacent α and γ chains.

While a slower process than the cleavage of FpA, thrombin cleaves fibrinopeptide B (FpB) from the terminal of the β chain. Fibrinogen

molecules which have been cleaved at both the α and β terminals are termed fibrin II. Fibrin II will aggregate and form cross-links between polymers in the same manner as fibrin I.

The conversion of fibrinogen to fibrin produces a lattice of strands that is not inert, in that approximately 40% of the thrombin which has been generated within the plasma is bound within the latice. Therefore this bound thrombin cannot be deactivated due to the inabiliy of inhibitors to penetrate through the lattice. As such, the fibrin strands themselves play an additional thrombin inhibitor role. These lattice bound thrombin molecules may then cause further localised thrombosis following the removal of the encasing fibrin strands during fibrinolysis.

Three types of thrombin formed following prothrombin activation have been identified: α-; β-; and γ-thrombin. The latter two are formed following autodegradation of the α-thrombin, and as such have very limited physiological function. This degradation can be brought about by elastase: an enzyme released by activated neutrophils which also serves to degrade the structure of the fibrin clots themselves.

3. Tissue Factor

   This surface glycoprotein is present in platelets, leukocytes and subendothelial tissue, and serves to activate thrombin during the extrinsic pathway of secondary haemostasis [71]. Tissue factor was incorrectly thought to be thromboplastin, a laboratory produced glycoprotein derived from placental blood and used in the prothrombin time (PT) assay, a method for measuring the rate of thrombus formation when the extrinsic pathway was activated. A derivative of thromboplastin was subsequently generated, termed partial thromboplastin and used in the investigation of the intrinsic pathway through an assay termed activated partial thromboplastin time (aPTT). Further study enabled the identification and separation of two components within thromboplastin; phospholipids and tissue factor, both of which are required for the activation of the extrinsic pathway. Investigation of the composition of the partial thromboplastin determined that partial thromboplastin only contained the phospholipid component, thus showing that tissue factor was not required for the activation of the intrinsic pathway.

   When presented on cellular surfaces, tissue factor serves as a receptor of high-affinity to factor VII. Following the binding of factor VII a

complex is formed which serves as a catalyst for the subsequent protease reactions within the coagulation cascade. Tissue factor also exists in a soluble extracellular form, which is no less effective once activated.

4. Calcium

   The calcium ion (Ca^{2+}) is critical as a catalyst for all of the protease reactions that constitute the coagulation cascade.

5. Factor V (Proaccelerin)

   This large soluble plasma protein is critical for haemostasis to occur normally [72]. Indeed, the factor was discovered by Owren in 1943 following the study of a patient who exhibited a bleeding disorder which was unexplainable with the knowledge of coagulation at the time. It was concluded that a deficiency in an activity which affected the rate of conversion of prothrombin to thrombin.

   By the 1940's, improvals in the assays for prothrombin had shown that the two stage theory proposed by Morawitz demonstrated that there were other factors required for the protease reaction initiated by tissue factor which converted prothrombin to thrombin. Factor V was the first of these to be identified[73]. It was termed proaccelerin or labile factor, the latter name referring to its *ex vivo* instability when in storage in plasma and its subsequent absence from blood serums.

   It has since been shown that the catalytic action on the protease reaction resulting in thrombin generation is due to a complex formed between the active forms of factor V and factor X (Va and Xa respectively) on the negatively charged phospholipid surface of the platelets when in the presence of calcium ions. This complex, known as prothrombinase, enables an increase in the rate of generation of thrombin by 300,000 times when compared with the rate of development due to factor Xa alone.

6. Factor VII (Stable Factor)

   The second factor to be identified following the work by Owren. This was initially named stable factor due to the fact that the protein remained stable when in plasma storage and thus was found to exist in high levels in blood serums [74]. However, the identification of the separate actions of factor VII and factor X was not accomplished until Telfer et al in 1956[75].

Once activated, factor VII binds to the expressed tissue factor on the platelet surface when in the presence of calcium ion. The formation of the factor VII-tissue factor complex has two critical results. Firstly, the bound factor VII is far more sensitive to the actions of activating proteases increasing the rate at which it's activation occurs. Secondly, the formation of the complex increases the efficacy of factor VIIa with the respect to the cleaving of factor IX and factor X into their active forms by three orders of magnitude.

Individuals suffering from acute myocardial infarction have been reported to have increased levels of factor VII, although separate reports have stated that factor VII levels do not provide an independent means for the prediction of cardiac events or the formation and progression of atherosclerosis.

7. Factor VIII (Antihaemophilic Factor A)

   Factor VIII is one of the largest of all the coagulation factors, and also one of the least stable [76].

   The critical role of factor VIII in coagulation cascade is evidenced by the severe bleeding seen in any mammal which is deficient. This deficiency is known as haemophilia A.

   Factor VIII has been found to have a marked catalytic effect on the activation of factor X by factor IXa. While this activation can occur in the absence of factor VIII, it is comparatively slow. In the presence of factor VIII however, the rate of the protease reaction is increased 200,000 times.

   This factor is therefore part of a feedback loop within the cascade, for while it is activated by thrombin, it is also activated by factor Xa.

8. Factor IX (Antihaemophilic Factor B)

   Pavlovsky showed in 1947 that the mixing of blood *in vitro* from different patients with haemophilia would occasionally result in the clotting time being brought back within the normal range. This resulted in the identification of two types of haemophilia, stemming from deficiencies in separate clotting factors. Haemophilia B is markedly less common than A and results from a deficiency in factor IX, also known as Christmas factor after the surname of the index patient [77].

Activated Factor IX serves to catalyse factor X activation by the cleaving of a peptide bond within the factor X chain which releases a glycoprotein fragment with an N-terminal. In order for the activation to occur at the required rate, interaction is required between the activated factor IX and platelet surface membrane molecules together with the activated factor VIII. Each of these reactions occur at different regions within the factor IX molecule. Factor IX also has a strong affinity for binding sites on the surface membranes of the endothelial cells which line the blood vessels. Indeed, as the activation of factor IX by either factor VIIIa or factor XIa can occur at these binding sites, resulting in activation of factor X and thrombin generation, they clearly play an important role in the process of coagulation.

9. Factor X (Stuart-Prower Factor)

   The factor X enzyme is critical to both the intrinsic and extrinsic coagulation pathways, in fact it is at this activation step that the two pathways converge [78].

   It is a glycoprotein consisting of both light and heavy chains bound by disulphide bridges. Activated factor IX serves an important role as the main generator of thrombin following the initial burst during primary haemostasis.

10. Factor XI (Plasma Thromboplastin Anticendent)

    Factor XI is a homo-dimeric plasma protein which exhibits a half-life of 52 days. It is part of the intrinsic pathway, serving to activate factor IX. Deficiency of this factor causes the very rare Haemophilia C, a condition in which there is little spontaneous bleeding following trauma, but the potential for rapid fatal blood loss during surgical procedures. The typical concentration of factor XI is approximately 5mg/l, with higher concentrations being linked to thrombosis.

11. Factor XII (Hageman Factor)

    Hageman factor is a plasma protein produced in the liver. It was discovered in 1955 following the assessment for operation of a patient named John Hageman who exhibited clotting times greater than 200s despite having no symptoms of haemorrhage.

    Factor XII serves to activate prekallikrein and factor IX. It is itself activated through contact with a negatively charged surface. Factor XII plays no part in the extrinsic pathway.

Despite the increase in clotting times found in patients who are factor XII deficient, the deficiency poses no risk of haemorrhage as the factor has no direct role in the generation of thrombin. However, deficient patients stand a higher risk of thrombosis. This is due to a reduced activation of fibrinolysis which can lead to fatal embolism.

12. Factor XIII (Fibrin Stabilising Factor)

    This factor circulates within the blood. A protransglutinase molecule which acts in the final stages of coagulation, factor XIII is activated by thrombin and serves to stabilise the forming fibrin clot through the catalisation of intermolecular bonds within the lattice. A large molecule, factor XIII consists of a pair of a and a pair of b protein chains which form a complex with fibrinogen and calcium ion. The cleavage of factor XIII by thrombin produces three distinct molecules determined by the protein chains of which they are constructed. In terms of the thrombi stabilisation, the most important of these is the active a'_2 dimer which is fibrin bound and it is this molecule which begins the cross-linking of the polymerised fibrin strands bound within the clot.

13. von Willebrand Factor (vWF)

    This factor is a multimeric glycoprotein which circulates in a free floating state within the plasma. It forms a non-covalent complex with activated factor VIII. Indeed, vWF serves as a carrier for factor VIII enhancing its stability. In locations where high shear regimes are dominant, it is vWF which enables platelet adhesion by binding to the subendothelial collagen matrix. The factor then binds to the platelet glycoprotein GpIIb/IIIa. The formation of this bond is dependent on the presence of calcium cations and is governed by ADP secreted from the platelets.

5.2.5 Plasma

Blood plasma constitutes 55% of the volume of blood. It is the slightly yellow liquid in which the blood components are suspended and serves as the main transport for all the excretory compounds within the blood including carbon dioxide.

5.3 Haemostasis

Haemostasis is the means by which the cardiovascular system is able to undergo self repair. It can be readily split into two distinct phases: Primary and Secondary haemostasis. While this body of work is mainly concerned with the changes occurring in the blood during the secondary phase, for completeness, the primary phase shall be briefly discussed first.

5.3.1 Historical Developments in Understanding

The observation of the coagulation of blood is recorded in antiquity [79]. The Ancient Greek philosopher Hippocrates stated that the coagulation was brought about by the cooling of the blood once outside the body. It was not until 1627 that Mercurialis reported finding blood clots forming in veins without cooling, although this was largely considered to be impossible, leading to his work being ignored, with the majority of belief being that blood clotted only when not in motion and died upon removal from the body. Other explanations linked to proposed chemical interactions were proposed such as the absence of ammonia of the formation of acid resulting in thrombus formation.

The induction of the clotting cascade by tissues was first reported in 1819 by Thackrah. This was later confirmed by de Blainville in 1834, whose work involved the infusion of a suspension formed of brain matter into animals resulted in the formation of a multitude of widespread thrombi within blood vessels, resulting in the death of the animal. The suggestion that tissues contained a substance (later named thromboplastin) which would directly convert prothrombin to thrombin was put forward by Schmidt in 1892.

The next critical development occurred in 1905, with the proposal of a theory of coagulation by Paul Morawitz based upon the four factors that had thus far been identified. The theory stated that prothrombin could be activated in the presence of calcium and thromboplastin (this was prior to the identification of tissue factor), and that the generated thrombin could convert fibrinogen into insoluble fibrin thus forming a clot.

In 1944 factor V was described by Paul Owren and the following years saw a flurry of activity in the investigation of coagulation resulting in the identification and description of the majority of the remaining coagulation factors. The intrinsic and extrinsic coagulation pathways were proposed in the mid 1950's, dependent on the requirement for tissue factor.

In 1964 Macfarlane et al produced the description of the reactions involved in thrombus generation which is still in use today: a cascade of protease reactions in which each proenzyme is activated by the previous factor.

5.3.2 Primary Haemostasis

This phase of haemostasis is characterised by the adhesion of platelets to the area of vessel damage and their subsequent localised aggregation [80].

Adhesion occurs due to the exposure of the sub-endothelial matrix following damage to the endothelial layer lining the vessel. The mechanism by which the platelets adhere is dependent upon the nature of flow in the area of the damage. If the damage occurs in a region of low flow then the platelets will adhere to local fibronectin and collagen strands exposed from lower layers. If the damage occurs in a region of high flow, then the platelets will adhere to Von Willebrand Factor. In either case, this adherence results in the platelets changing to their activated state.

Following activation the platelets undergo a number of changes resulting in the initial stages of signaling by which aggregation is brought about. These changes result in the platelets becoming increasingly spherical and causes the formation of pseudopods on the platelet surface.

The most important points from figure 5.3 are the release of fibrinogen from the α granules together with the adenosine di-phosphate (ADP) and the seratonin from the dense granules. These are released due to the increased levels of calcium and promote further activation and aggregation of the surrounding free platelets.

The third stage of primary haemostasis is platelet aggregation. At this point the direction of signaling reverses to run from outside the agglomerating platelet structure to the inside. The outside-in signaling is due to the binding of fibrinogen between the platelets causing a cross-linked aggregate. The platelet-platelet aggregation itself is enabled by the $\alpha_{IIb}\beta_3$ receptors in the surface membrane of the platelets. The initial aggregation, termed *primary* aggregation, is reversible and is a direct systemic response to stimulation. Subsequent, termed *secondary*, aggregation includes the secretion of granules from the platelets and cytoskeletal rearrangements of both the platelets and the embedded fibrinogen. This secondary stage of aggregation is irreversible.

Both thrombin and collagen are strong agonists for the aggregation of platelets, causing a rapid local response. ADP and epinephrine are also

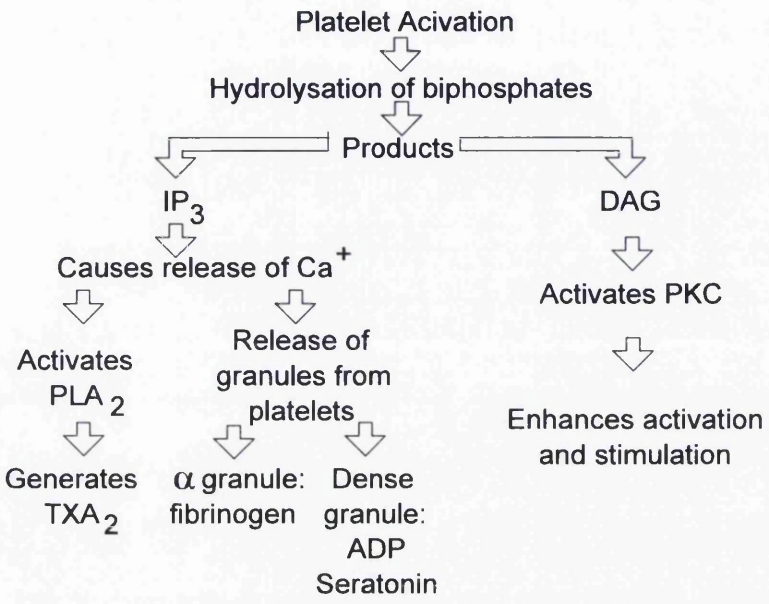

Figure 5.3: *Primary Haemostasis steps following platelet activation. Terms:IP_3 - Inositol triphosphate, DAG - Diacylglycerate, PLA_2 - Phospholipase A_2, ADP - Adenosine diphosphate, PKC - Protein kinase C, TXA_2 - Thromboxane A_2.*

agonists but their effects are much less pronounced.

Haemostatic Balance

This is a means of viewing the manner in which the initial steps of coagulation are regulated in order to remove unwanted thrombi at an early stage [81]. Consider a beam upon a fulcrum. At one end of the beam are the factors which regulate the primary phase of haemostasis. Platelets and plasma factors are the triggers, while antithrombin III, the protein C - protein S complex and heparin cofactor II are inhibitors.

At the other end of the beam are the triggers and inhibitors of fibrinolysis (discussed later in this chapter). Plasminogen activators, both tissue- and urokinase-type, factor XII and fibrin serve as the triggers. plasminogen activation inhibitor, α_2-antiplasmin and histidine-rich glycoprotein acting as inhibitors.

5.3.3 Secondary Haemostasis

Following the formation of the initial platelet plug, secondary haemostasis involves the formation of the complete thrombi, together with the mechanisms by which the rate of thrombosis is controlled. A number of pathways may be followed in the formation of the clot depending on the nature of the activation: these are the intrinsic and extrinsic pathways. The method by which the clot is formed and the rapidity of thrombosis is regulated can most easily be shown through the use of a diagram of the coagulation cascade process presented in figure 5.4.

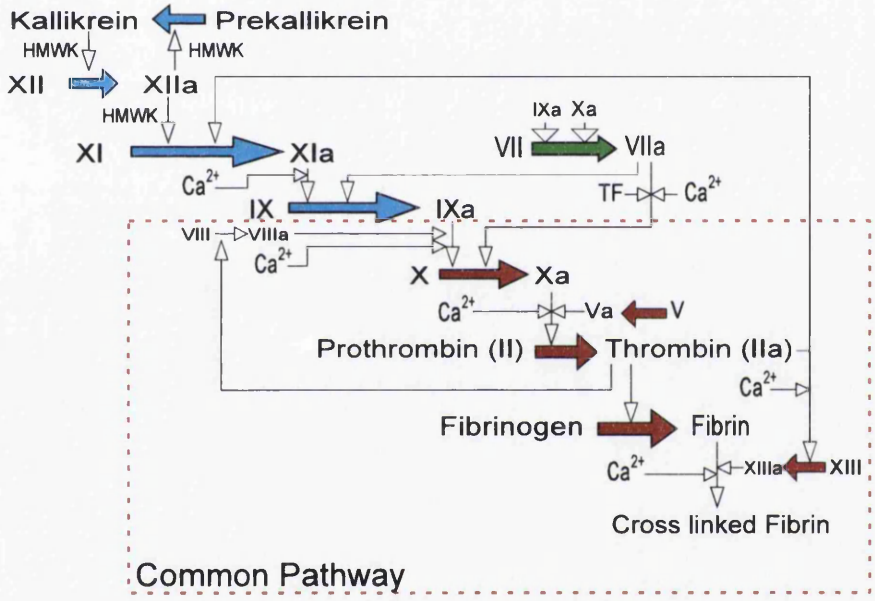

Figure 5.4: *Secondary Haemostasis cascade reactions leading to clot formation. Blue arrows refer to the intrinsic pathway, while green refer to the extrinsic pathway.*

Intrinsic Pathway

This pathway is dominant in the case of any external stimulus such as that due to removal of blood from the body. The fact that thrombi can spontaneously form following the removal of blood from the body suggests that all necessary components for haemostasis are contained within the blood. It is thought that the intrinsic pathway is started by the activation of factor XII through contact with activators such as negatively charged surfaces.

Extrinsic Pathway

This pathway is initiated by the presence of raised levels of active factor VII and presented cellular Tissue Factor. Normally, only 1% of all factor VII is present in the active form. Together with presented Tissue Factor, activated factor VII serves to activate factor factors IX and X. The main role for the factor VII/tissue factor complex is to enable the generation of sufficient levels of factor Xa that small amounts of thrombin can be created.

Generated thrombin begins the activation of platelets, however further Xa production is limited by Tissue Factor Pathway Inhibitor (TFPI). TFPI and antithrombin are much less efficient at inhibiting the generation of factor IXa which is then able to diffuse through the plasma to the platelet surface where the main process of thrombin generation occurs.

High concentrations of Tissue Factor bearing cells are found in the Tunica Adventitia. Blood borne Tissue Factor is also generated in order that thrombus growth is not halted when the original area of vessel wall in which Tissue Factor was exposed has been covered.

Common Pathway

The common pathway begins with the formation of a complex containing calcium, thrombin, cofactor Va and factor Xa on the negative platelet surface. This complex is called prothrombinase. This complex results in the cleaving of prothrombin, which causes the release of thrombin into the surrounding area. This reaction is limited by the availability of factor Xa. The thrombin then acts upon the soluble fibrinogen to fibrin monomers by removal of the fibrinopeptides FPA and FPB. These monomers then form long fibrin strands which may be branched following polymerisation at the FPB site. This branching enables cross linking between the fibrin strands to occur. The resulting mesh is able to trap blood cells and thus cover vessel damage.

The structure of the fibrin network which is formed is highly dependent on the conditions under which it formed. A fine network comprising a large number of fine fibrin strands is far more rigid than a network composed of thick fibrin strands encompassing larger liquid filled voids within it. This is of importance due to the fact that men suffering from myocardial infarction at a young age have been found to form finer, more rigid fibrin clots *in vivo*. These finer clots have been shown to be far more difficult for the body to break down through fibrinolysis, despite the fact that thin fibres can be cleaved more rapidly than thicker ones, the massively larger numbers of the

fine fibres in clots of comparable size require a much longer lysing time.

It is important to note that only 15% of the thrombin available acts upon the fibrinogen; suggesting the importance of thrombin through a number of points within the cascade. It is also suggested that due to the fact that only 35-40% of FPA is released the majority of available fibrinogen at the clotting site is trapped within the initial thrombus. This is backed up by an 80% reduction in the levels of fibrinogen within the blood plasma.

5.3.4 Clot Retraction

The retraction of the thrombus occurs once it's formation has been completed. There are three major reasons for the desirability of retraction: firstly, retraction aids in concentrating the plug to the damaged area; secondly it enables the edges of the wounded area to be drawn together and finally it aids in the opening of an otherwise occluded vessel to flow.

Retraction is mediated by the platelets and is highly dependent on the platelets binding to the polymerising fibrin strands. The platelet binding is in part regulated by the glycoprotein IIb/IIa receptor which forms a link between the fibrin strands and the network of actin and myosin which forms the cytoskeletal structure of the platelets.

5.3.5 Fibrinolysis

Once the damaged section of the vessel has been repaired it is imperative that the clot can be readily removed. The removal is carried out by the fibrinolytic system which utilises plasmin to degrade the fibrin network into fibrin degradation products (FDP) and D-dimers.

The term stems from the earliest studies into the breakdown or lysis of thrombi when it was thought that the action of plasmin was limited to the lysing of fibrin in circulation. As discussed above, the haemostatic and fibrinolytic components in a state of mutual compensation. This is maintained in terms of fibrin through the binding of tissue plasminogen factor (tPA), plasminogen and α_2-antigen onto the surface of the fibrin molecule itself. The complex formed from these fibrinolytic precursor enzymes produces plasmin which then causes the cleavage of fibrin through a hydrolytic reaction.

Control and regulation of the fibrinolytic system has been widely linked to tPA. This protein is synthesised in the endothelial lining of the blood vessels.

Once released into circulation however, the protein has a very short half life of only a few minutes. Indeed, if an individual responds poorly to stimuli, such as venous occlusion, which would normally result in a marked increase in localised tPA concentrations within the blood, then they are likely to be at far greater risk from Deep Vein Thrombosis.

5.4 Flow Pattern Complications

Localised changes in the nature of the flow throughout the cardiovascular system can lead to the generation of undesired and potentially harmful thromboses [82]. The means of generation is dependent upon whether the vessel in question is an artery or a vein.

5.4.1 Atherosclerotic Plaques

These plaques are preferentially formed at points in the arterial vessel network such as bends and bifurcations. This is due to the nature of the flow in these locations, which results in eddy formation and other low flow regimes resulting in the adhesion of both leukocytes and platelets to the vessel wall, together with wall penetration by lipoproteins.

The lesions typically begin as accumulations of macrophages that have taken up the low density lipoprotein once it has been oxidised. These are found in some children prior to the age of 1 and in all children after the age of ten. These deposited macrophages become known as foam cells once they have accreted a certain amount of cytoplasm. Upon the death of the foam cells, the release of the cell contents causes the attraction of further numbers of macrophages resulting in the formation of an extracellular lipid core within the growing plaque. In contrast the outlying plaque regions become increasingly calcified and exhibit a greatly reduced metabolic function as the lifetime of the plaque increases.

The swelling itself is not directly on the internal surface of the artery but rather in between the Intima and Media layers. As the size of this swelling increases, the arterial tissue will undergo stretching in order that the internal bore of the vessel can remain as unchanged as possible. This stretching can continue until the point where the plaque constitutes 50% of the cross sectional area of the arterial wall.

Once the ability for the artery to expand at a rate matching the growth of the plaque is exceeded, narrowing of the area available for flow will begin

to occur. This will result in localised areas of high shear in the region around the narrowing potentially causing the plaque to rupture. The occurrence of a rupture in the endothelium separating the plaque growth from the blood flow results in the initiation of a rapid platelet and hence clotting response. However, the rupture may result in a shower of debris being ejected into the blood stream.

The narrowing of the artery due to the clot formed over the rupture causes a further degree of localised high shear and narrowing of the available flow area. However the more dangerous region is now the area of localised low shear downstream from the plaques. Eddy formation in this region results in the formation of strong secondary fibrin clots which are rich in red blood cells. The low flow regimes can also result in the deposition of debris in smaller vessels locally causing further blockages. The combination of these complications can result in the complete occlusion of the arterial vessel resulting in the loss of blood flow to regions after the location of the plaque. This is the principal cause of myocardial infarction (heart attack).

This is not the sole danger posed by the formation of atherosclerotic plaque. If the arterial wall is caused to stretch to between 2 and 3 times its original size to accomodate the growing plaque the elastic tissue in the vessel walls can become increasingly weak. At this point even the minor pressure increase due to the pulse can cause a rupture of the vessel leading to a potentially fatal haemorrhage. The atrophy of the muscular support in the Medial region of the wall can result in the formation of an aneurysm where the vessel balloons out at the weakened region resulting in massive localised pressure on the surrounding tissue.

It has been postulated that atherosclerotic plaques may be generated due to oxidative stresses on the cell wall, possibly caused by the presence of foreign nanoparticles (such as diesel particulates or carbon nanotubes) within the blood.

5.4.2 Deep Vein Thromboses

These develop most often in the areas of eddying flow directly after the venous valves. This flow pattern can cause the aggregation of platelets within the valve 'pockets' resulting in the initiation of coagulation.

They can become particularly dangerous in the small, deep veins (hence the name) where an expanding thrombus may become lodged. This can

result in death largely due to the separation of all or parts of the thrombus from the initial generation site, followed by their lodging in the pulmonary system resulting in pulmonary embolism.

5.5 Procedures for Haemostasis Analysis

The work in this thesis involves two systems which are used for the clinical analysis of haemostasis; the Thromboelastograph (TEG) and the Sonoclot.

5.5.1 Thromboelastograph

Thromboelastography was first conceived following the 1^{st} World War. In the intervening years it has been developed as a clinical tool for the diagnosis of pro-coagulant states as well as the assessment of coagulation function in patients following major trauma such as serious injury or surgery.

The TEG machine utilises a cuvette heated to 37°C which is filled with 360μl of blood (work has been carried out on both whole and citrated blood). This cuvette is oscillated through an angle of 4° 45' over a period of 10 seconds to provide a low shear regime which resembles sluggish venous flow. A pin, freely suspended in the cuvette from a torsion wire, is monitored for motion.

As the fibrin strands form, the motion of the cuvette is coupled to the pin, causing a transfer of torque. The rate of the formation of the clot together with the clots' strength affect the motion of the pin. The electrical signal generated by the coupling is amplified to generate the TEG trace. The deflection of the trace from the baseline increases as the strength of the clot increases and decreases as the clot is lysed.

However, false readings can be generated due to the nature of the force which the TEG applies, which results in a stress that is outside the linear viscoelastic range of blood. Due to the fact that the applied torque is constant, this can lead to false lysis readings due to separation of the clot from either cuvette or pin surface during retraction, or to an increase in measured clotting times as the growing fibrin strands may be sheared apart.

Variables Measured

1. *r* time

   This is a measurement of the period of latency taken from the commencement of the test until the deflection of the plot is 2mm. The

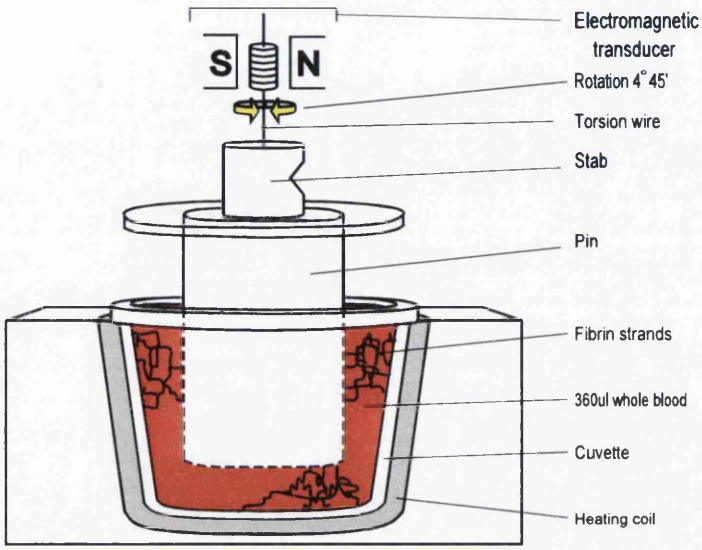

Figure 5.5: *Simple schematic of the thrombolestograph bob and cup system.*

normal range for the r time is between 15 and 23 minutes.

The value of the r time may be increased due to defficiency in clotting factors, the addition of anticoagulants into the blood or by cases of severe hypofibrinogenaemia of thrombocytopenia.

The r time is decreased in patients with hypercoagulability syndromes.

2. k time

   The k time is the time taken after the detection of the initial fibrin to achieve a defined level of clot strength equivalent to a clot amplitude of 20mm. The normal range for the k time is between 5 and 10 minutes.

   As with the r time, the k time will be increased in patients with a deficiency in clotting factors, hypofibrinogenaemia, thrombocytopenia and also thrombocytopathy.

   Values for the k time are also reduced in patients exhibiting hypercoagulability.

3. α angle

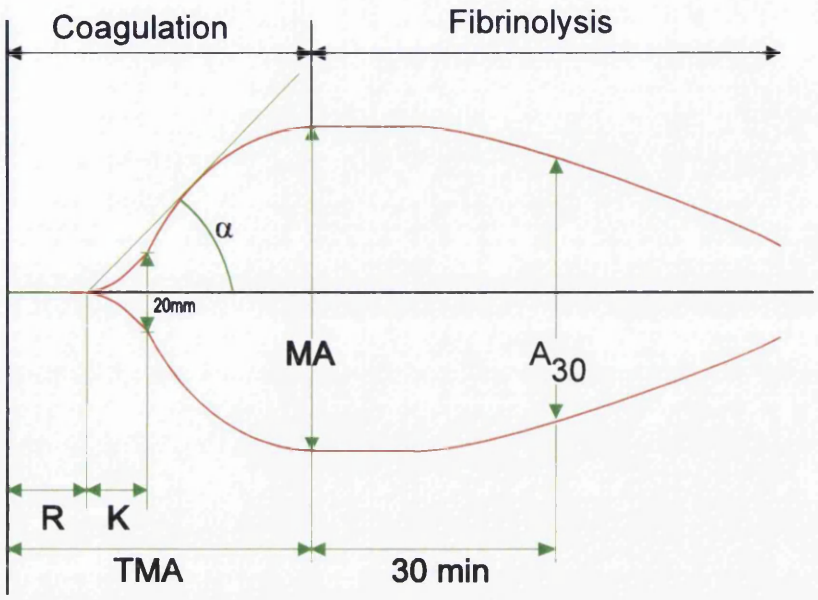

Figure 5.6: *An example of a TEG plot of haemostasis showing the points at which values are recorded*

The α angle measures the rapidity of the build-up of the fibrin clot and the level of cross linking as this relates directly to clot strength. It's normal range is between 22° and 38°.

The α angle is increased in individuals exhibiting hypercoagulability and decreased in patients with hypofibrinogenaemia and thrombocytopenia.

4. Maximum Amplitude (MA)

   The maximum amplitude value is a direct function of the maximum dynamic properties of the bonding of fibrin and platelets through the GpIIb/IIIa receptors and represents the ultimate strength of the clot formed. It correlates to platelet function as 80% of the clot consists of platelets. The normal range for the MA is 47 to 58mm.

   It is again increased in cases of hypercoagulability and decreased in cases of thrombocytopenia, thrombocytopathy and hypofibrinogenaemia.

5. LY_{30}

LY_{30} refers to the percentage of lysis which has occured 30 minutes after the clot has reached maximum amplitude. It is calculated using the following formula:

$$LY_{30} = \frac{MA - A_{30}}{MA} \tag{5.1}$$

Where A_{30} is the amplitude 30 minutes after maximum amplitude has been reached. The normal range is $\leq$7.5%.

The variables which the TEG system records are illustrated in figure 5.6.

Explanation of Disorders Mentioned

Thrombocytopenia refers to disorders which result in a reduced platelet count due to the fact that platelets are lost from circulation at a higher rate than they can be replaced.

Thrombocytopathy refers to disorders in which platelet function is reduced or compromised.

Hypofibrinogenaemia is a deficiency in levels of fibrinogen in blood. This deficiency may be congenital, due to liver disease or brought about following complications in pregnancy. While the normal fibrinogen range is between 1.5 and 2.77g/l, clotting deficiencies only occur when the concentration has dropped below the threshold of 750mg/l.

5.5.2 Sonoclot

The Sonoclot was developed by Sienco in 1986. The mechanical components of the machine consist of: a 360μl cuvette, which is maintained at 37° prior to the addition of blood by the use of the top of the machine as a pseudo hot plate; a disposable hollow cylindrical probe; and an electronic oscillator.

The probe is affixed to the oscillator and lowered into the blood sample. The probe is oscillated over a 1mm distance at a rate of 200Hz. The machine then monitors the impedance of the oscillation in order to determine the development of the clot.

No reason has been found by the author for the selection of the frequency or range of the movement, certainly the operating parameters are outside the linear viscoelastic range for whole blood.

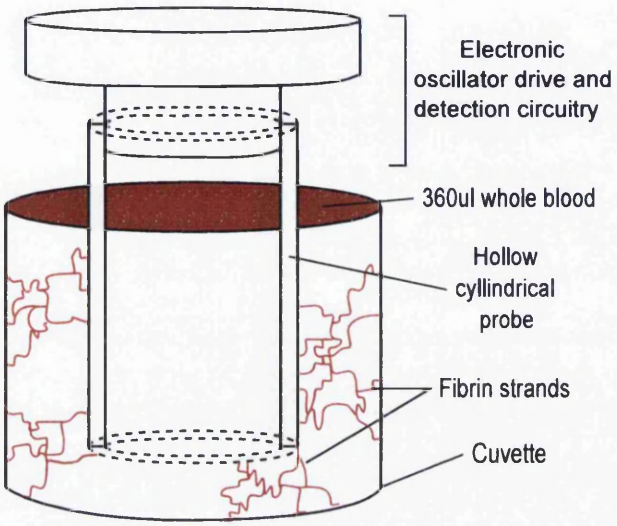

Figure 5.7: *Simple schematic of the Sonoclot system.*

The Sonoclot presents the results through a graphical display. The presented curve as shown in figure 5.5.2 can be split into four distinct sections:

1. Liquid Phase: this phase ends at the point at which thrombin generation within the blood sample causes initial fibrin strand formation resulting in the sample viscosity beginning to increase rapidly.

2. Clot Rate: The slope of the signature during fibrin formation together with the final value of the signature when the gel formation is complete enable the rate of fibrin formation to be assessed.

3. Clot Retraction: This phase can be split into two. The first is characterised by the upward slope which corresponds to the retraction of the clot, while the second phase involves the clot pulling away from the surfaces of the sonoclot and is characterised by the downward slope after the final peak.

4. Time to Peak: While not strictly a distinct phase unlike the three listed above, this measurement provides a useful means of assessment for clot retraction, and can be used to determine platelet function. In general, the faster the time to peak, the greater the platelet function.

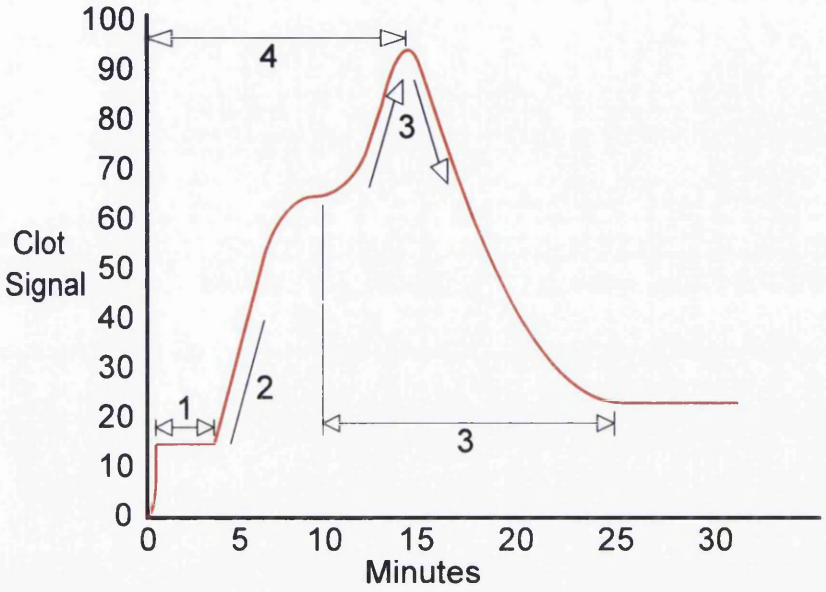

Figure 5.8: *A typical example of a Sonoclot trace.*

The frequency of use of the sonoclot in literature is much lower than that of the thromboelastograph and the validity and relevance of results is somewhat debated.

The first investigation of a calibrated version of the machine was undertaken by Chandler and Schmer [83] who found it to be a useful technique for providing information on the viscosity of whole blood and plasma. This was followed by an investigation by Hett et al who reviewed the operation and performance, determining that while the sonoclot could provide useful data on platelet function, further testing was required before the machine could be adopted for clinical use.

McKenzie et al [84] discussed the sonoclot with reference to the other systems available for clinical use. They highlighted two main advantages with the system: its' high level of convenience due to the small size, both of the machine and the volumes of sample required, and the short time required for the procedure; and the ability to immediately infer the location of the abnormality within the clotting cascade through changes in the plotted output curve. They also highlighted a pair of disadvantages in the potential for subjective analysis of the results curve and the lack of supporting evidence for physical correlation.

Following studies undertaken by Tucci et al [85] it was found that the Sonoclot glass bead activated test could reliably detect inhibition of the glycoprotein IIb/IIa receptor by tirofiban in unheparinised whole blood. Miyashita et al [86] were able to show that approximate platelet function can be assessed through the investigation of the time to peak value on the Sonoclot. The time to peak was found to be predicted by the platelet count, whole blood platelet aggregation measurement and the fibrinogen level.

5.5.3 Rheological Techniques

The techniques utilised in this thesis are discussed in Chapter 1.

5.6 Rheology of Blood

The rheological properties of blood are extremely difficult to accurately quantify due to the continuing interaction between the cellular and molecular species which it contains and the fact that the system is sensitive to any disturbances or external stimuli. Theoretical calculation of properties *in vivo* is almost impossible due to the pulsal nature of the flow and the nature of blood vessels themselves.

Blood rheology has an impact upon the location and nature of thrombi formed within the circulation.

Chapter 6

Hypothesis

1. The addition of any of the nanoparticle types into whole blood will have a prothrombotic effect. This will become increasingly marked as the concentration of nanoparticles is increased.

2. The Carboxyl functionalised Nanotubes will have a greater prothrombotic effect as they will be able to disperse more readily throughout the blood sample due to their increased solubility.

3. The relatively insoluble nature of the as-produced nanotubes may result in their being less well dispersed and thus the effects of the contact activation due to them being confined to a much smaller region of the blood sample resulting in a reduced prothrombotic effect.

4. As the diesel samples exhibit a solubility between the functionalised and as-produced nanotubes it is expected that the prothrombotic response from the blood will lie between the two extremes above.

Chapter 7

Materials and Methods

7.1 Nanoparticles Used

The following nanoparticles were used in this work: Blended Combustion Derived Diesel Particulates (red, bio- and) provided by Cardiff University Mechanical Engineering Department; As-produced Single- and Multi-walled Carbon Nanotubes provided by SES Research (as used by Radomski et al); Carboxyl functionalised Single- and Multi-walled Nanotubes provided by Cheap Tubes.

7.2 Sample Preparation

7.2.1 Concentrations

Following initial gel point studies it was found that a 5% spike of the desired nanoparticle solution into freshly drawn whole blood provided the best results. As such it was required that the concentration of nanoparticles in suspension be 20 times greater than the desired final concentration once added to blood. The final concentrations investigated of nanoparticles per litre of whole blood were 0.01g, 0.005g, 0.001g, 0.0005g and 0.0001g.

7.2.2 TBS Preparation

TBS was prepared as required from a stock solution of 10 times standard concentration. This was diluted using de-ionised water.

7.2.3 Addition of Nanoparticles

The required amount of nanoparticles was carefully weighed using an analytical balance. 10ml of TBS was then decanted into a vial using a pipette. The vial was placed in a water bath set to 15°C. The nanoparticles were added in small increments. Following each addition of nanoparticles the sample was sonicated for 15 seconds at an amplitude of 60 units.

The water bath was used to cool the sample in order to provide some mitigation of the boil-off of the solvent, caused by the heat generated by sonication thus enabling the maintenance of accuracy in the final sample concentration.

The samples were used as soon as possible due to the fact that TBS denatures over time when at room temperature. Cold storage was not appropriate as this caused all nanoparticles to agglomerate and thus be removed from suspension incredibly rapidly.

7.2.4 Final Treatment

Prior to the drawing of blood, the desired sample of nanoparticles was sonicated for 30s at an amplitude of 60 units. 0.7ml was then drawn off and decanted into a vial.

7.3 Blood Collection

All drawing of blood was taken from healthy volunteers and performed by a trained phlebotomist from the Accident and Emergency department of Morriston Hospital. Blood was drawn using a 21G standard bevel hypodermic needle affixed to a 20ml syringe. 15ml of blood was drawn for each complete experiment.

Once the blood had been drawn, the final 1ml was discarded. The remaining 14ml of blood was gently injected into the vial containing the nanoparticle suspension. The vial was then sealed and then gently inverted 4 times in order to mix the nanoparticle sample into the blood and also to ensure that the blood cells were evenly spatially distributed.

7.4 Experiments Run

7.4.1 Oscillatory Rheometry

Upon arrival each day and between each experiment the geometry was removed from the G2 machine and cleaned using soap and water to remove any surface contaminants that may have accumulated. The geometry was then dried using lint-free material. Once dry the geometry was reassembled and placed back in the machine. The G2 uses a 'smart-swap' programme to identify the geometry upon attachment. Following this identification the geometry was then rotationally mapped using 4 iterations to enable accurate assessment of the inertia of the geometry.

Once this was completed a specifically designed oscillation procedure was selected. This procedure utilised the following frequency sweep: a 0.200Hz base frequency followed by oscillations at 0.4309Hz, 0.9283Hz and 2.000Hz. Temperature within the geometry was maintained through the use of the inbuilt water bath.

7.4.2 TEG

Prior to any experiments being run, quality control tests were run on each of the two channels of the TEG machine. 365μl was transferred via pipette from the bulk sample into a TEG cup mounted in the machine. This cup was then raised and the experiment begun. All TEG samples were run until a value for lysis after 30 mins (LY30) had been recorded.

7.4.3 Sonoclot

A non-activated test cuvette was removed from the packaging and placed into one of the holders in the heating unit which makes up the top surface of the Sonoclot in order to bring the cuvette to blood temperature prior to the experiment commencing. While the cup was being heated a quality control (QC) test was run using a QC cuvette, a fresh probe and the provided QC oil. This was run using the inbuilt QC test programme on the Sonoclot.

Once the QC test had been successfully completed, the QC cup was disposed of and the probe removed and replaced with a fresh one. The appropriate test regime was then selected from the inbuilt list on the Sonoclot machine. The metal stirring rod was removed from the Sonoclot cuvette by inverting the cuvette and gently tapping it against the top surface of the

Sonoclot. This was done to ensure that the contact activation caused by the presence of the stirring rod was removed. The cuvette was then placed in the holder.

Once the blood had been collected and added to the nanoparticle suspension, 3.65μl was drawn off using a pipette and gently injected into the cuvette. The test was then run following the instructions provided by the manufacturer. Upon completion of a test, measured values were recorded and the used probe and cuvette were removed and disposed of.

7.4.4 Order and Timing

The order in which the machines are listed above was the order in which the samples were placed in to the machines. Total time from commencement of drawing of blood to the starting of each of the tests was as follows: G2 - 40 seconds, TEG - 50 seconds, Sonoclot - 50 seconds.

7.5 Safety

For all steps involving the handling of nanoparticles both in and out of suspension, and all work undertaken on blood, nitrile gloves were worn and all appropriate laboratory safety precautions were followed. All sharps were disposed of in a specific sharps container provided by Morriston Hospital. All contaminated materials (gloves, syringes, vials etc) were disposed of using the biohazard bin also provided by the hospital. Prior to commencement of experiments and upon completion, all surfaces were cleaned with alcohol wipes.

Chapter 8

Results from As-Produced Single Walled Nanotube Experiments

The results for tests on AP-SWNT presented in figure 8.1 show a random scatter of points in a band between 63 and 72°, with an average of 67.5° corresponding to an average fractal dimension of 1.67. While the values recorded for the concentrations are elevated when compared to those for untreated whole blood, and markedly higher than the baseline control value provided by the pure TBS spike in whole blood, the other values show very little variance, preventing any clear conclusions from being drawn.

Both the gel time and G' data (figures 8.3 and 8.4 respectively) show a peak at 0.001g/l. In the case of the gel time plot 0.001g/l is the only concentration at which the recorded gel time of 312 seconds is greater than the baseline whole blood and TBS value. In the case of the G' data, the peak value is 375 Pa. All of the G' values are raised in comparison to the baseline value. This suggests that the inclusion of the nanotubes within the clot results in a more elastic structure. These peaks are not seen in the data from the TEG or Sonoclot machines.

Both the r-time and k-time plots (figures 8.5 and 8.6 respectively) show downward trends with increasing nanotube concentration. The r-time values halve over the range, falling from 12 minutes at 0.0001g/l and 15 minutes at 0.0005g/l to a minimum of 7.3 minutes at 0.01g/l. This is still over 120 seconds longer than the maximum gel time recorded on the G2, highlighting the difference in sensitivity between the two systems.

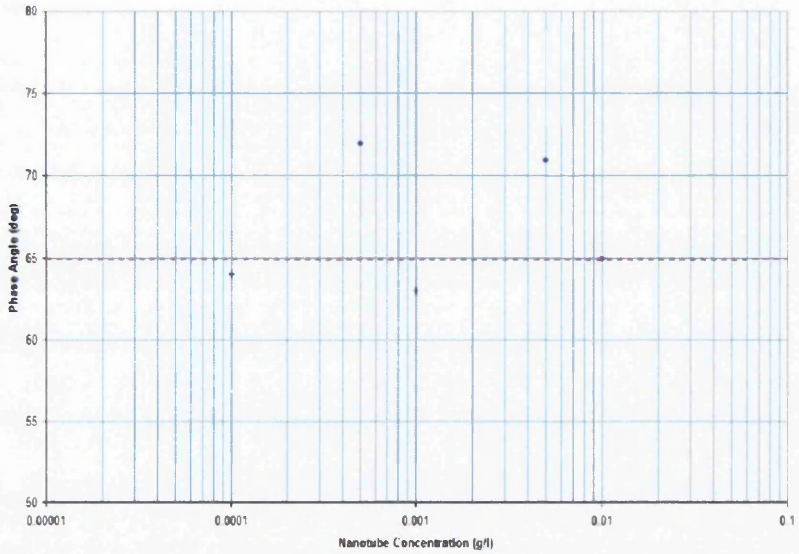

Figure 8.1: *Variance in Phase Angle δ of whole blood with 5% spike of As-produced Single Walled Nanotubes in TBS. The dashed red line indicates the value recorded for whole blood with a 5% spike of pure TBS.*

The reduction in both r- and k-times suggests a prothrombotic state resulting in more rapid clot formation. This is supported by an increase in α angle (figure 8.7) from 39.3° to 53.4°, which points to rapid initial clot growth.

The data for both Maximum Amplitude and Lysis Percentage at 30 minutes show no obvious trends, suggesting that the inclusion of nanotubes within the structure has very little effect on the resulting clot dimensions and does not inhibit the fibrinolytic process.

The decrease in clotting time as shown by the TEG r-time data is partially supported by a decrease in the Activated Clotting Time recorded on the Sonoclot. In the case of this data, the value corresponding to the lowest concentration is 124 seconds greater than that for a pure TBS addition (572 seconds compared to 448 seconds), suggesting that low concentrations inhibit the clotting process. Indeed, only the two highest concentrations (0.005g/l and 0.01g/l) exhibit ACT values below that of the baseline at 430 seconds and 394 seconds. Again, these values are still over 100 seconds greater than the gel times recorded by the G2.

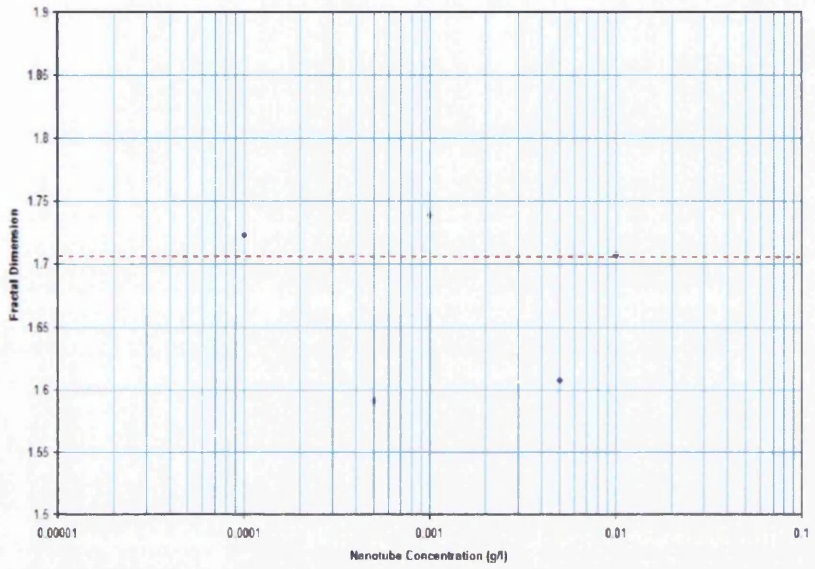

Figure 8.2: *Variance in Fractal Dimension of whole blood with 5% spike of As-produced Single Walled Nanotubes in TBS.*

The increasing rapidity of the clot growth as shown by the trends in the k-time and α angle recorded by the TEG is supported by an increase in the Sonoclot Clot Rate parameter (figure 8.11). The increase is not linear however, with a peak of 4.6 occurring at 0.001g/l.

The Platelet Function data shows a clear increase from an initial of 1.6, equal to that of the pure TBS addition, to a value of 2.6 at the two highest concentrations. This would suggest the prothrombotic effect of the nanotubes is increased with concentration. Due to the nature of the platelet activation taking place (contact - intrinsic pathway) this would be expected as an increase in particle concentration would result in an increase in the surface area available for the activation.

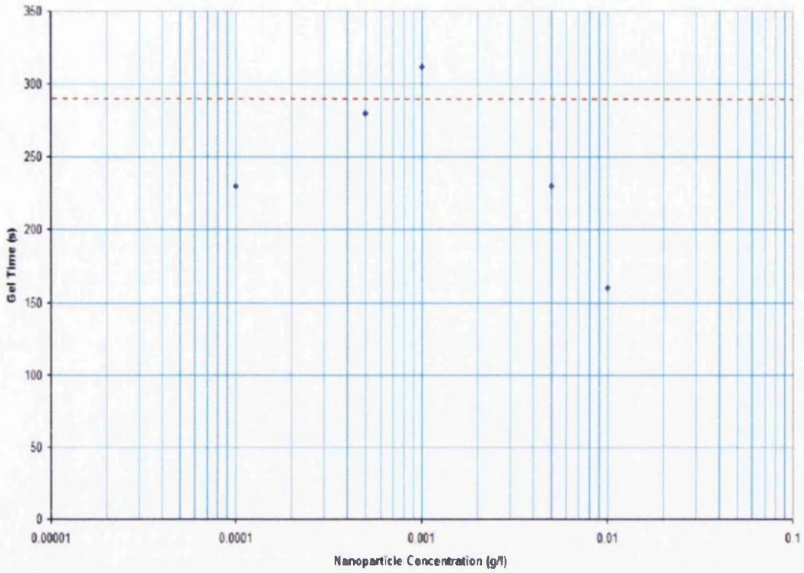

Figure 8.3: *Variance in gel time of whole blood with 5% spike of As-produced Single Walled Nanotubes in TBS.*

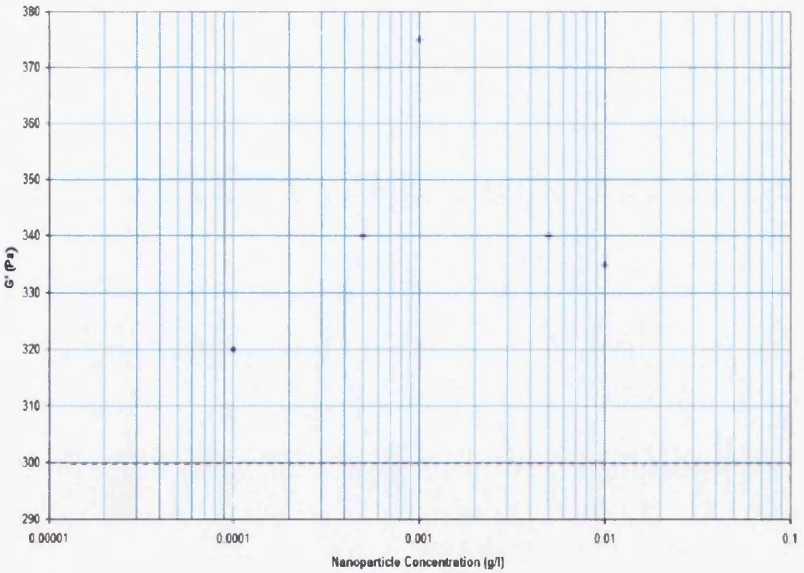

Figure 8.4: *Variance in G' max of whole blood with 5% spike of As-produced Single Walled Nanotubes in TBS.*

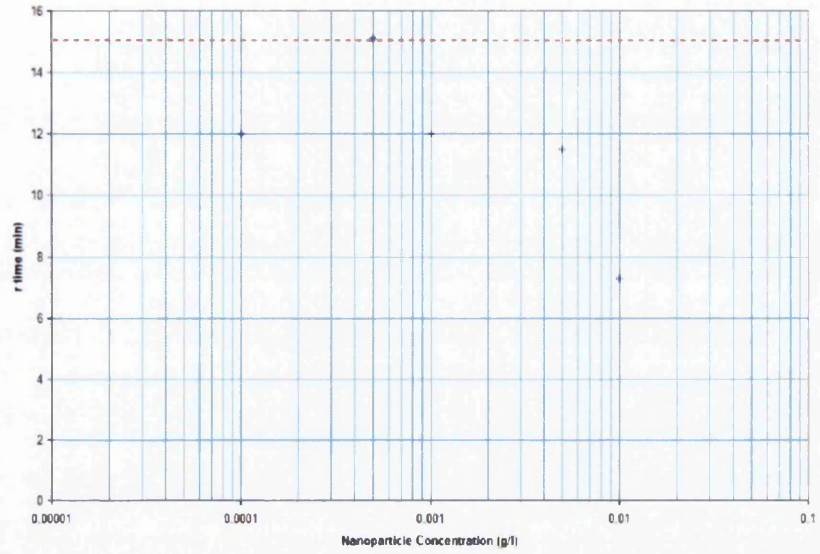

Figure 8.5: *Variance in TEG r time of whole blood with 5% spike of As-produced Single Walled Nanotubes in TBS.*

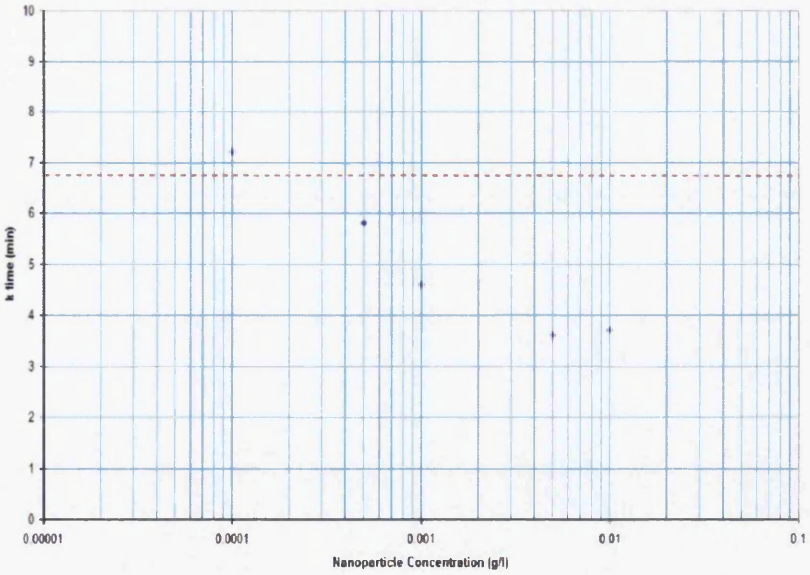

Figure 8.6: *Variance in TEG k time of whole blood with 5% spike of As-produced Single Walled Nanotubes in TBS.*

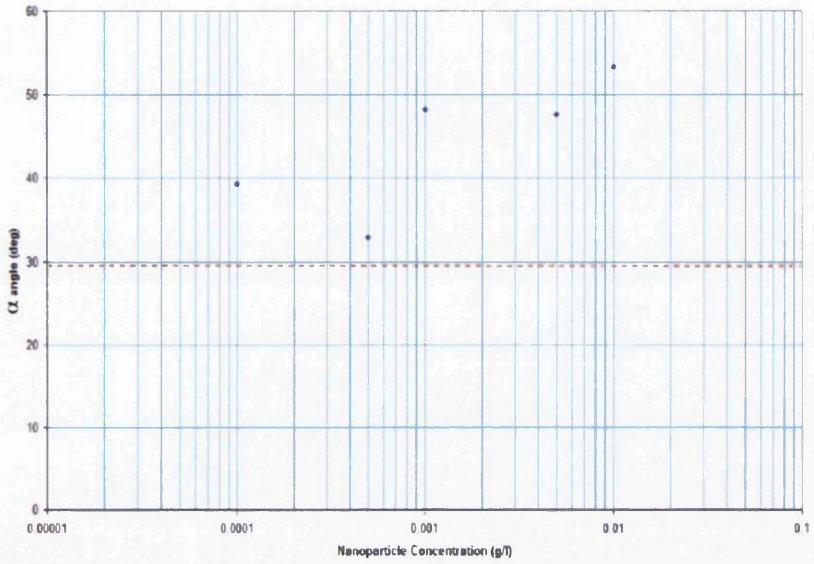

Figure 8.7: *Variance in TEG α angle of whole blood with 5% spike of As-produced Single Walled Nanotubes in TBS.*

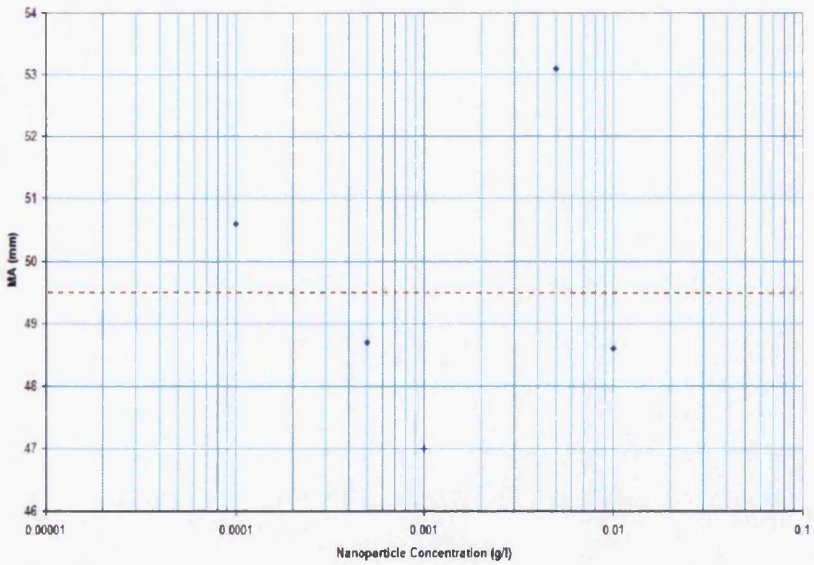

Figure 8.8: *Variance in TEG Maximum Amplitude of whole blood with 5% spike of As-produced Single Walled Nanotubes in TBS.*

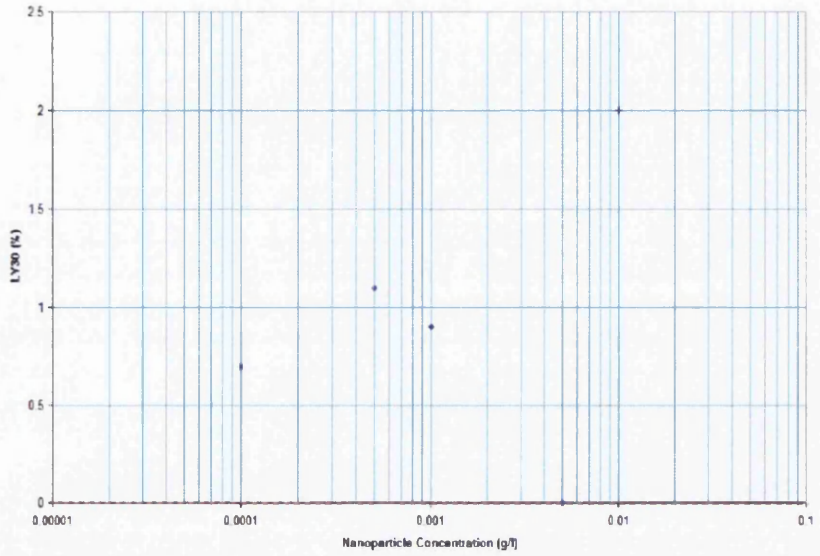

Figure 8.9: *Variance in TEG LY_{30} of whole blood with 5% spike of As-produced Single Walled Nanotubes in TBS.*

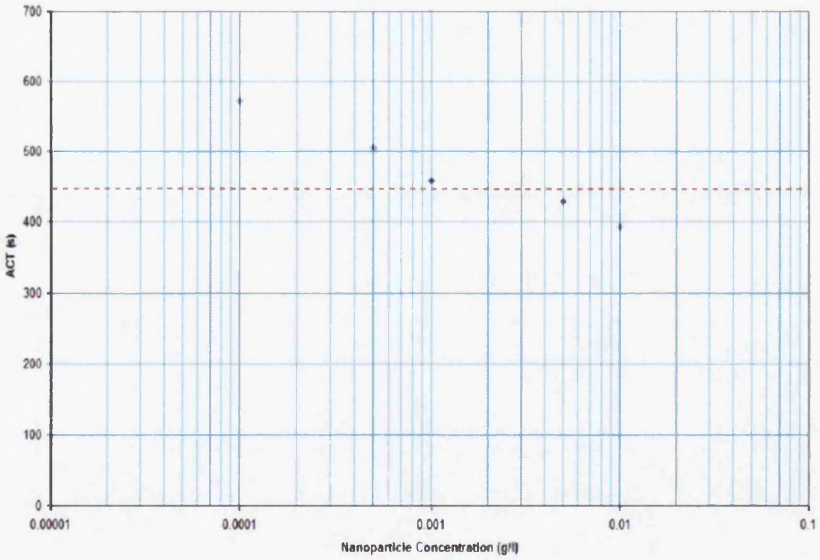

Figure 8.10: *Variance in Sonoclot ACT of whole blood with 5% spike of As-produced Single Walled Nanotubes in TBS.*

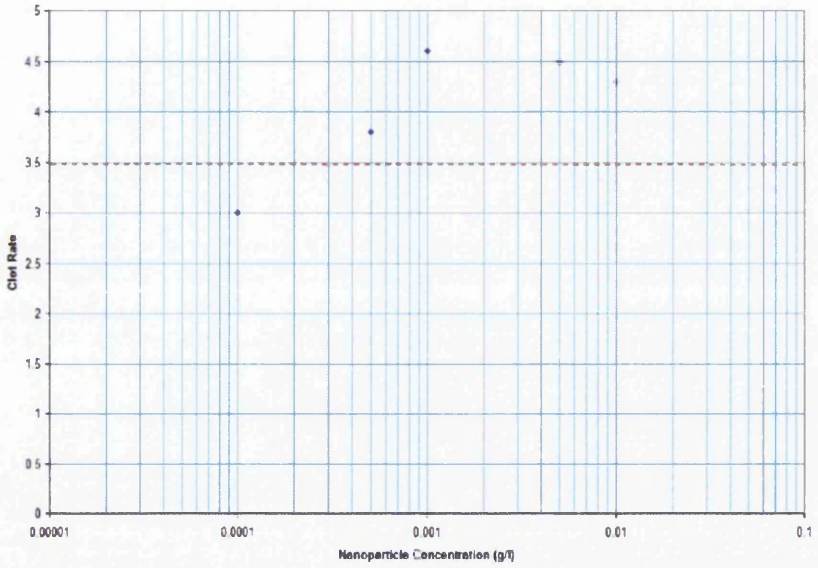

Figure 8.11: *Variance in Sonoclot Clot Rate of whole blood with 5% spike of As-produced Single Walled Nanotubes in TBS.*

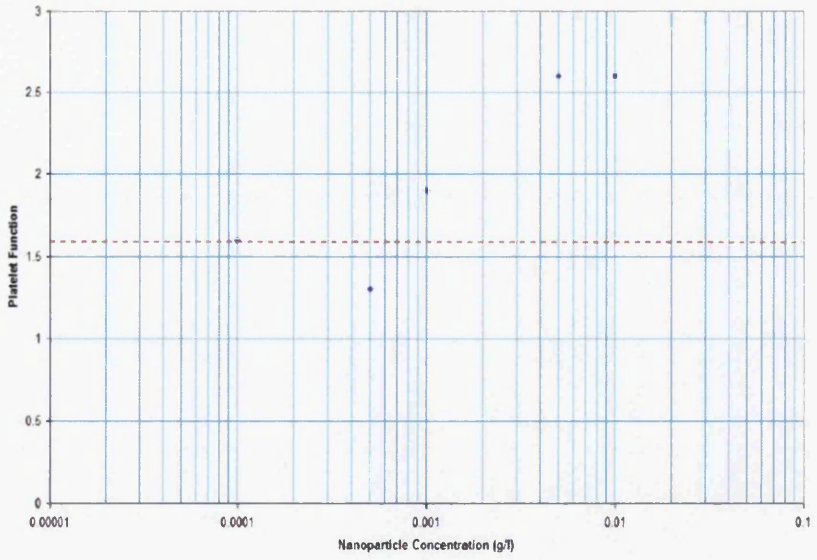

Figure 8.12: *Variance in Sonoclot Platelet Function of whole blood with 5% spike of As-produced Single Walled Nanotubes in TBS.*

Chapter 9

Results from As-Produced Multi Walled Nanotubes Experiments

A decrease in the measured phase angle at the gel point with increasing concentration (figure 9.1) gives an increasing fractal dimension (figure 9.2) corresponding to an increase in the density of the initial clot due to the fibres within the mesh structure becoming finer.

All gel time values are reduced in comparison to the TBS control value, and are scattered in a band around 200 seconds suggesting that further concentration increases above 0.0001g/l have little effect on the clotting time.

The G' values show a rapid decrease from a value of 400 Pa at a concentration of 0.0001g/l to 290 Pa at 0.001g/l. The G' values then increase to 320 Pa at the highest concentration. Indeed, all the concentrations above 0.0001g/l exhibit G' values in a band around 315 Pa.

The r-time values presented in figure 9.5 increase from the initial value of 7.8 minutes at 0.0001g/l to 11.3 minutes at 0.01g/l. All of these values are below that of the pure TBS addition. This suggests that while any nanotube addition has prothrombotic effects, increasing the concentration of the as-produced multi walled nanotubes has an inhibiting effect on the initial fibrin formation.

Measured k-times show an increase to a peak of 5.5 minutes at a concentration of 0.001g/l from an initial value of 4.3 minutes at 0.0001g/l. Further increases above 0.001g/l result in a sharp decrease in the k-time to a minimum

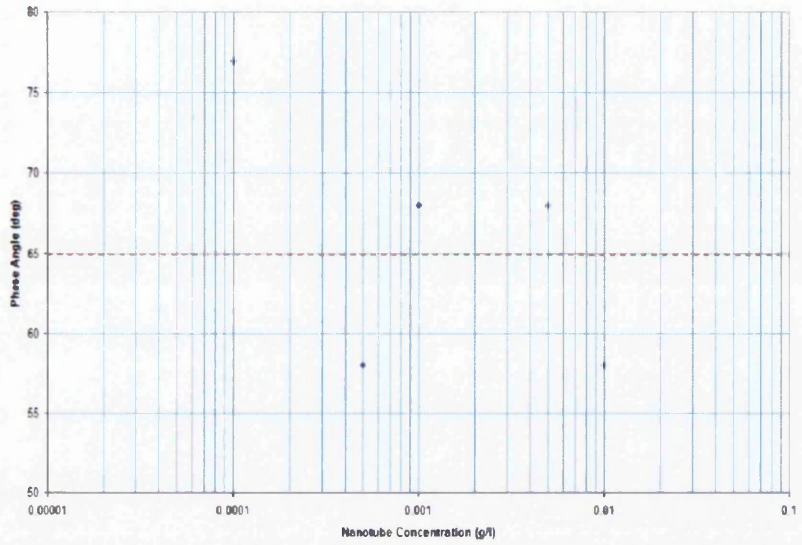

Figure 9.1: *Variance in Phase Angle δ of whole blood with 5% spike of As-produced Multi Walled Nanotubes in TBS.*

of 2.2 minutes. All values are below the baseline for a pure TBS addition suggesting that any addition is prothrombotic in comparison. However the initial increase suggests that up to a concentration of 0.001g/l increasing the concentration of nanotubes is inhibitive to the growth of the clot. Further increases are massively prothrombotic however.

The α angle data supports the second part of the k-time data but disagrees with the increasing inhibition of clot growth up to a concentration of 0.001g/l. In this instance there is a decrease in the values from 49.5° to 39° with an increase of concentration from 0.0001g/l to 0.0005g/l, followed by a rapid linear increase to a maximum value of 73.2°.

The recorded Maximum Amplitude data falls in a band between 52 and 61.4mm. The data for lysis percentage after 30 minutes shows a slight increase, but this is well within the normal range stated in chapter 5.6.

The Activated Clotting Time recorded by the Sonoclot shows initial inhibition at lower concentrations. The result for the lowest concentration of addition is equal to that recorded with a pure TBS addition. As the concentration is then increased the ACT is lengthened to a peak value of 541 seconds

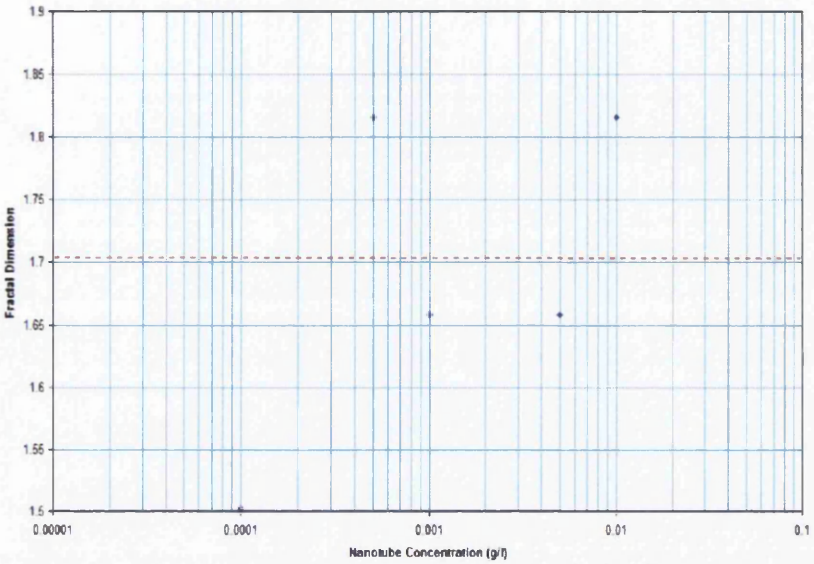

Figure 9.2: *Variance in Fractal Dimension of whole blood with 5% spike of As-produced Multi Walled Nanotubes in TBS.*

at a concentration of 0.001g/l. Once the concentration passes 0.001g/l the effect of the nanotubes is highly prothrombotic, as evidenced by the rapid decrease in the ACT values to 376 seconds and 394 seconds at 0.005g/l and 0.01g/l respectively.

The Clot Rate for the three lowest concentrations of nanotubes was just below that of the pure TBS addition suggesting a small level of inhibition. As with the Activated Clotting Time data, once the concentration passed 0.001g/l then the nanotubes become increasingly prothrombotic as evidenced by a rapid increase to 6.4 and 6 for 0.005g/l and 0.01g/l respectively.

The Platelet Function data shown in figure 9.12 exhibits a rapid increase from an initial value of 1.3 at 0.0001g/l to values of 3.2 and 3.1 at 0.005g/l and 0.01g/l respectively. The two lowest concentrations are below that of the pure TBS addition, again suggesting that low concentrations have an inhibitive effect on the growth of the clot through the reduction of the platelet activity. The value for the Platelet Function at 0.001g/l is equal to that recorded for a pure TBS addition at 1.6. Further increase of concentration then results in the nanotubes exhibiting an increasingly prothrombotic effect.

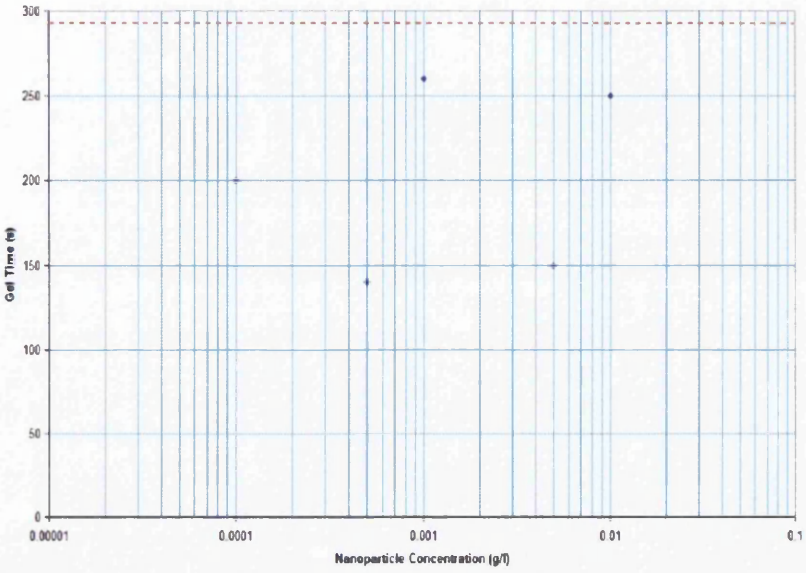

Figure 9.3: *Variance in Gel Time of whole blood with 5% spike of As-produced Multi Walled Nanotubes in TBS.*

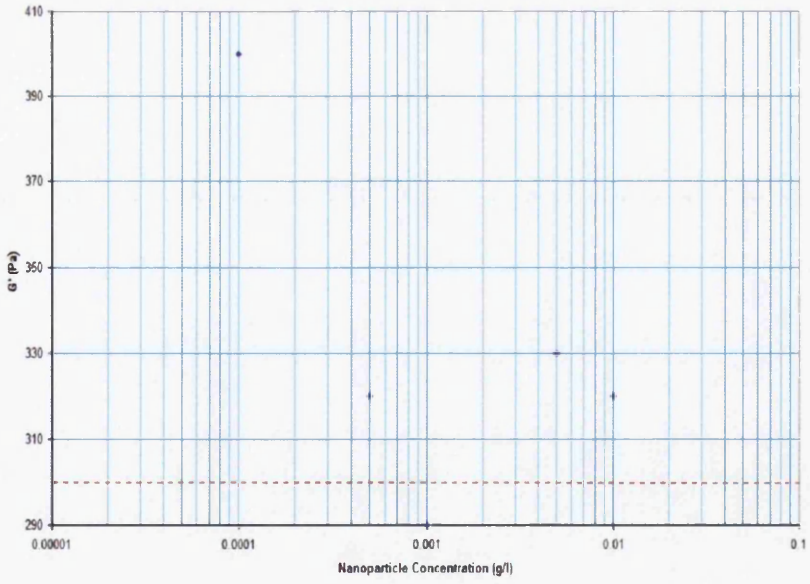

Figure 9.4: *Variance in G' max of whole blood with 5% spike of As-produced Multi Walled Nanotubes in TBS.*

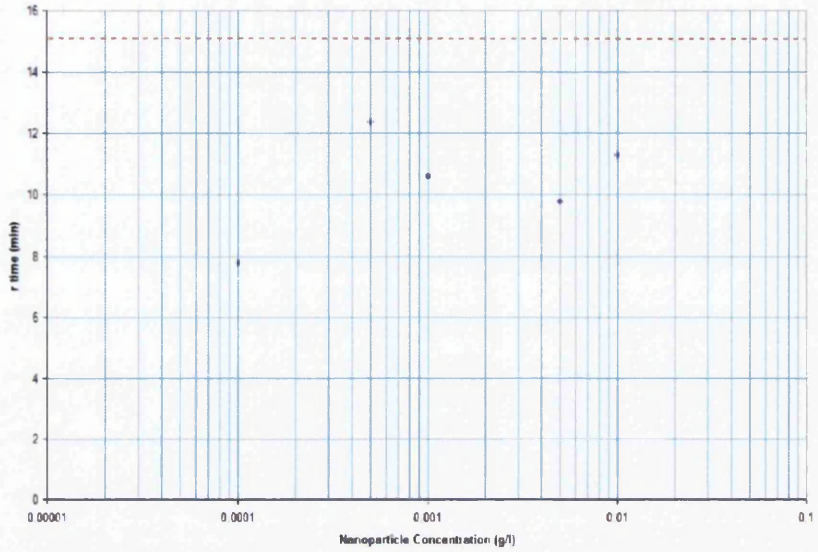

Figure 9.5: *Variance in TEG r time of whole blood with 5% spike of As-produced Multi Walled Nanotubes in TBS.*

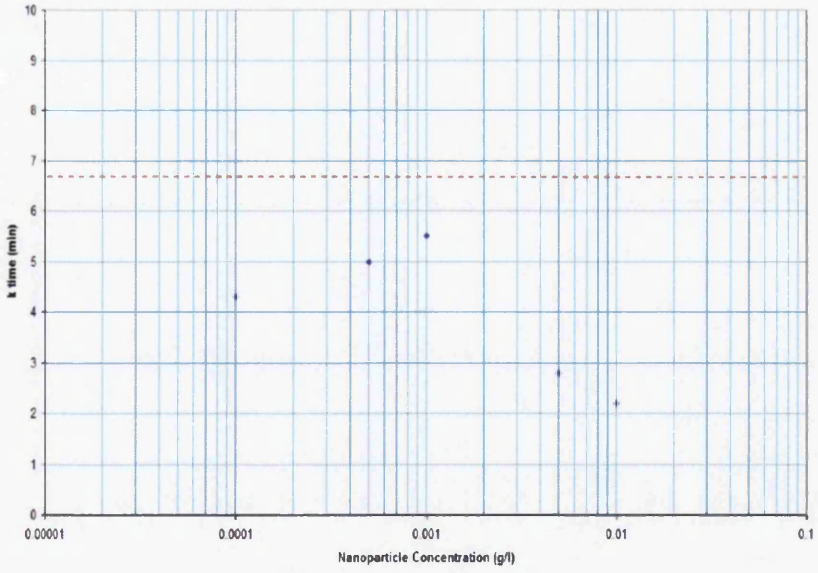

Figure 9.6: *Variance in TEG k time of whole blood with 5% spike of As-produced Multi Walled Nanotubes in TBS.*

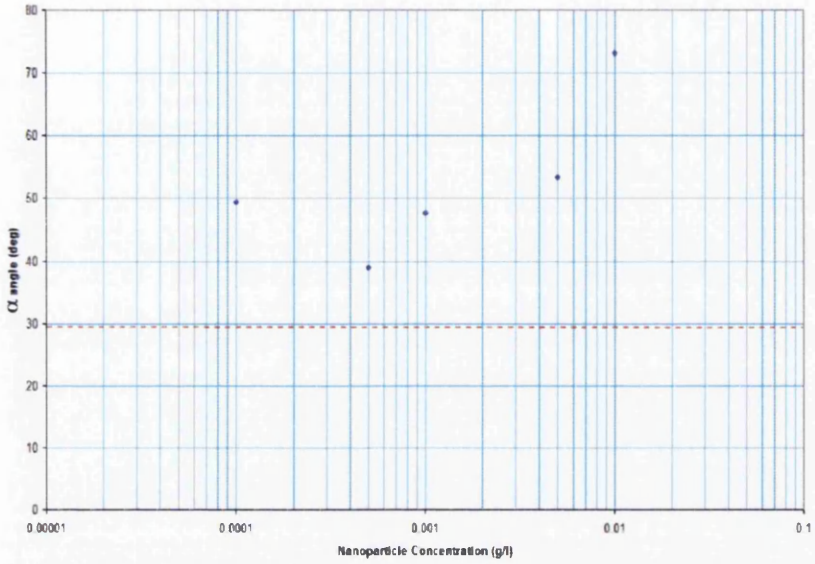

Figure 9.7: *Variance in TEG α angle of whole blood with 5% spike of As-produced Multi Walled Nanotubes in TBS.*

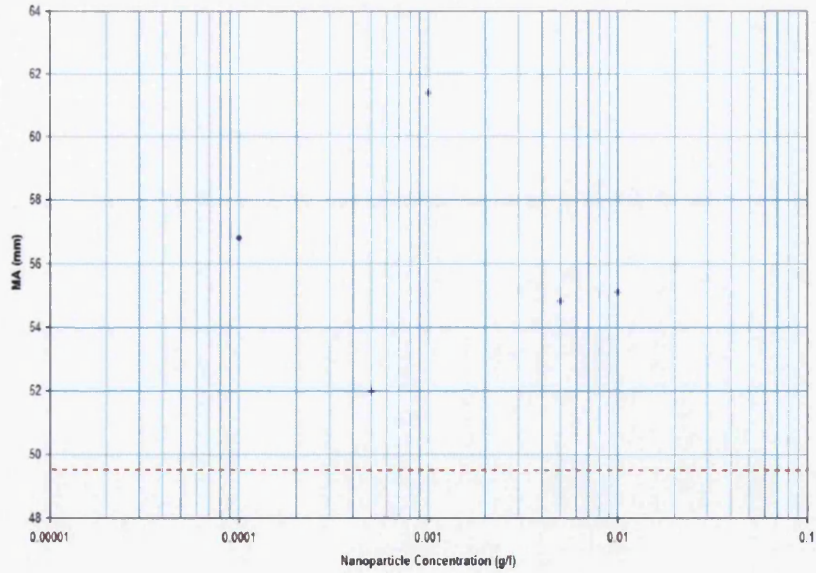

Figure 9.8: *Variance in TEG Maximum Amplitude of whole blood with 5% spike of As-produced Multi Walled Nanotubes in TBS.*

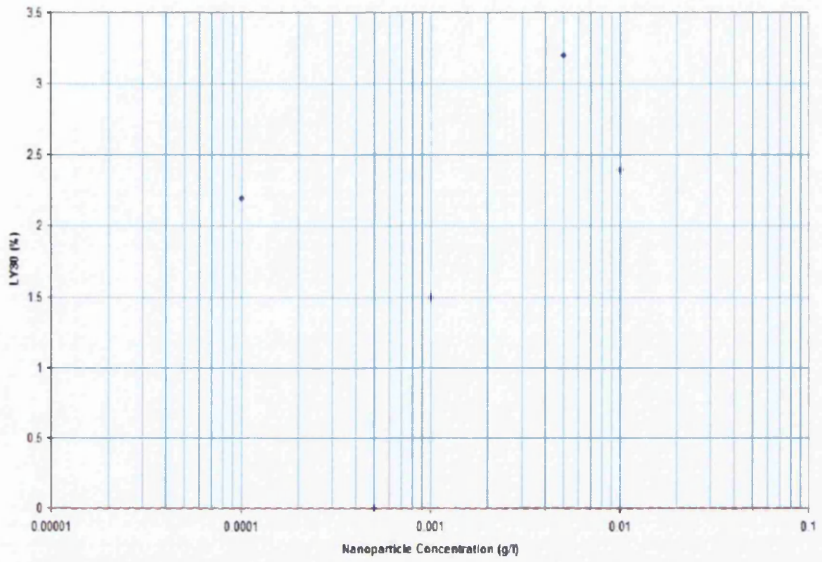

Figure 9.9: *Variance in TEG LY_{30} of whole blood with 5% spike of As-produced Multi Walled Nanotubes in TBS.*

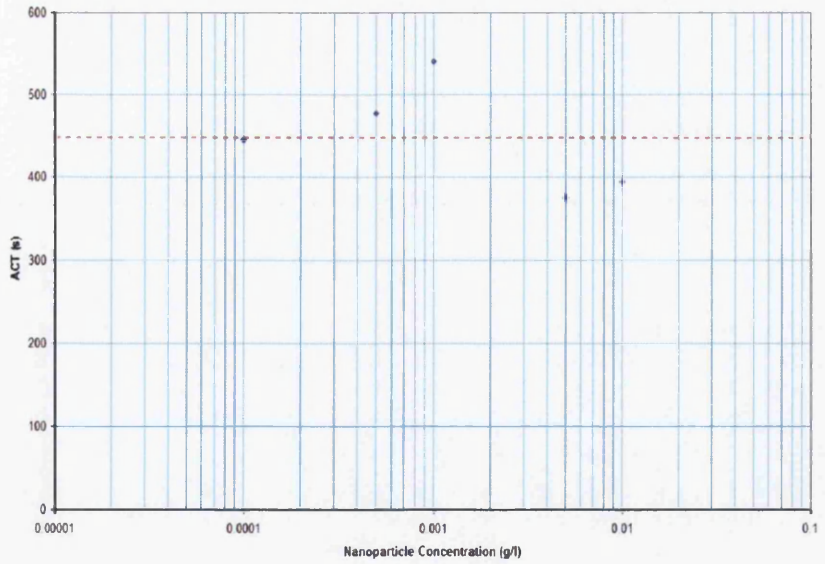

Figure 9.10: *Variance in Sonoclot ACT of whole blood with 5% spike of As-produced Multi Walled Nanotubes in TBS.*

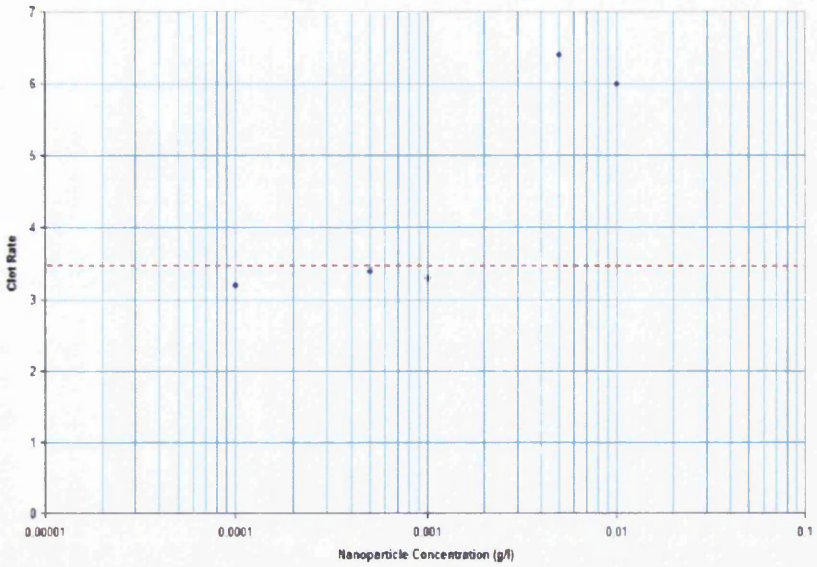

Figure 9.11: *Variance in Sonoclot Clot Rate of whole blood with 5% spike of As-produced Multi Walled Nanotubes in TBS.*

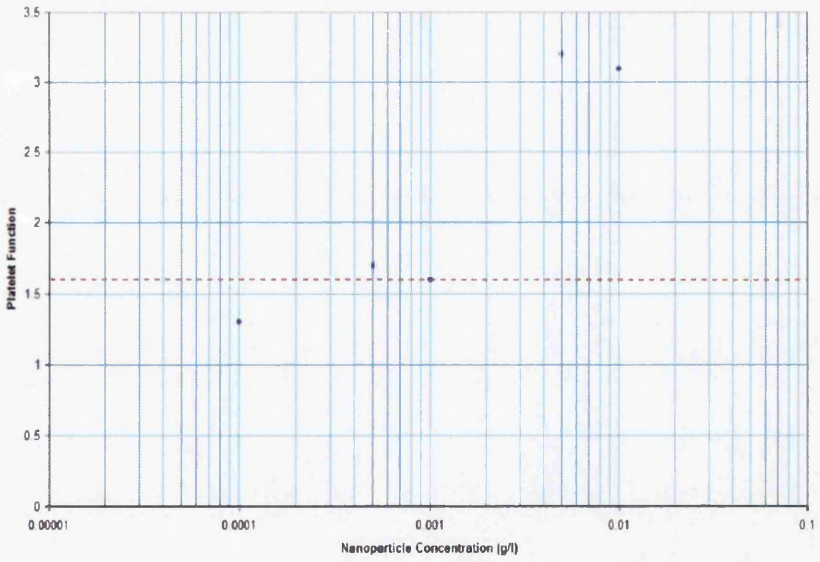

Figure 9.12: *Variance in Sonoclot Platelet Function of whole blood with 5% spike of As-produced Multi Walled Nanotubes in TBS.*

Chapter 10

Results from Diesel Particulate Experiments

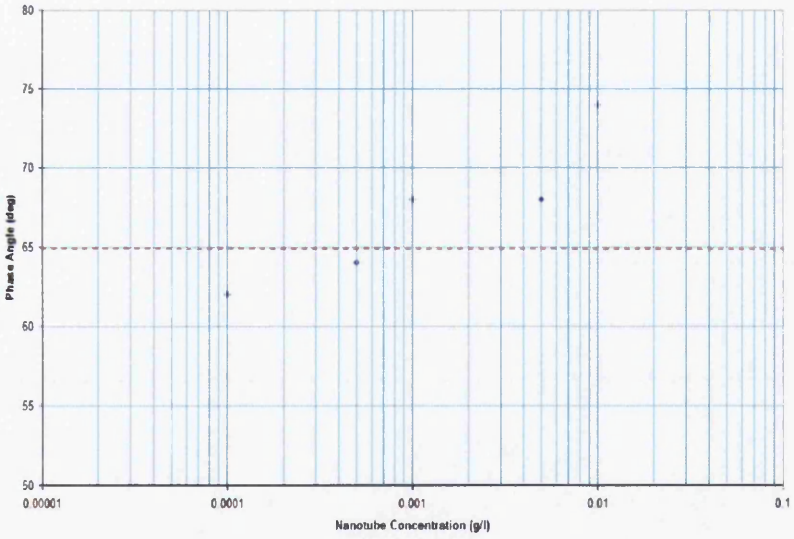

Figure 10.1: *Variance in Phase Angle δ of whole blood with 5% spike of Diesel particles in TBS.*

The introduction of diesel particles into whole blood at low concentrations leads to a reduction in the phase angle at the gel point corresponding to the formation of more rigid clots than those formed in the presence of pure TBS (figure 10.1). As the concentration of the particles is increased however the phase angle increases from in a fairly linear fashion, corresponding to the

formation of clots with an increasingly loose structure. This may be due to the change in the manner in which platelets are able to act as the particulate concentration is increased.

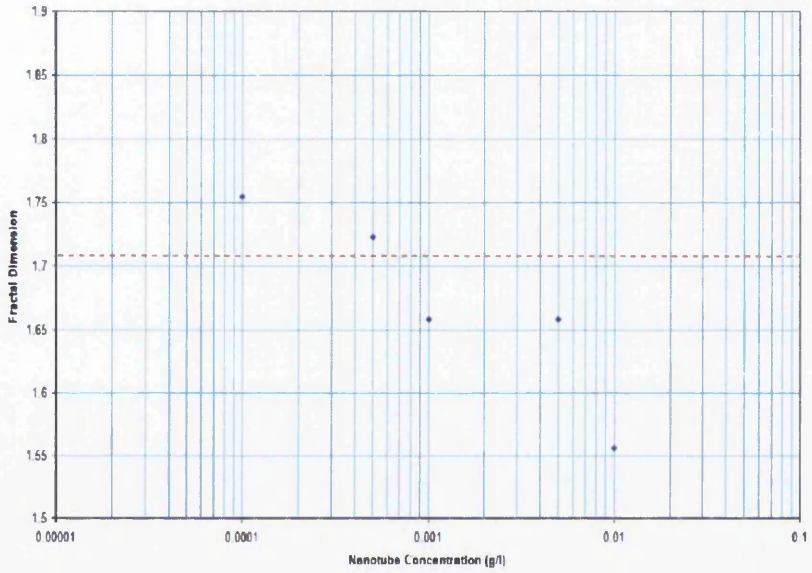

Figure 10.2: *Variance in Fractal Dimension of whole blood with 5% spike of Diesel particles in TBS.*

At the lowest concentrations, the particles are far more widely dispersed such that the volume of blood per particle is much greater. This enables platelets which are activated through contact with the particles (intrinsic pathway) to reach more of the surrounding blood and activate thrombin as opposed to repeated collisions with particles which may result in the platelet becoming bound to a particle and thus having its effectiveness reduced. As the fibrin mesh is formed, some of these particles will become trapped within the spaces together with platelets and fibrinogen. The trapped particles would then serve as activation sites for the platelets within the gaps in the matrix leading to the formation of a much denser structure.

As the concentration of particulates in suspension is increased it may be that once a threshold level has been passed the particles begin to from sweep flocs. This would result in particles and the platelets and fibrin strands surrounding them settling rapidly out of suspension. If this were to be the case then the availability of activated platelets throughout the solution may

become sporadic, with the largest amount located in the settled layer. This would result in the formation of increasingly looser clots as the concentration is further increased past the threshold level.

This mechanism is supported by the gel time data presented in figure 10.3. While all values are markedly below that for the TBS baseline, the gel times show a loose upward trend with increasing concentration, suggesting increasing thrombosis inhibition.

Despite the increase in gel time and the decrease in fractal dimension, the final clot elasticity of the clot as measured by G' shows a dramatic increase with a very tight correlation. This suggests that while the initial clot takes longer to form as the particulate concentration is increased, the final clot is more elastic.

It may be that the initial clot has taken longer to form due to the manner of the fibrin strands formed within the mesh or the manner in which the particulates are bound within it. As mentioned earlier in this discussion, the binding of particulates within the mesh would enable further activation of the platelets and thrombinogen which are also bound. While this activation would have little effect on the nature of the incipient clot, it would result in increasing clot retraction during the latter stages of formation.

The r time data presented in figure 10.5 drops from a value equal to the baseline at the lowest concentration of particulates to 7 minutes at the highest concentration. This value is still markedly longer than the gel time measured using the rheometer.

The k time data shows a loose upward trend (figure 10.6), with all data points below the baseline. This increase fits with the results from the G2 together with the loose downward trend in the α angle data (10.7), suggesting that at higher concentrations the diesel particulates may have inhibitive properties in the very early stages of thrombosis.

The increased elasticity as measured by the G' data is mirrored in the MA data from the TEG (10.8) which shows a clear upward trend, suggesting that the increasingly loose structure found in the incipient clot continues to the mature clot, resulting in a larger structure. This larger structure may also be due to the particulates interfering with the ability of the platelets to effect clot retraction.

Very little variance is in evidence within the lysis data, with all of the

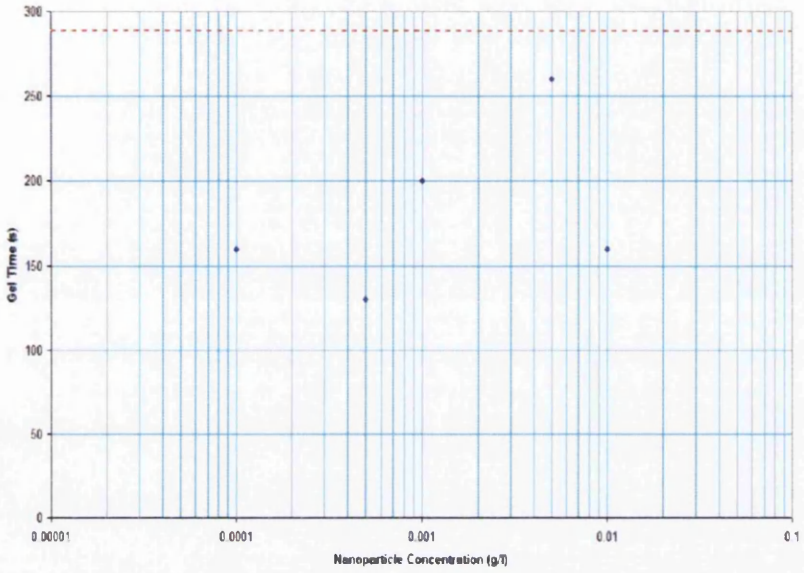

Figure 10.3: *Variance in Gel Time of whole blood with 5% spike of Diesel particles in TBS.*

data points remaining within the normal range.

The Activated Clotting Times (ACT) measured by the Sonoclot are grouped in a horizontal band with an average slightly above the baseline value. Clot Rate data shows a loose upward trend. This is in agreement with the k time and α angle data.

Inferred Platelet Function is raised on all data points compared to the baseline value. A slight upward trend is visible, although very loose. As such it would appear to support the suggestion that the diesel particulates may inhibit the clot retraction stage while enhancing the contact activation of the platelets, resulting in the large, loose structures measured.

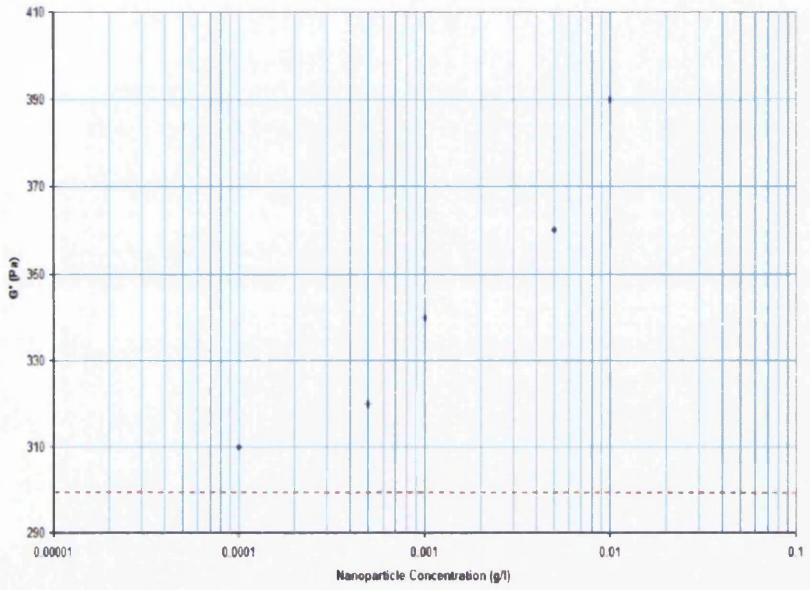

Figure 10.4: *Variance in G' max of whole blood with 5% spike of Diesel particles in TBS.*

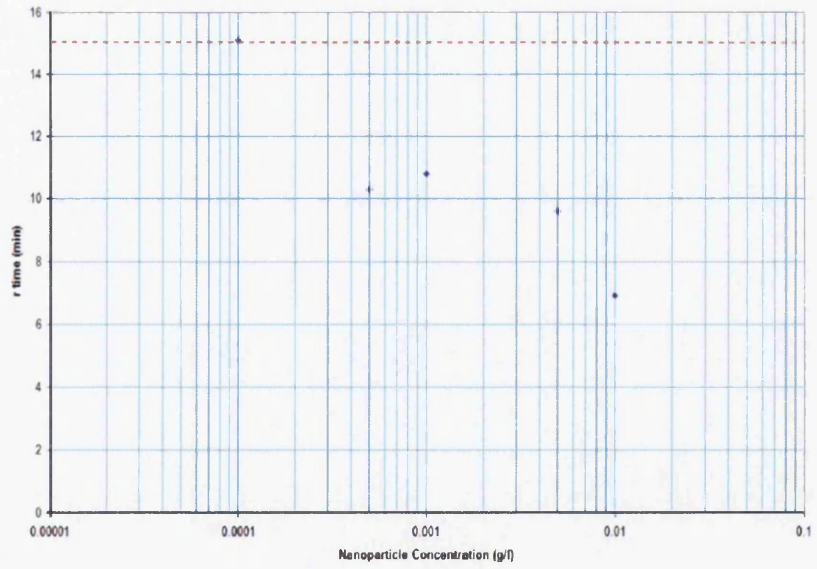

Figure 10.5: *Variance in TEG r time of whole blood with 5% spike of Diesel particles in TBS.*

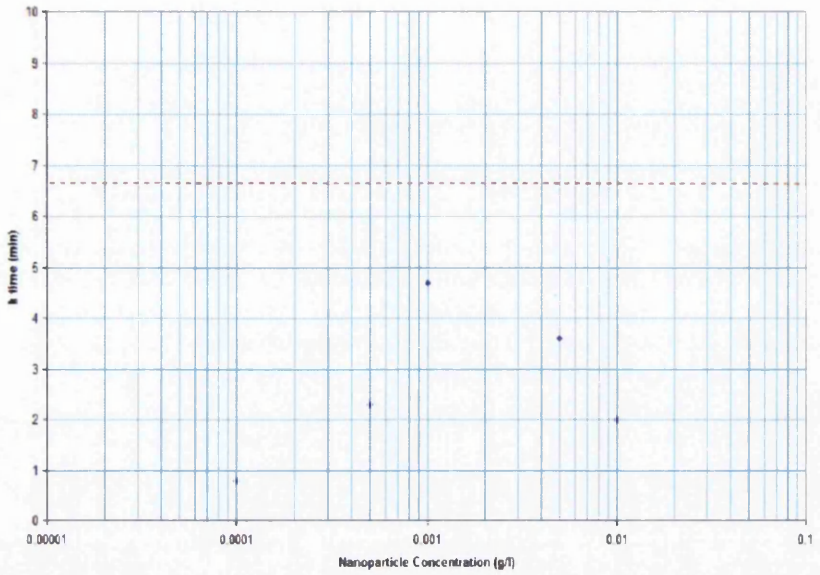

Figure 10.6: *Variance in TEG k time of whole blood with 5% spike of Diesel particles in TBS.*

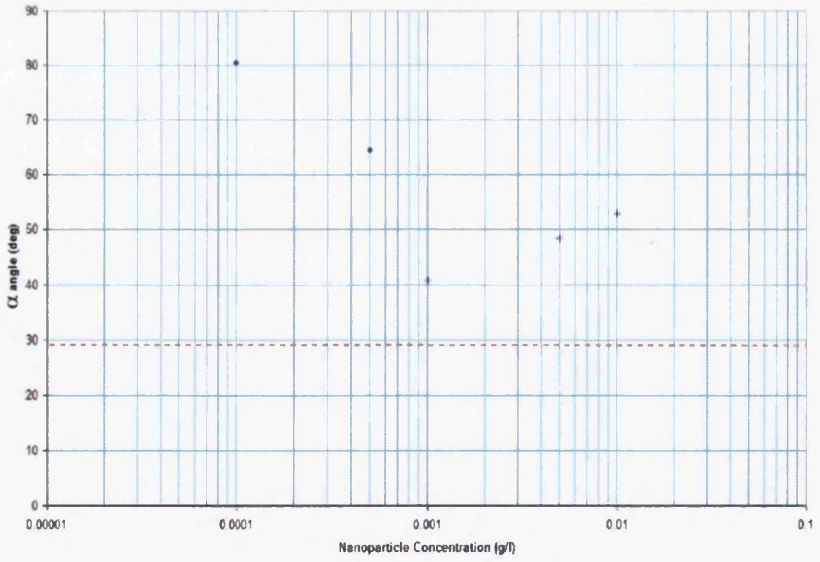

Figure 10.7: *Variance in TEG α angle of whole blood with 5% spike of Diesel particles in TBS.*

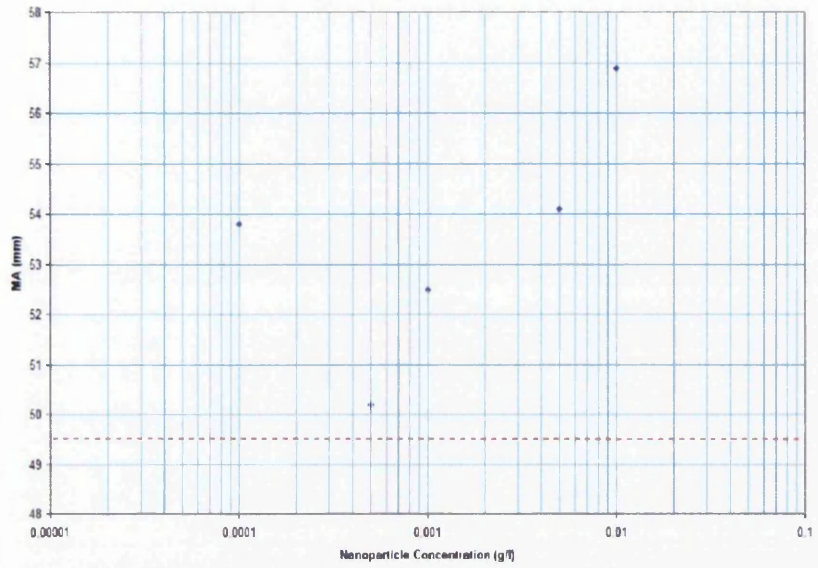

Figure 10.8: *Variance in TEG Maximum Amplitude of whole blood with 5% spike of Diesel particles in TBS.*

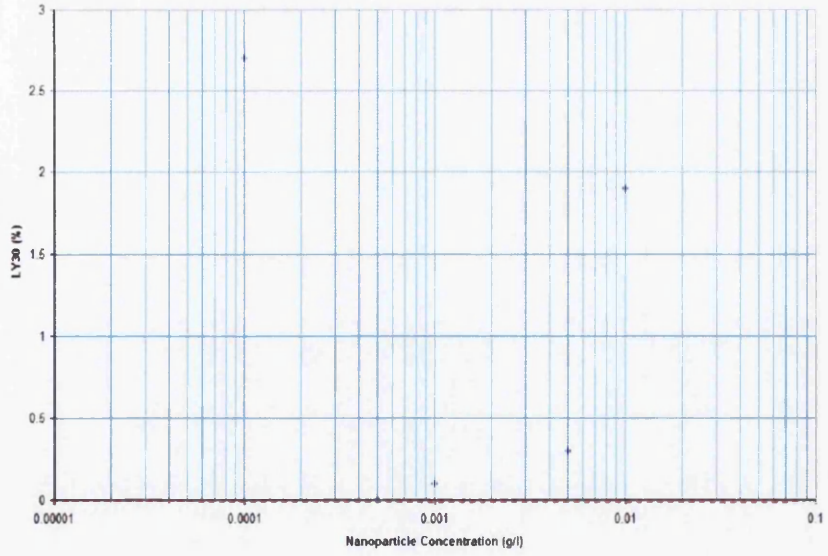

Figure 10.9: *Variance in TEG LY_{30} of whole blood with 5% spike of Diesel particles in TBS.*

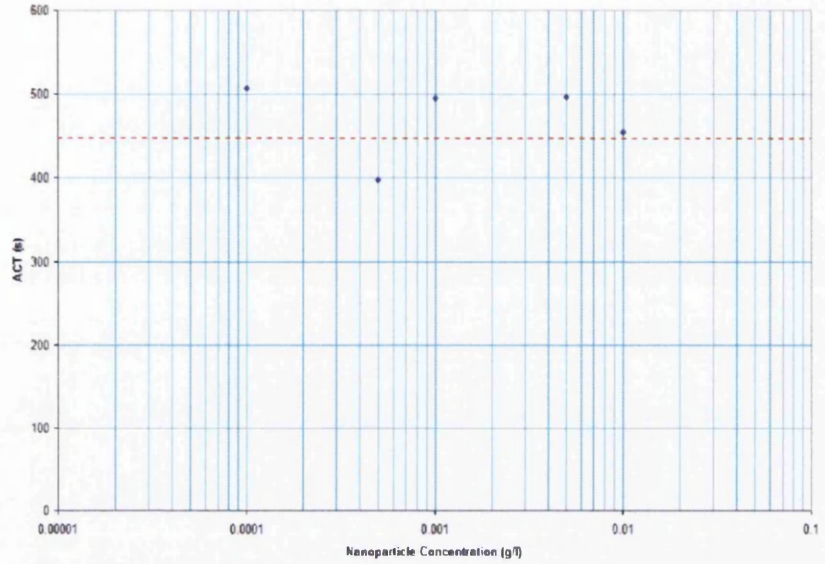

Figure 10.10: *Variance in Sonoclot ACT of whole blood with 5% spike of Diesel particles in TBS.*

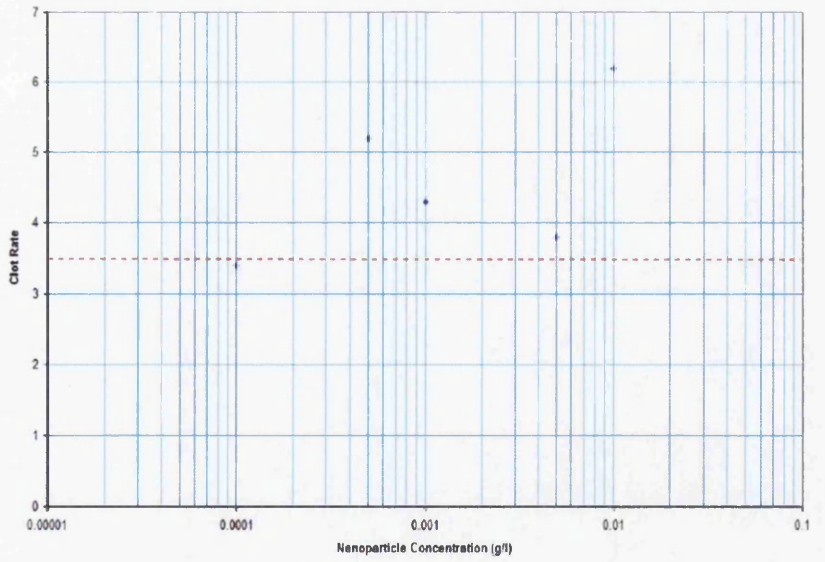

Figure 10.11: *Variance in Sonoclot Clot Rate of whole blood with 5% spike of Diesel particles in TBS.*

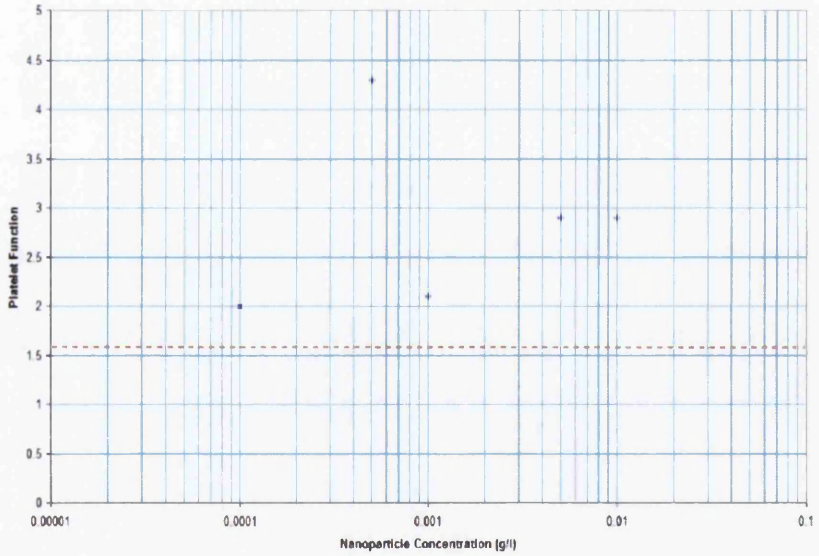

Figure 10.12: *Variance in Sonoclot Platelet Function of whole blood with 5% spike of Diesel particles in TBS.*

Chapter 11

Results from Carboxyl-Functionalised Single Walled Nanotube Experiments

The effect on the nature of the thrombus formed following the inclusion of the carboxyl-functionalised single walled nanotubes differ somewhat from machine to machine. In the case of the G2, an increase in the phase angle at the gel point (and a corresponding decrease in fractal dimension) are evident in figures 11.1 and 11.2.

The initial phase angle value measured at a concentration of 0.0001g/l was 63°, suggesting that the lower concentration produces a clot that has a slightly higher level of structural order than that with an addition of pure TBS. Subsequent increasing concentrations exhibit an increase in the phase angle up to 68°, a value above that of the pure TBS addition meaning that the initial clot has an increasingly loose structure as the concentrations are increased.

The gel time data is in a band around 200 seconds, below that of the value of the pure TBS addition, showing that despite the effect on the initial structure as shown by the phase angle, any addition of these nanotubes is prothrombotic, serving to increase the rate of initial platelet activation.

The G' values show a marked increase from a minimum of 210 Pa at 0.0005g/l to a maximum of 320 Pa. The final clot structure is thus less rigid in the lower concentration additions than at the higher concentrations. In comparison to the baseline value from the pure TBS addition, the structural elasticity is reduced by all concentrations apart from the highest. This

suggests an inhibitive function of the nanotubes at lower concentrations.

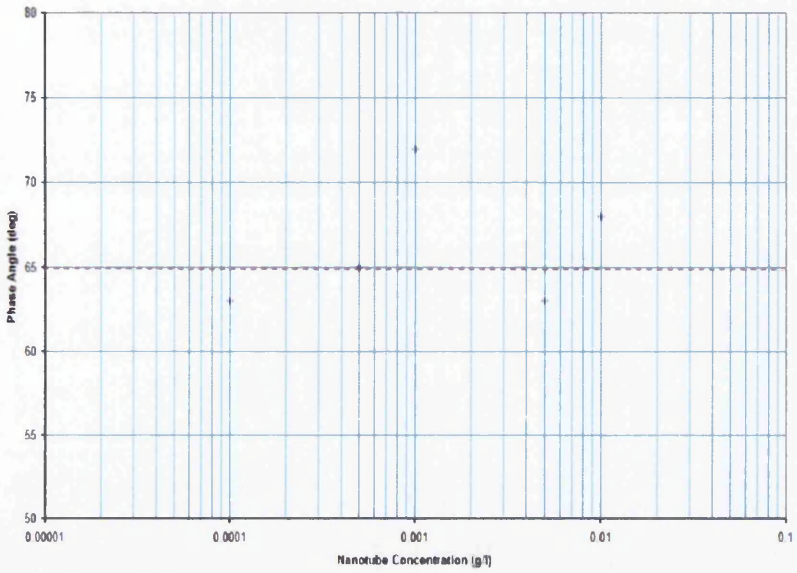

Figure 11.1: *Variance in Phase Angle δ of whole blood with 5% spike of Carboxyl-functionalised Single Walled Nanotubes in TBS.*

The rate of formation of the initial fibrin strands increases with increasing nanotube concentration as shown by the marked decrease in the r-time measured by the TEG. The values drop from 11.5 minutes at 0.0001g/l to 5.9 minutes at 0.01g/l. This partially supports the results from the gel time measurements made on the G2 in that all data points show the addition to have prothrombotic effects.

An increase in the rate of thrombus formation following the generation of the initial fibrin strand is clearly shown through a decrease in the k-time from 5 minutes to 2.3 minutes and a corresponding increase in the α angle from 39.3 to 61.3°. This shows that the action of the nanotubes is highly prothrombotic. However, while the addition of the nanotubes results in a faster rate of growth and thus a reduced time for the clot to reach maturity, the G' data discussed earlier suggests that this enhanced rate of growth results in a reduced structural integrity within the clot.

This reduced structural integrity couples with the looser structure of the initial clot measured by the phase angle data results in an increase in the

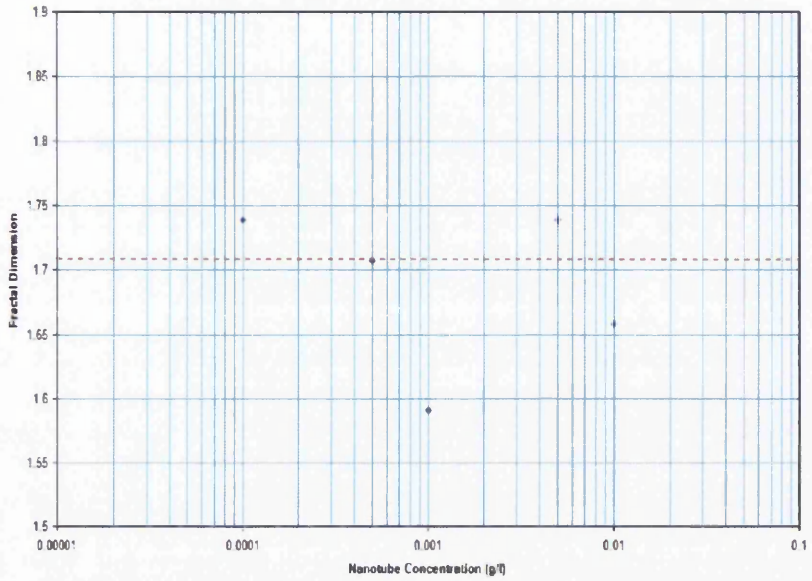

Figure 11.2: *Variance in Fractal Dimension of whole blood with 5% spike of Carboxyl-functionalised Single Walled Nanotubes in TBS.*

Maximum Amplitude of the mature clot measured on the TEG. This change in the clot structure has no effect on the lysis as measured by the TEG.

The marked increase in the prothrombotic effect of increasing concentrations of the carboxyl-functionalised single-walled nanotubes on the initial clot formation as measured on the TEG is also in evidence in the Activated Clotting Times measured by the Sonoclot. A decrease from a value of 354 seconds at a concentration on 0.0001g/l to 305 seconds at the highest concentration of 0.01g/l represents a marked increase in the rate at which the platelets are activated during the initial stages of thrombosis. This increase may well be due to the increase in the solubility of the nanotubes due to the addition of the carboxyl molecules.

The increase in the rate of the growth of the clot to maturity as shown by the increase in the k-time and α angle measured by the TEG is also shown in the clot rate data from the Sonoclot with an increase from 4.4 at 0.0001g/l to a plateau value of around 6.7 which is reached at 0.0005g/l. The platelet function data is not a distinct linear trend, instead exhibiting a peak of 3.6 at 0.001g/l. This is followed by a decrease to 2.4 as the concentration is increased to 0.01g/l, suggesting that the activity of the platelets throughout the clot formation from the initial fibrin to maturity is enhanced by the

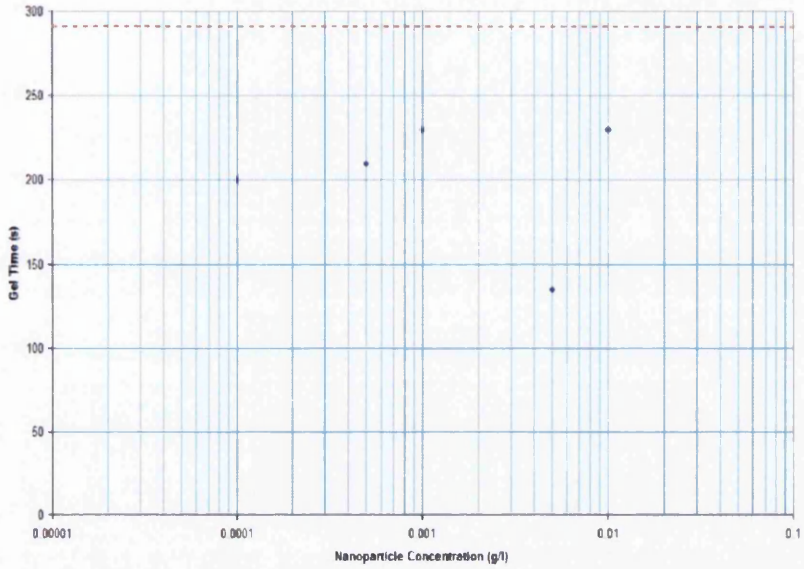

Figure 11.3: *Variance in Gel Time of whole blood with 5% spike of Carboxyl-functionalised Single Walled Nanotubes in TBS.*

addition of nanotubes up to the concentration of 0.001g/l. Further increases in the concentration added then exhibit inhibitory properties. This peak is not seen in any of the other data sets for this type of nanotube.

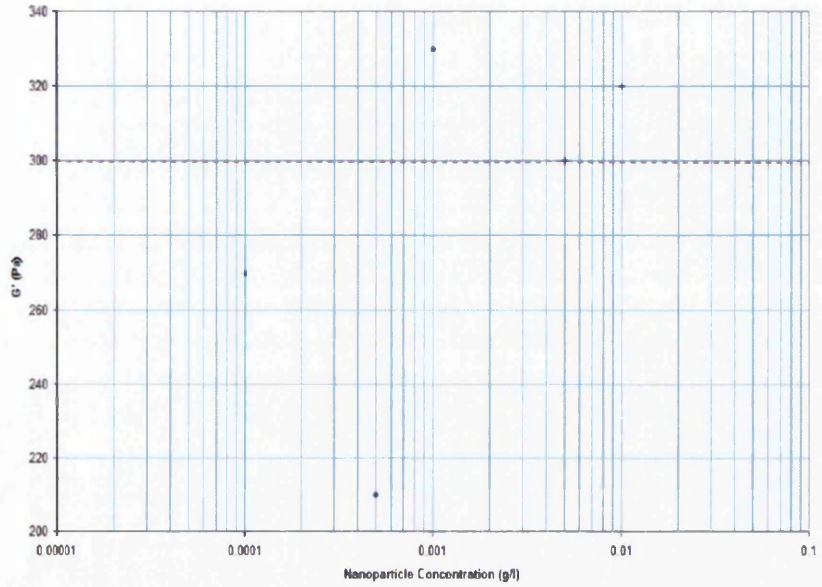

Figure 11.4: *Variance in G' max of whole blood with 5% spike of Carboxyl-functionalised Single Walled Nanotubes in TBS.*

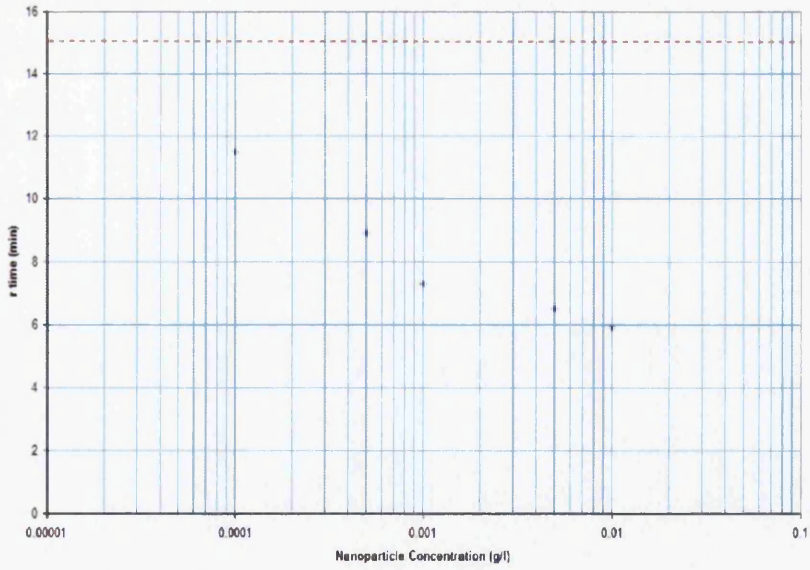

Figure 11.5: *Variance in TEG r time of whole blood with 5% spike of Carboxyl-functionalised Single Walled Nanotubes in TBS*

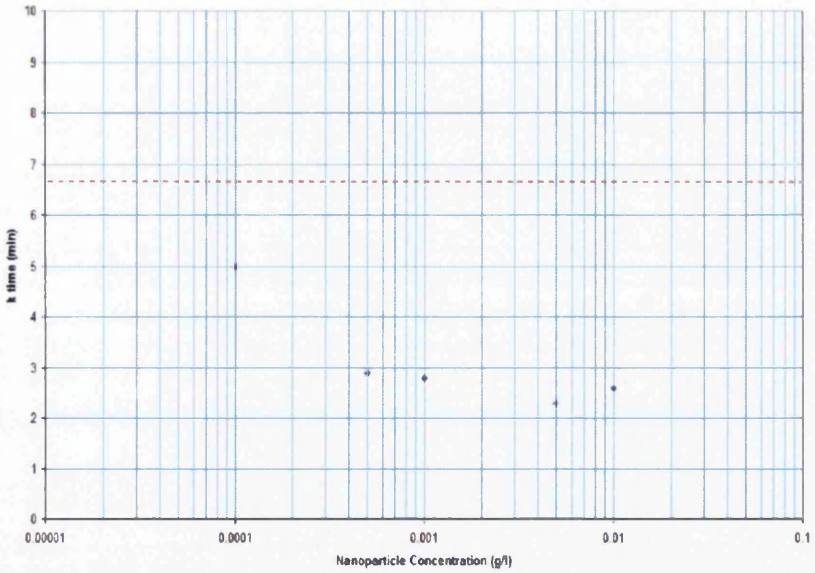

Figure 11.6: *Variance in TEG k time of whole blood with 5% spike of Carboxyl-functionalised Single Walled Nanotubes in TBS*

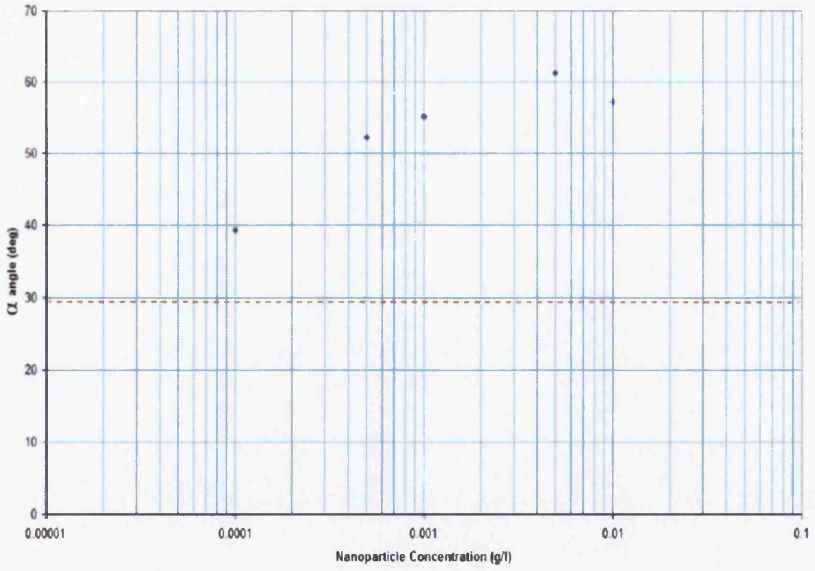

Figure 11.7: *Variance in TEG α angle of whole blood with 5% spike of Carboxyl-functionalised Single Walled Nanotubes in TBS*

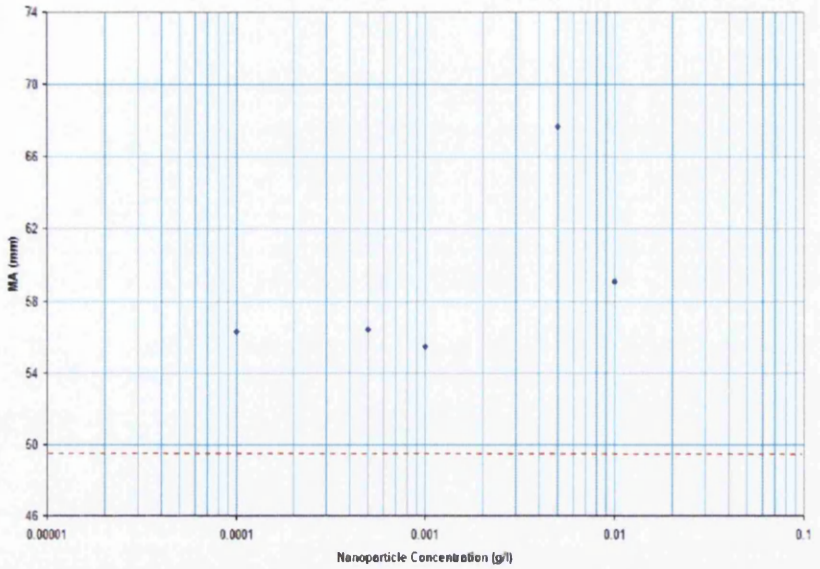

Figure 11.8: *Variance in TEG Maximum Amplitude of whole blood with 5% spike of Carboxyl-functionalised Single Walled Nanotubes in TBS*

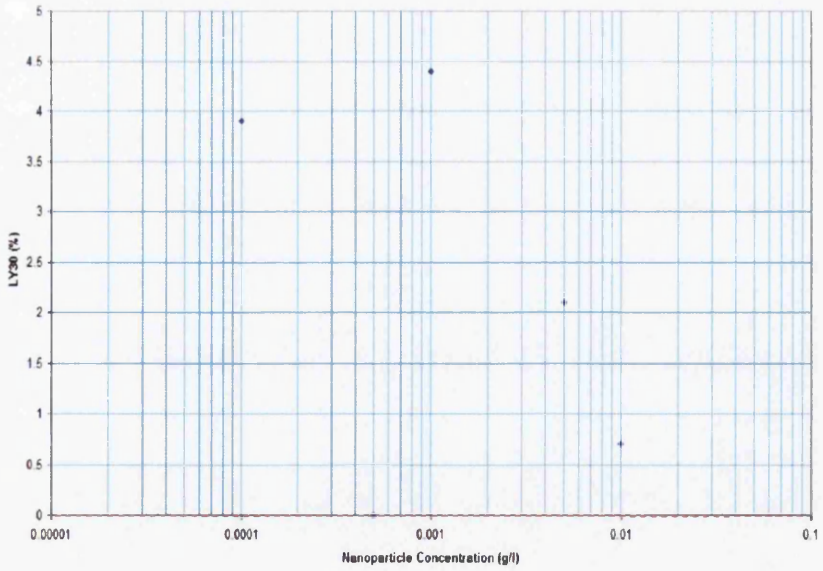

Figure 11.9: *Variance in TEG LY_{30} of whole blood with 5% spike of Carboxyl-functionalised Single Walled Nanotubes in TBS*

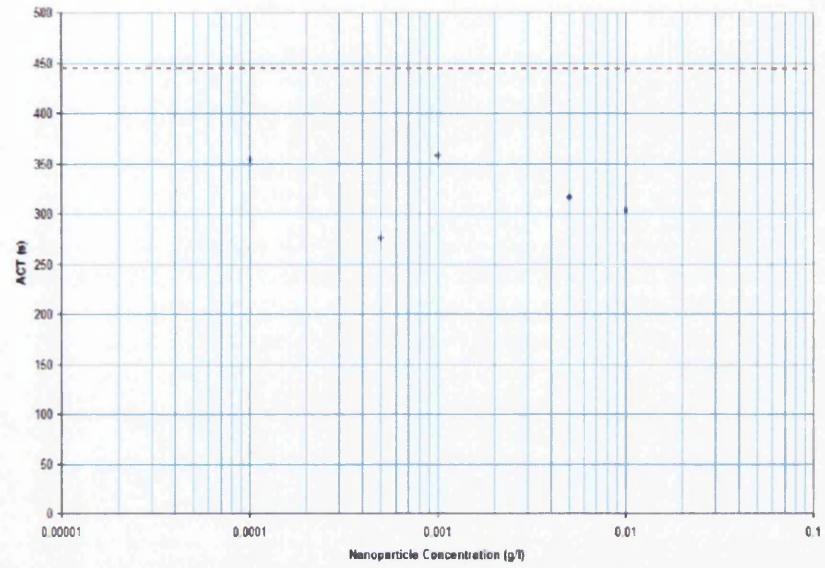

Figure 11.10: *Variance in Sonoclot ACT of whole blood with 5% spike of Carboxyl-functionalised Single Walled Nanotubes in TBS*

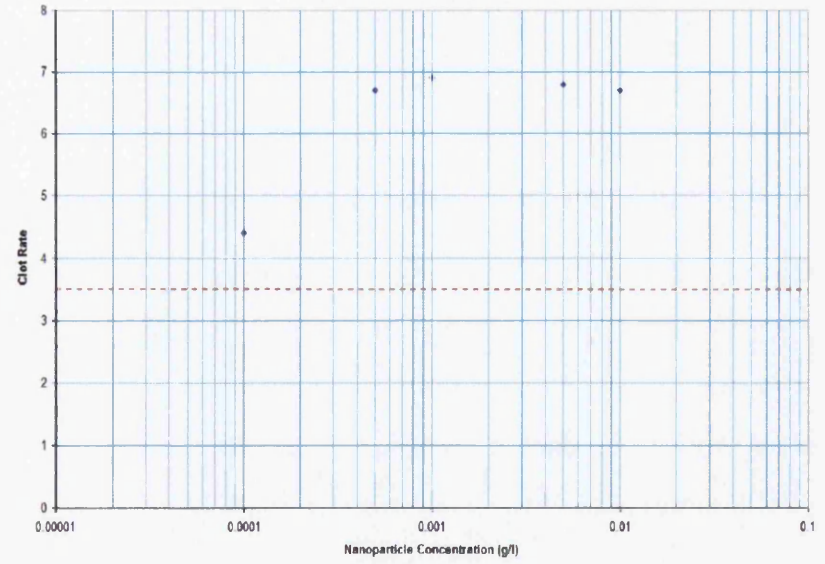

Figure 11.11: *Variance in Sonoclot Clot Rate of whole blood with 5% spike of Carboxyl-functionalised Single Walled Nanotubes in TBS*

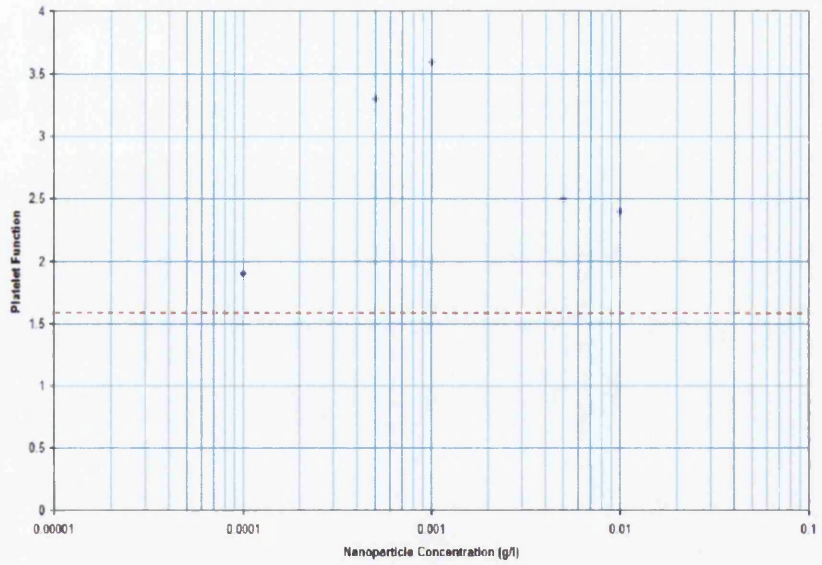

Figure 11.12: *Variance in Sonoclot Platelet Function of whole blood with 5% spike of Carboxyl-functionalised Single Walled Nanotubes in TBS*

Chapter 12

Results from Carboxyl-Functionalised Multi-Walled Nanotubes Experiments

The results from the work undertaken with the carboxyl-functionalised multi-walled nanotubes have provided the clearest data sets of all of the particles tested.

The small increase in fractal dimension in the data presented in figure 12.2 points to an increasing level of structure within the initial clot. This suggests that the inclusion of the nanotubes within the blood causes increasingly thin fibrin strand formation.

The sharp decrease in the recorded gel time from 250 seconds to 100 seconds reflects a very high prothrombotic effect in the initial thrombus formation.

Recorded G' values shown in figure 12.4 start initially below that of the TBS control value of 300 Pa with a G' of 200 Pa recorded following the addition of 0.0001g/l. These values increase sharply to 320 Pa at 0.01g/l. This shows an initial reduction in the elastic properties of the clot with nanotube addition. Increasing G' with increasing nanotube concentration points towards prothrombotic effects of the nanotubes in the later stages of clot formation.

A sharp decrease in the r-time values from 13.3 minutes at a concentration

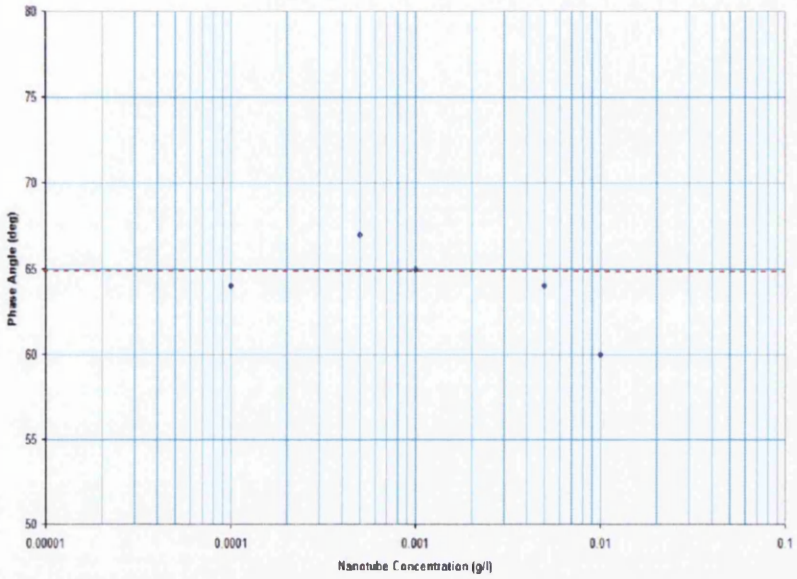

Figure 12.1: *Variance in Phase Angle δ of whole blood with 5% spike of Carboxyl-functionalised Multi Walled Nanotubes in TBS.*

of 0.0001g/l to 3.3 minutes at 0.01g/l agrees with the rapid reduction seen in the gel time measured on the G2. This reduction in the time required for the initial fibrin formation is likely due to the increased solubility of these nanoparticles enabling a good dispersion throughout the blood sample. As such, a very large surface area is available for the contact activation of the platelets.

The k-time data shows a sharp decrease coupled with a sharp increase in the α angle, showing a rapid level of clot growth following the initial fibrin formation. The continued high level of increase in the rate of clot growth suggest that the particles remain in suspension effectively even at the higher concentrations enabling continuing platelet activation throughout thrombus formation.

The continuing activation throughout the clot formation is supported by an increase in the values of maximum amplitude recorded as the nanotube concentration is increased. This further suggests that the nanotubes are effectively suspended throughout the suspension enabling the continued activation to occur at the extremities of the clot, thus resulting in the larger final clots.

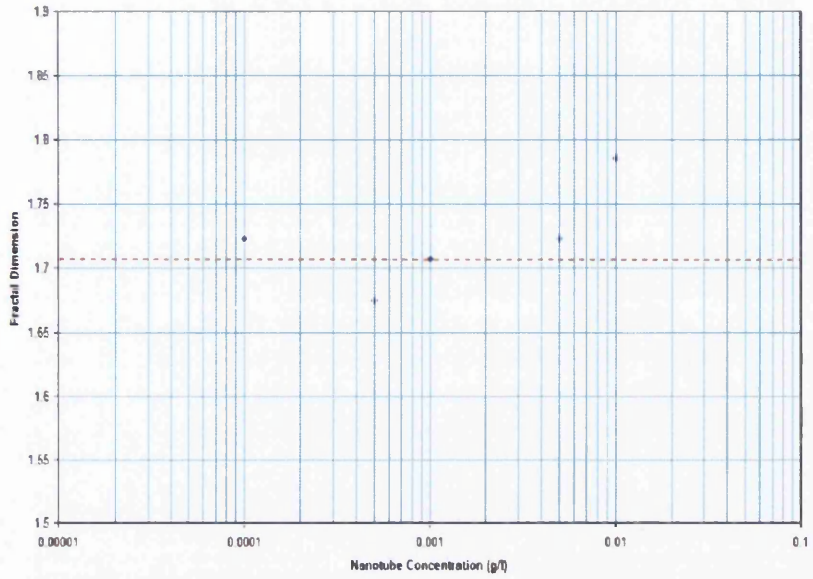

Figure 12.2: *Variance in Fractal Dimension of whole blood with 5% spike of Carboxyl-functionalised Multi Walled Nanotubes in TBS.*

No trend is evident in the data recorded for the percentage of lysis.

An increase in the clot size and the level of fine structure within it may lead to a reduction in the ability of the body to effectively remove the clot resulting in the possibility of dangerous free floating thrombi which could potentially lodge in smaller blood vessels downstream from the original clot.

The reduction in the time for the fibrin formation seen in the gel time and r-time data is also evident in the Activated Clotting Time measured on the Sonoclot with a sharp reduction from 450 seconds to 182 seconds.

The Clot Rate and Platelet Function data both dramatically increase from 3.6 to 12 and from 2 to 4.3 respectively. This supports the findings from the k-time and α angle recorded on the TEG.

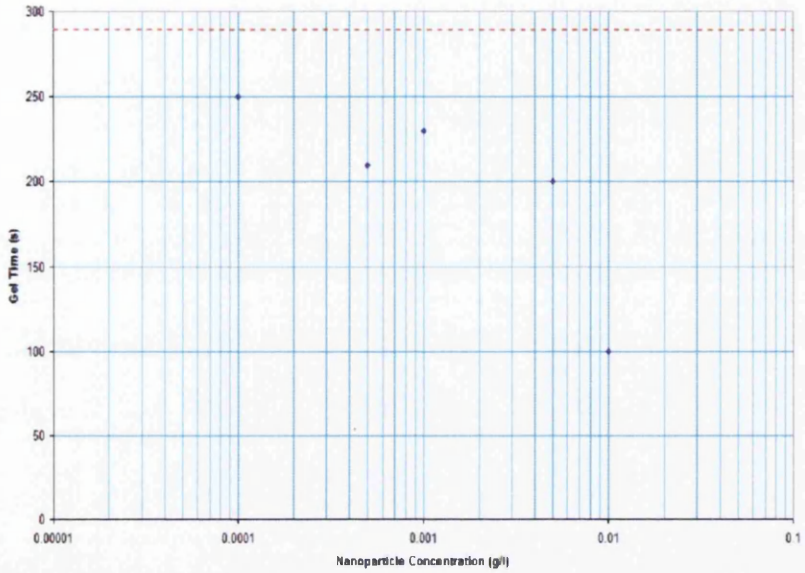

Figure 12.3: *Variance in Gel Time of whole blood with 5% spike of Carboxyl-functionalised Multi Walled Nanotubes in TBS.*

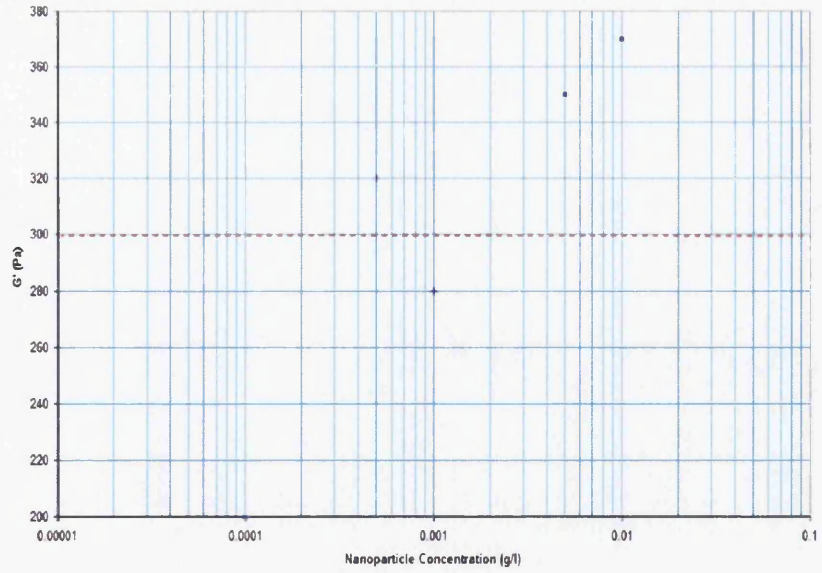

Figure 12.4: *Variance in G' max of whole blood with 5% spike of Carboxyl-functionalised Multi Walled Nanotubes in TBS.*

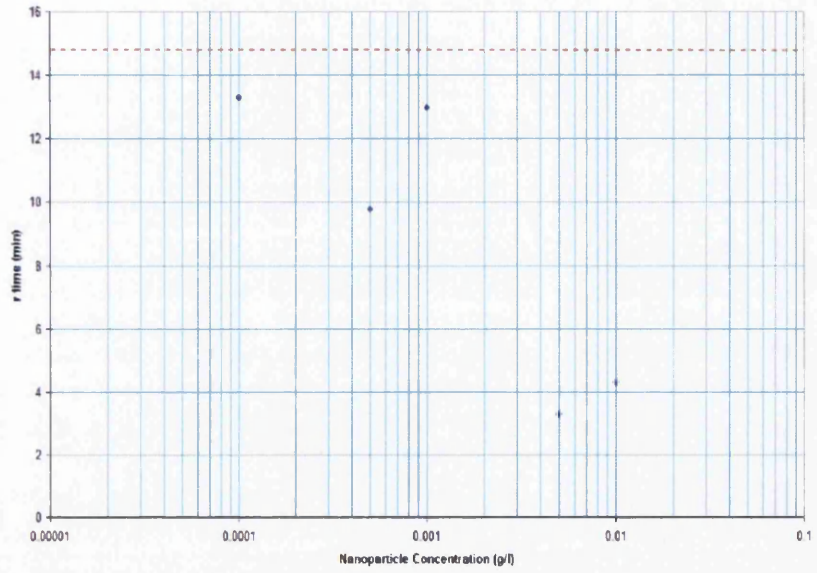

Figure 12.5: *Variance in TEG r time of whole blood with 5% spike of Carboxyl-functionalised Multi Walled Nanotubes in TBS.*

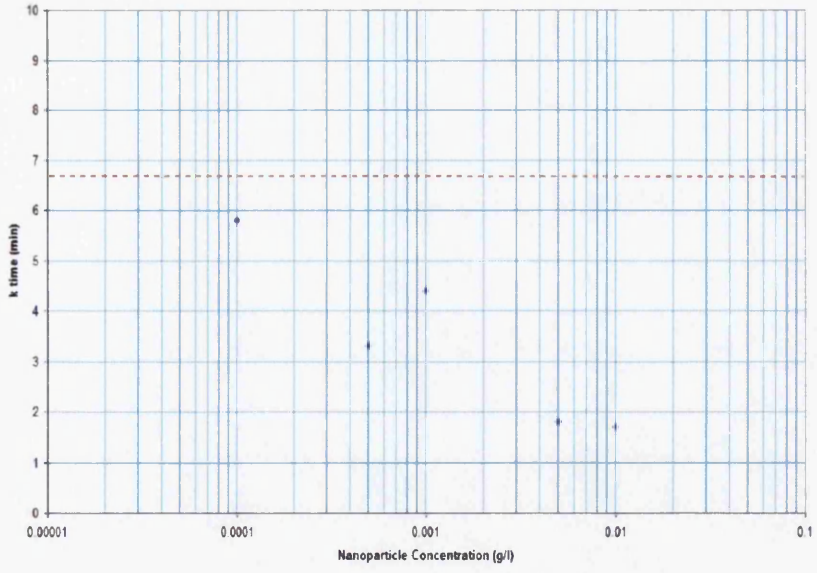

Figure 12.6: *Variance in TEG k time of whole blood with 5% spike of Carboxyl-functionalised Multi Walled Nanotubes in TBS.*

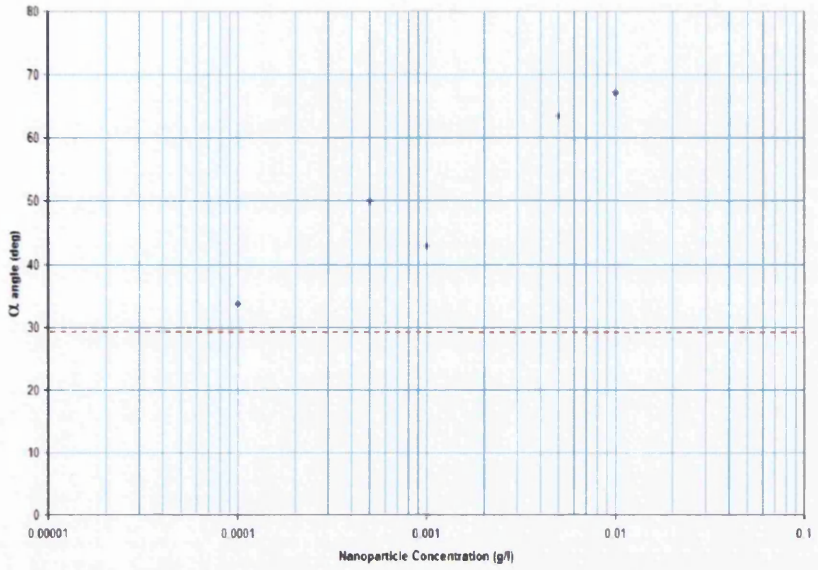

Figure 12.7: *Variance in TEG α angle of whole blood with 5% spike of Carboxyl-functionalised Multi Walled Nanotubes in TBS.*

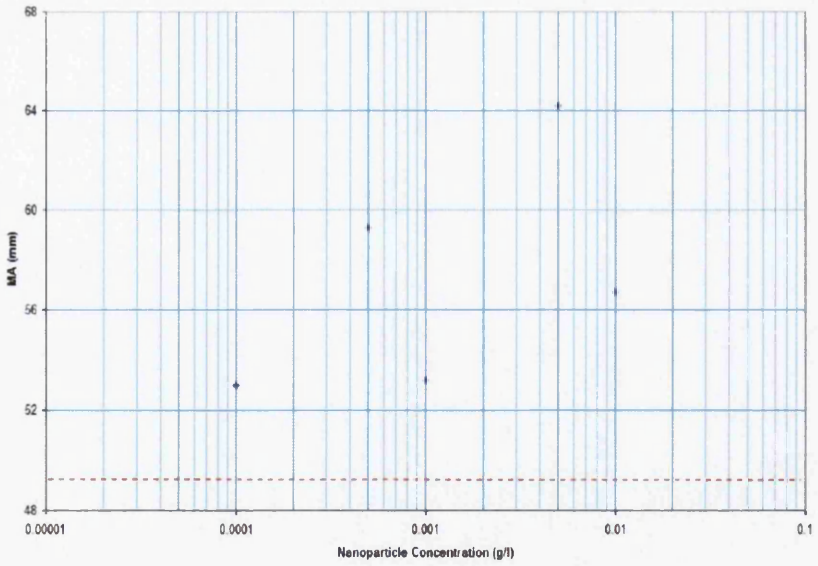

Figure 12.8: *Variance in TEG Maximum Amplitude of whole blood with 5% spike of Carboxyl-functionalised Multi Walled Nanotubes in TBS.*

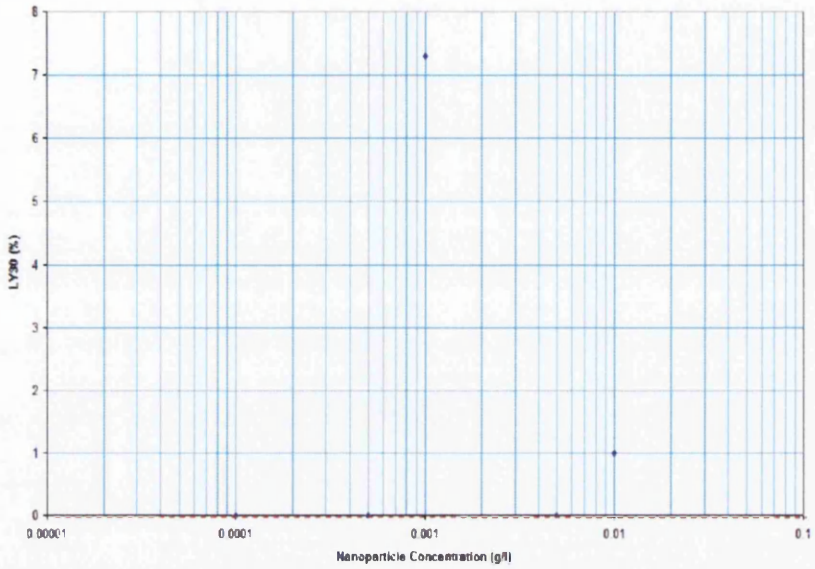

Figure 12.9: *Variance in TEG LY_{30} of whole blood with 5% spike of Carboxyl-functionalised Multi Walled Nanotubes in TBS.*

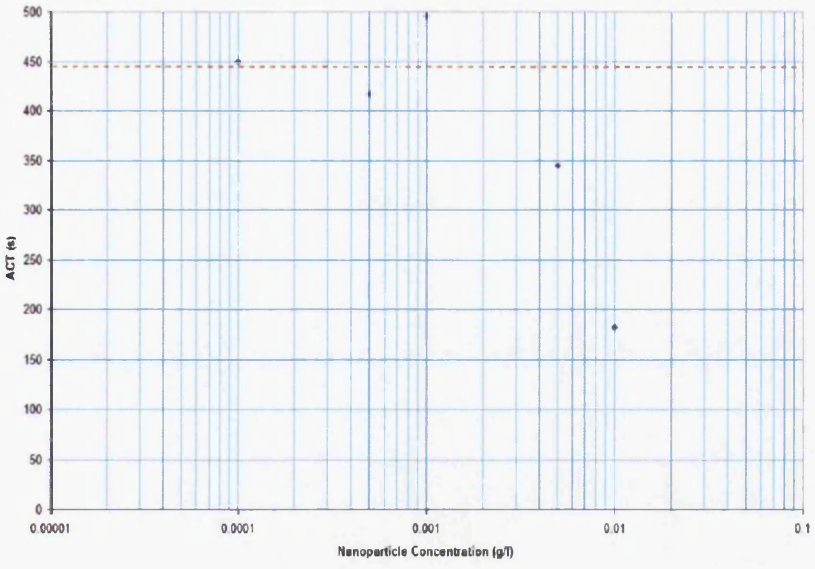

Figure 12.10: *Variance in Sonoclot ACT of whole blood with 5% spike of Carboxyl-functionalised Multi Walled Nanotubes in TBS.*

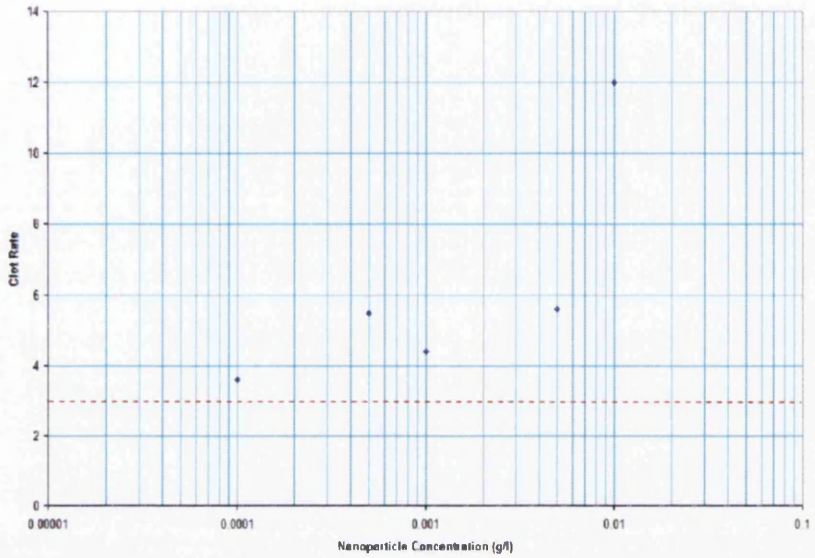

Figure 12.11: *Variance in Sonoclot Clot Rate of whole blood with 5% spike of Carboxyl-functionalised Multi Walled Nanotubes in TBS.*

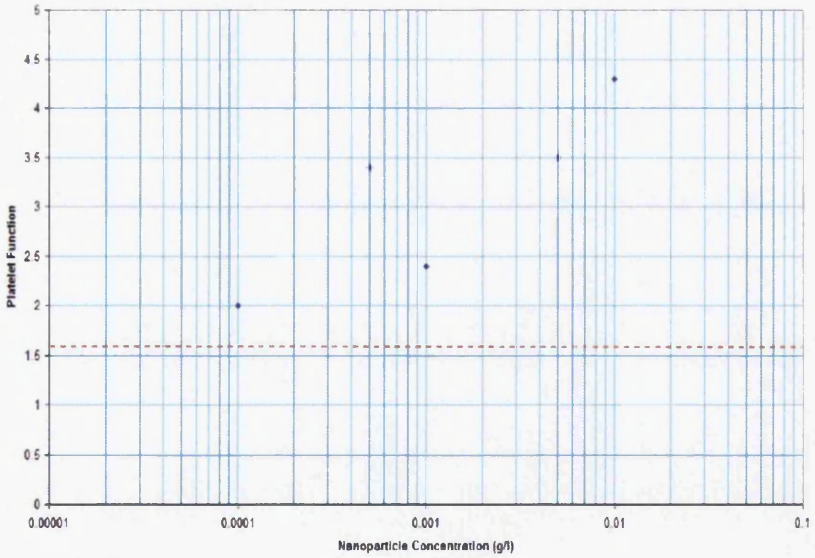

Figure 12.12: *Variance in Sonoclot Platelet Function of whole blood with 5% spike of Carboxyl-functionalised Multi Walled Nanotubes in TBS.*

Chapter 13

Conclusions

13.1 Rheology

The assessment of initial clot formation through Gel Point detection using oscillatory shear rheometry enables a far more rapid detection of the early stages of thrombosis than is possible in either of the clinical haemostasis measurement techniques. The machine is also able to maintain the applied stress within the linear range of the system while it undergoes gelation, something which neither of the clinical machines is capable of.

However, the rheological system at present does have a number of drawbacks: a long preparation time; the requirement of compressed air for the bearing; and the size of the machine. All of which preclude it from application in point of care locations, thus limiting the use of the currently available systems to suitable laboratories.

As such further work would be required to develop a rheometer which would be suitable for point of care facilities, as it has clear advantages in detecting structural abnormalities in the initial clot. It would also be necessary to generate standard procedures within the software for the assessment of particular abnormalities or the effect of dilutions as these will alter the material properties of the blood sample, thus changing the required frequencies for Gel Point detection and the critical stress value.

13.2 Fractal Analysis

The use of the fractal dimension calculated from the phase angle at the Gel Point is of vital importance as it enables an assessment of the microstructure

of the initial clot that would otherwise be impossible. The only other method being the use of SEM imaging which requires the clot to be ethanol dried, embedded in wax and cleaved into fine sections, a process which means the final clot which is imaged may be little resemblance to that originally formed.

At present the fractal dimension is limited to the description of the structure of the initial clot. Development of the work undertaken by Avrami et al [36][37] may enable the structural analysis to be extended to cover the manner in which the clot grows to maturity. This clearly presents itself as being the next step required to further develop this method of thrombosis analysis.

13.3 Carbon Nanoparticles

While all of the nanoparticles examined in this thesis have prothrombotic effects when added to whole blood, there is a clear difference in the degree to which these effects occur. In the case of the nanotubes this difference is linked to the increased solubility of the functionalised nanotubes which enables them to more readily become suspended.

The range of nanoparticles investigated in this thesis is necessarily limited however. As such a broader range requires investigation with respect to the functionalisation of the nanotubes with protein molecules such as heparin. The expansion should be tailored towards the nanoparticles, both carbon and otherwise, which are at the forefront of the development for uses in targeted drug delivery.

13.4 Nanoparticle Characterisation

The characterisation of nanoparticles, both as individual entities and their behaviour within any prospective solvent is very important, both to ensure that the nanoparticles fall within the suspected size ranges and that the proposed solvent produces as stable a suspension as possible.

Further developments in the field of SEM which enable higher resolution at lower applied beam strength are of profound importance for the improvement of nanoparticle imaging. At standard beam strengths (above 3kV) the nanotubes in particular exhibit charging which can result in the destruction of sections of sample.

In terms of the solvent, a larger number of medical solutions should be investigated. This investigation should also include assessment of the effect of the solvents on the initial clot formation as measured on the rheometer.

13.5 Blood

Prior to the work presented here, very little had been carried out to assess the effects of nanoparticle addition to whole blood in vitro. This is of critical importance both to the prospects of the utilisation of nanoparticles for drug delivery and in continuing the assessment of the effects of urban particulate exposure.

The work presented needs to be expanded to a full clinical study for each nanoparticle type with a large volunteer base and should include haematological tests such as aPTT to enable a complete assessment of the effects of the nanoparticles utilising all standard test procedures applicable.

13.5.1 Clot Measurement Techniques

Sensitivity

It is clearly evident through the measured values of the time taken for the initial sample spanning fibrin strands to form that the rheometrical techniques as used on the G2 are far more sensitive than either the Sonoclot of the TEG. This is due to a number of factors.

Firstly the G2 is able to maintain the applied force below the critical strain value of 2%, the numerical value of which will change as the structure of the clot develops. In contrast neither the Sonoclot or the TEG are able to do this and as such may well shear apart the earliest formed fibrin strands, thus delaying their measurement of the sample spanning network. This also means that neither of the clinical machines are operating within the linear range of the blood sample.

Secondly, while the geometry used to conduct the experiments on the G2 is completely rigid, the probe used by the Sonoclot is easily deformed, which may well allow the growing blood clot to cause an alteration in the shape of the probe resulting in the development of inaccuracies.

Ease of Use

In terms of ease of use the two systems set up as clinical devices, the TEG and the Sonoclot, are both far more straightforward to set up and run. This is true of the tests and the preparation times. The G2 also requires a knowledge of rheometry in order to set up the parameters for the tests.

Finally, the G2 and other similar rheometrical devices are at present too bulky to be used for point of care blood analysis due to the requirement for pressurised air for the bearings.

13.6 Comparison of Nanoparticles' Effects on Thrombosis

13.6.1 Effect on Thrombus Structure

Initial Thrombus

The fractal dimension derived from the phase angle value at the Gel Point is the only relatively noninvasive means by which the microstructure of the initial clot can be characterised. A comparison of the alterations in the fractal dimension due to the inclusion of the various types of nanoparticles will therefore provide a means of assessing the level of effect on the initial clot formation of each particle type.

In this case the nanoparticles with the clearest effect on the fractal dimension of the initial clot are as-produced multi-walled nanotubes which exhibit the most dramatic increase from 1.50 following a 0.0001g/l addition to 1.82 following a 0.01g/l addition. This represents an increase in structural complexity within the fibrin mesh as the concentration of the nanotubes is increased.

The carboxyl-functionalised single-walled nanotubes also exhibit a rise in the fractal dimension, although less marked than that found following the addition of the as-produced multi-walled nanotubes, meaning that the structural complexity increase is reduced.

The next greatest effect is seen from the carboxyl-functionalised multi-walled nanotubes which show a small increase in fractal dimension from 1.67 to 1.79. This data set is one of the tightest enabling a ready ascertation of the trend. This is also the last of the nanoparticles to exhibit a rise in

structural complexity with increasing concentration.

Data points from the as-produced single-walled nanotubes fall in a band with no increase or decrease in fractal dimension evident with increasing nanoparticle concentration. The average is still raised above that of the baseline provided by the pure TBS addition showing that the particles still cause a small level of increase in the structural complexity.

In stark contrast to the results from all of the nanoparticles, the addition of increasing concentrations of diesel particles leads to a decrease in the fractal dimension from 1.75 to 1.56, as the initial clot structure becomes increasingly loose.

Therefore, the order of level of effect is as follows:

$$\text{APMN} \geq \text{SCOOH} \geq \text{MCOOH} \geq \text{APSN} \geq \text{DIESEL}$$

Mature Thrombus

The maximum value of G' reached by the clot reflects its structural complexity once mature.

The carboxyl-functionalised multi-walled nanotubes clearly have the most dramatic effect on the final clot structure, a fact which becomes even more apparent as the concentration of the nanotubes is increased with the G' values increasing from 200Pa.s to 370Pa.s.

The addition of diesel particles to the blood, in marked contrast to the results from the initial clot, also showed a clear increase in G', from 310Pa.s to 390Pa.s.

Carboxyl-functionalised single-walled nanotubes also exhibit a marked increase in the G' values, although to a lesser extent than that seen in the data for the carboxyl-functionalised multi-walled nanotubes or the diesel particles.

While the results from the as-produced single walled nanotubes are all above the TBS baseline, the data points exhibit a peak of 375Pa.s at 0.001g/l. The average value of the data points is below that of the nanoparticles already described in this section.

The G' data from the as-produced multi-walled nanotubes shows a marked decrease from 400Pa.s to a final plateau around 310Pa.s.

The results from both the diesel particulates and the as-produced multi-walled nanotubes suggest that the initial clot structure as determined by the fractal dimension cannot necessarily be used as pointer to the structure of the mature clot in the case of nanoparticle addition.

The order of level of effect on the G'max is:

$$\text{MCOOH} \geq \text{DIESEL} \geq \text{SCOOH} \geq \text{APSN} \geq \text{APMN}$$

Both the carboxyl-functionalised single-walled nanotubes and carboxyl-functionalised multi-walled nanotubes exhibit increases (56.3mm to 59.1mm and 59.3mm to 64.7mm respectively) in the maximum amplitude with increasing particle concentration.

As-produced multi-walled nanotubes data reveals a band elevated above the TBS baseline, and with an average greater than that of the carboxyl-functionalised multi walled nanotubes.

The diesel particles produce a very slight increase from 53.8mm to 59.9mm in the measured maximum amplitude as their concentration is increased.

The data for the as-produced single-walled nanotubes shows no obvious trend.

The order of the level of effect on the Maximum Amplitude recorded by the TEG is:

$$\text{SCOOH} \geq \text{APMN} \geq \text{MCOOH} \geq \text{DIESEL} \geq \text{APSN}$$

The rate of lysis is an important marker, both of clot stability and therefore structure and as a way of showing any effect the nanoparticles may have on the fibrinolytic system.

The average of the scattered data of lysis percentage for the carboxyl-functionalised single walled nanotubes is the highest, suggesting either a small enhancement of the fibrinolytic system or a reduction in the stability of the mature clot.

A high average in the lysis values is also seen to a lesser extent in the data generated following the addition of the diesel particles.

The as-produced multi-walled nanotubes, carboxyl-functionalised multi-walled nanotubes and the as-produced single-walled nanotubes all exhibit scattered data with low averages.

The order of the effect on the percentage of lysis after 30 minutes recorded by the TEG is:

$$\text{SCOOH} \geq \text{DIESEL} \geq \text{APMN} \geq \text{MCOOH} \geq \text{APSN}$$

13.6.2 Effect on Rate of Initial Thrombus Formation

The time required for initial clot formation is measured by the variables of gel time, r-time and activated clotting time on the G2, TEG and Sonoclot respectively. A reduction in the time required for the formation of the initial clot is a clear indicator of a hypercoagulability with the blood due to increased levels of activation of the platelets through contact with the added nanoparticles.

The most dramatic effect on the gel times following the addition of any of the nanoparticles is seen in the data from the experiments using the carboxyl-functionalised multi walled nanotubes which show a reduction in gel time from 250 seconds to 100 seconds.

Addition of carboxyl-functionalised single-walled nanotubes resulted in reduced gel times with an average of 220 seconds except for the addition of 0.005g/l which exhibited a gel time of 135 seconds.

The as-produced single-walled nanotube additions all resulted in gel times below the TBS baseline of 290 seconds apart from a peak at 0.001g/l of 312 seconds.

As-produced multi-walled nanotubes also caused a reduction in gel times, although to a lesser extent than the single-walled.

In contrast to this, the measured gel times following the addition of diesel particulates showed an initial large reduction to 160 seconds with an increase to a peak of 260 seconds at a concentration of 0.005g/l.

The order of the level of effect on the gel time is:

$$\text{MCOOH} \geq \text{SCOOH} \geq \text{APSN} \geq \text{APMN} \geq \text{DIESEL}$$

The TEG machine is the least sensitive to the initial fibrin formation with the values for the r-time being markedly higher than those for either the gel time or the activated clotting time.

Again the clearest effect was from the addition of the carboxyl-functionalised multi walled nanotubes, exhibiting a sharp decrease from 13.3 minutes to 4.3 minutes with increasing concentration.

Decreases were evident to smaller degree in the data for the carboxyl-functionalised single walled nanotubes (11.5 minutes to 5.9 minutes), the diesel particulates (15.1 minutes to 6.9 minutes) and the as-produced single walled nanotubes (12 minutes to 7.3 minutes).

The r-times recorded following the addition of increasing concentrations of as-produced multi walled nanotubes showed an increase from 7.8 minutes to 11.3 minutes, reflecting the TEG measuring an inhibitive effect.

The order of the level of effect on the r-time is:

$$\text{MCOOH} \geq \text{SCOOH} \geq \text{DIESEL} \geq \text{APSN} \geq \text{APMN}$$

The activated clotting time measured by the Sonoclot falls between the gel time and the r-time measured by the other machines.

In this case the greatest effect was seen from the carboxyl-functionalised multi-walled nanotubes which showed a sharp decrease in the activated clotting times from 450 seconds to 182 seconds with increasing concentration. All of the activated clotting times were below the pure TBS value.

A decrease was also evident in the data from the carboxyl-functionalised single-walled nanotubes, although smaller than that seen with the carboxyl-functionalised multi-walled nanotubes, with the values dropping from 354 seconds to 305 seconds.

The addition of as-produced single-walled nanotubes also resulted in marked decrease with activated clotting times falling from 572 seconds to 394 seconds. While this decrease is sharper than that of the carboxyl-functionalised single-walled nanotubes, at no point do the values cross, meaning that the greater effect is caused by the functionalised nanotubes.

The as-produced multi-walled nanotubes exhibited a slightly decreasing trend in the recorded activated clotting times with increasing concentrations.

The activated clotting times recorded following the addition of increasing concentrations of diesel particulates showed no obvious trend.

Therefore, the order of the level of effect on the activated clotting time is:

$$\text{SCOOH} \geq \text{MCOOH} \geq \text{APSN} \geq \text{APMN} \geq \text{DIESEL}$$

13.6.3 Effect on Thrombus Development

The k-time is a measure of the time taken for the clot to show an impedance to the movement of the cuvette equivalent to it having reached a size of 20mm. As such any reduction of the time would indicate prothrombotic effects.

The carboxyl-functionalised multi-walled nanotubes again showed the greatest effect with a distinct and tight decrease from 5.8 minutes to 1.7 minutes with increasing concentration.

A decrease in the k-times from 5 minutes to 2.6 minutes was evident in the data from the carboxyl-functionalised single-walled nanotubes.

Decreases in the k-time are also seen in the data collected following the addition of as-produced multi- and single walled nanotubes (4.3 minutes to 2.2 minutes and 7.2 minutes to 3.7 minutes respectively).

The data generated following the addition of diesel particulates to whole blood the k-times show an increase from 0.8 minutes to a peak of 4.7 minutes at 0.001g/l followed by a decrease to 2 minutes at 0.01g/l to with increasing concentration, again suggesting that the diesel particulates may have an inhibitive effect at certain concentrations concentrations.

The order of the level of effect on the k-time is therefore:

$$\text{MCOOH} \geq \text{SCOOH} \geq \text{APMN} \geq \text{APSN} \geq \text{DIESEL}$$

The α angle provides a measurement of the rate of clotting through the use of a line applied at a tangent to the TEG curve. An increase in the angle reflects an increase in the rate of thrombosis.

As with the k-time the most marked increase was seen in the data from the addition of the carboxyl-functionalised multi-walled nanotubes: 33.8° to 67.2°.

The next most distinct effect was seen following the addition of the as-produced multi-walled nanotubes with an increase 49.5° to 73.2°.

A lesser increase is also seen in the data from the carboxyl-functionalised single-walled nanotubes.

An slight rise with increasing concentration is evident in the results from the as-produced single-walled nanotubes.

The data for the diesel particulates shows a decrease from 80.6° at 0.0001g/l to 40.9° at 0.001g/l followed by an increase to 52.9° at 0.01g/l.

The order of the level of effect on the α angle is:

$$\text{MCOOH} \geq \text{APMN} \geq \text{SCOOH} \geq \text{APSN} \geq \text{DIESEL}$$

The clot rate as measured by the Sonoclot is taken as the gradient of the rapid increase seen in the second stage of the sonoclot signature. As such it provided a value for the increase in the impedance of the sonoclot probe as the sample clots.

The values for the clot rate measured following the addition of the carboxyl-functionalised multi walled nanotubes exhibited a sharp increase from 3.6 to 12 with increasing concentration again pointing to the highly prothrombotic action of these nanoparticles.

Addition of increasing concentrations of carboxyl-funcionalised single walled nanotubes also resulted in the measured clot rate rising to a value of 6.7 at 0.01g/l from 4.4 at 0.0001g/l.

A lesser increase in the clot rate was seen following the addition of as-produced multi walled nanotubes, with the values rising from 3.2 to 6.

The addition of diesel particulates caused a similar climb in the clot rate with increasing concentration, from 3.4 at 0.0001g/l to 6.2 at 0.01g/l. This data is fairly loose.

As-produced single walled nanotubes produced the smallest increase in clot rate rising from 3 to 4.3.

Therefore, the order of the level of effect in the clot rate is:

$$\text{MCOOH} \geq \text{SCOOH} \geq \text{APMN} \geq \text{DIESEL} \geq \text{APSN}$$

The platelet function is one of the most important variables inferred by the sonoclot as it is the activation of the platelets through contact with the nanoparticles which causes the prothrombotic effects.

Again the most distinct and rapid rise in platelet function was recorded following the addition of increasing concentrations of the carboxyl-functionalised multi-walled nanotubes with values climbing from 2 at 0.0001g/l to 4.3 at 0.01g/l.

The as-produced multi-walled nanotubes produced the next most marked increase in platelet function (1.3 to 3.1) with increasing concentration.

Results from the tests on carboxyl-functionalised single-walled nanotubes also exhibited a sharp upward trend, although to a lesser extent than the particles already mentioned, ranging from 1.9 at 0.0001g/l to 2.4 at 0.01g/l.

The addition of both diesel particulates and as-produced single-walled nanotubes resulted in only a slight climb in the inferred platelet function for each particle (2 to 2.9 and 1.6 to 2.6 respectively).

Thus, the order of the level of effect on the platelet function is:

$$\text{MCOOH} \geq \text{APMN} \geq \text{SCOOH} \geq \text{DIESEL} \geq \text{APSN}$$

13.6.4 Conclusions From Comparisons of Nanoparticles

From the work presented above it can be stated that all of the nanoparticles examined had a prothrombotic effect on healthy, whole blood under the test conditions.

Overall Order of Effect

The comparison of the individual parameters given above enables an assessment of the overall levels of effect of each of the nanoparticles investigated.

$$\text{MCOOH} \geq \text{SCOOH} \geq \text{LPMN} \geq \text{LPSN} \geq \text{DIESEL}$$

This differs from the hypothesis in that it was expected that the diesel particulates would have a greater effect on the clot formation and structure than the as-produced nanotubes due to the greater solubility of the diesel particulates.

The reason for the reduced effect of the diesel particles may well lie in the inherent structural differences between them and the other nanoparticles. While the diesel particulates have a fairly uniform spherical structure, the nanotubes are, as per the name, cylindrical. The sizes of the nanotubes closely resemble the size and have similar surface roughness to the collagen fibres which trigger clotting in the case of vessel injury.

As suggested in the results chapters for the Diesel particles and the as-produced nanoparticles, the inhibitive effect as seen at certain concentrations may be due to floc formation and settlement within the asample as the nanoparticles agglomerate. This floc formation would result in the concentration of both nanoparticles and and cellular bodies such as platelets at the bottom of the sample thus preventing an even distribution of thrombin generation. This inhibitive effect may be reduced at the highest concentrations due to the simple number of particles in solution resulting in a limited amount of movement thus reducing he potential for agglomeration.

A full clinical study with these techniques utilising a broader range of the newly developed functionalities of nanotubes such as heparin, a number of solvents and a wider spread of concentrations is required.

Bibliography

[1] E.C Bingham. *The History of the Society of Rheology 1924-1944.* 1944.

[2] I.C Newton. *Philosophiae Naturalis Principia Mathematica 1st Ed.* 1687.

[3] R.J Hooke. *De Potentia Restitutiva.* J. Martyn. London, 1678.

[4] A.L Cauchy. *Ex. de Math*, 2:42, 1827.

[5] H Markowitz. The emergence of rheology. *Physics Today*, April:23, 1968.

[6] G.H.L Hagen. *Ann. Phy. Chem.*, 46:423, 1839.

[7] J.L Poiseiulle. *Comptes Rendus*, 12:112, 1841.

[8] C.L.M.H Navier. *Bull. Soc. Philomath*, page 75, 1823.

[9] G.G Stokes. *Trans. Camb. Phil. Soc.*, 8:287, 1845.

[10] G Weidemann. *Ann. Phy. Chem.*, 99:177, 1856.

[11] W Weber. *Ann. Phy. Chem.*, 34:247, 1835.

[12] J.C Maxwell. *Phil. Trans. Roy. Soc. London*, 157:49–88, 1867.

[13] L Boltzmann. *Weid. Ann.*, 5:430, 1878.

[14] T Schwedoff. *J. Physique*, 2, 9:34, 1890.

[15] W.R Hess. *Kolloid Z. Klin. Med.*, 71:421, 1910.

[16] E Hatchek. *Koll. Z.*, 13:88, 1913.

[17] E.C Bingham. *Fluidity and Plasticity.* McGraw-Hill, 1922.

[18] A Einstein. *Ann. Physik.*, 19:289, 1906.

[19] J.D Ferry. *Viscoelastic Properties of Polymers.* J. Wiley and Sons, 1970.

[20] P.J Flory. *J. Am. Chem. Soc.*, 63:3083, 1941.

[21] W.H Stockmayer. *J. Chem. Phys.*, 11:45, 1943.

[22] P.G de Gennes. *La Recherche*, 7:919, 1976.

[23] H.E Stanley. *Real-Space Renormalization.* Springer, 1982.

[24] H.H Winter and F Chambon. Analysis of linear viscoelasticity of a cross linking polymer at the gel point. *Journal of Rheology*, 30 (2):367–382, 1986.

[25] P.J Flory. *Principles of Polymer Chemistry.* Cornell University Press, 1953.

[26] H.H Winter. *Prog. Colloid Polymer Sci.*, 75:104, 1987.

[27] C.M Tung and J.P Dynes. Relationships between viscoelastic properties and gelation in thermosetting resins. *App. Polym. Sci.*, 27:569–574, 1982.

[28] B Mandelbrot. *The Fractal Geometry of Nature.* Freeman, 1982.

[29] G Edgar, editor. *Classics on Fractals.* Addison-Wesley, 1993.

[30] J.E Martin. Viscoelasticity near the sol-gel transition. *Phys Rev A*, 39 (3):1325–1332, 1989.

[31] M Smoluchowski. Drei vortrage uber diffusion, brownsche molekularbewegung und koagulation von kolloidteichen. *Phys. Z.*, 17:557–571, 1916.

[32] M Doi and S.F Edwards. *The Theory of Polymer Dynamics.* Clarendon Press, 1999.

[33] A. Bunde. Localization in disordered structures: Breakdown of the self-averaging hypothesis. *Phys. Rev.*, 52:53–56, 1995.

[34] P.E Rouse. *J. Chem. Phys.*, 21:1272, 1953.

[35] M Muthukumar. Screening effect on viscoelasticity at the gel point. *Macromolecules*, 22 (12):4656–4658, 1989.

[36] M Avrami. *J. Chem. Phys*, 7:1103, 1939.

[37] X.Y Liu. Formation kinetics of fractal nanofibre networks in gels. *App. Phys. Lett.*, 79 (21):3518–3520, 2001.

[38] E Drexler. *Engines of Creation.* Anchor Books, 1986.

[39] A Seaton. Particulate air pollution and acute health effects. *Lancet*, 345:176–178, 1995.

[40] Greater London Authority. 50 years on. 2002.

[41] C Herder. Chemokines and incident coronary heart disease. *Atherosclerosis, Thrombosis, and Vascular Biology*, 26:2147, 2006.

[42] W Huang. Visibility, air quality and daily mortality in shabghai china. *Sci. Tot. Env.*, 407 (10):3295–3300, 2009.

[43] H Kan. Differentiating the effects of fine and coarse particles on daily mortality in shanghai, china. *Environ. Int.*, 33 (3):376–384, 2007.

[44] G Oberdorster. Association of air pollution and acute mortality: involvement of ultrafine particles. *Inhalation Toxicology*, 1995.

[45] C Venkataraman. Comparison of particle lung doses from the fine and coarse fractions of urban pm-10 aerosols. *Inhalation Toxicology*, 11 (2):151–169, 1999.

[46] W Roemer. Differences among black smoke, pm10 and pm1.0 levels at urban measurement sites. *Env. Health Perspesctives*, 109 (2):151–154, 2001.

[47] R Peng. Seasonal analysis of air pollution and mortality in 100 us cities. *Am. J. Epidemiology*, 161 (6):585–594, 2005.

[48] N Mills. Diesel exhaust inhalation causes vascular dysfunction and impaired endogenous fibrinolysis. *Circulation*, 112:3930–3936, 2005.

[49] H.W Kroto and R.E Smalley. C60: Buckminsterfullerene. *Nature*, 318:162, 1985.

[50] S Iijima. Helical microtubules of graphitic carbon. *Nature*, 354:56, 1991.

[51] M.S Dresselhaus. Physics of carbon nanotubes. *Carbon*, 33:883, 1995.

[52] L.A Chernozatinskii. Carbon carbon films of oriented multilayered nanotubes deposited on kbr ang glass by electron beam evaporation. *Chem. Phys. Lett.*, 228:94, 1994.

[53] T W Ebbesen and K Tanigaki. Purification of carbon nanotubes. *Nature*, 367:519, 1994.

[54] G.S Duesberg. Separation of carbon nanotubes by size exclusion chromatography. *J. Chem.Soc., Chem. Commun.*, 435, 1998.

[55] S Iijima. Single-shell carbon nanotubes of 1-nm diameter. *Nature*, 363:603, 1993.

[56] D.S Bethune. Cobalt-catalysed growth of carbon nanotubes with single layer atomic walls. *Nature*, 363:605, 1993.

[57] S Subramoney. Radial single-layer nanotubes. *Nature*, 366:637, 1993.

[58] R.E Smalley. Catalytic growth of single-walled nanotubes by laser vaporisation. *Chem. Phys. Lett.*, 243:49, 1995.

[59] J-M Bonard. Purification and size-selection of carbon nanotubes. *Advanced Materials*, 9:827, 1998.

[60] K Tohji. Purifying single-walled nanotubes. *Nature*, 383:697, 1996.

[61] A.J Gross. The oxidation of tyramine, tyrosine, and related compounds by peroxidase. *J. Bio. Chem.*, 234 (6):1611–1614, 1959.

[62] C.A Poland. Carbon nanotubes introduced into the abdominal cavity of mice show asbestos-like pathogenicity in a pilot study. *Nature Nanotechnology*, 3:423–428, 2008.

[63] A Radomski. Nanoparticle-induced platelet aggregation and vascular thrombosis. *Brit. J. Pharm.*, 146:882–893, 2005.

[64] A Nemmar. Passage of inhaled particles into the blood circulation in humans. *Circulation*, 105:411–414, 2002.

[65] A Nemmar. Diesel exhaust particles in lung acutely enhance experimental peripheral thrombosis. *Circulation*, 107:1202–1208, 2003.

[66] A Peters. Increased particulate air pollution and the triggering of myocardial infarction. *Circulation*, 103:2810–2815, 2001.

[67] R.F Doolittle. Sturctural aspect of the fibrinogen to fibrin conversion. *Adv. Protein Chem.*, 27:1–109, 1973.

[68] H Hemker. *Thrombin generation, an essential step in haemostasis and thrombosis. Haemostasis and Thrombosis*, volume 1. Churchill Livingstone, 3 edition, 1993.

[69] A. Loeliger. Behaviour of factor vii and prothrombin in late pregnancy and in the newborn. *Acta Haematologica*, 7, 1952.

[70] K-T. H. Vu. Molecular cloning of a functional thrombin receptor reveals a novel proteolytic mechanism of receptor activation. *Cell*, 64:1057–1068, 1991.

[71] N Mackman. The role of tissue factor in haemostasis, thrombosis and vascular development. *Arterioscler. Thromb. Vasc. Biol.*, 24 (6):1015–1022, 2004.

[72] R.J Jenny. *The physiology and biochemistry of factor V. Haemostasis and Thrombosis*, volume 1. Churchill Livingstone, 3 edition, 1993.

[73] P.A Owren. The fifth coagulation factor. (factor v). preparation and properties. *Biochem. J.*, 43:136, 1948.

[74] F Koller and A Loeliger. Experiments on a new clotting factor (fector vii). *Acta Haematoligica*, 6, 1951.

[75] T.P Telfer and K.W Denson. A 'new' coagulation defect. *Brit. J. Haemat.*, 2:308, 1956.

[76] D.P O'Brien. *The structure and function of factor VIII. Haemostasis and Thrombosis.*, volume 1. Churchill Livingstone, 3 edition, 1993.

[77] A.P Reiner. *The physiology and biochemistry of factor IX. Haemostasis and Thrombosis.*, volume 1. Churchill Livingstone, 3 edition, 1993.

[78] H.L James. *Physiology and biochemistry of factor X. Haemostasis and Thrombosis.*, volume 1. Churchill Livingstone, 3 edition, 1993.

[79] O.D Ratnoff. *The development of knowledge about haemostasis and thrombosis. Haemostasis and Thrombosis*, volume 1. Churchill Livingstone, 3 edition, 1993.

[80] S Ramstrom. *The role of platelets in whole blood coagulation.* Number 776. Linkoping University Medical Dissertations, 2003.

[81] J.M Thomson, editor. *Blood coagulation and Haemostasis: a practical guide.* Churchill Livingstone, 1991.

[82] M.H Prins. *Diagnosis and treatment of venous thromboembolism. Haemostasis and Thrombosis*, volume 2. Churchill Livingstone, 3 edition, 1993.

[83] W Chandler and G Schmer. Evaluation of a new dynamic viscometer for measuring the viscosity of whole blood and plasma. *Clin. Chem.*, 32 (3):505–507, 1986.

[84] M.E McKenzie. Clinical utility of available methods for determining platelet function. *Cardiology*, 92:240–247, 1999.

[85] M.A Tucci. Platelet function monitoring with the sonoclot analyser after in vitro tirofiban and heparin admininstration. *J. Thorac. Cardiovasc. Surg.*, 131:1314–1322, 2006.

[86] T Miyashita. Evaluation of platelet function by sonoclot analysis compared with other hemostatic variables in cardiac surgery. *Anesthesia and Analgesia*, 87:1228–1233, 1998.